



universität
wien

DIPLOMARBEIT

Towards the Understanding of Conformational Changes of the Alpha-Actinin2 Homodimer

angestrebter akademischer Grad

Magister/Magistra der Naturwissenschaften (Mag. rer.nat.)

Verfasserin / Verfasser:	Kerstin Schorn
Matrikel-Nummer:	0100270
Studienrichtung (lt. Studienblatt):	Molekulare Biologie
Betreuerin / Betreuer:	Kristina Djinovic-Carugo

Wien, am 07.11.07

Towards the Understanding of Conformational Changes of the Alpha-Actinin2 Homodimer

Diplomarbeit

Vorgelegt am Institut für biomolekulare Strukturchemie an der Universität Wien 2007

Verfasst
Von

Kerstin Schorn

Betreut
Von

Kristina Djinovic-Carugo
und
Anita Salmazo

Danksagung

An dieser Stelle möchte ich mich bei allen jenen bedanken, die es mir ermöglicht haben, diese Arbeit zu verfassen.

Vorrangig bedanke ich mich bei meiner Familie, meinen Eltern Alfred und Edeltraud Schorn und meiner Schwester Viola Krautschneider, die mich zu jeder Zeit und in jeglicher Hinsicht mit aller Kraft unterstützt haben.

Außerdem gebührt meinem Freund Peter Just größter Dank für seinen Beistand, seine Geduld und Fürsorge in dieser nicht immer ganz leichten Zeit.

Natürlich danke ich auch meinen Studienkollegen und Freunden, die mich auf dem Weg zu dieser Arbeit und durch diese hindurch begleitet und unterstützt haben, insbesondere Bettina Spitzenberger, Ara Hacobian und Georg Feichtinger.

Schließlich möchte ich mich bei allen jenen bedanken, die die Entstehung dieser Arbeit mit ihrer Betreuung, ihrem Wissen und der Bereitstellung aller nötigen Mittel ermöglicht haben: Anita Salmazo, Björn Sjöblom, Kristina DjinoVIC-Carugo und alle weiteren Mitglieder der Gruppe für Kristallographie und der Gruppe für NMR des Instituts für biomolekulare Strukturchemie.

Es würde den Rahmen dieser Ausführungen sprengen, jede helfende Hand namentlich zu nennen, und ich hoffe daher, dass jene, die nicht genannt wurden, sich dennoch meiner Dankbarkeit bewusst sind.

Zusammenfassung

Alpha-Aktinin ist ein Protein des Zytoskeletts, das Aktin Filamente quervernetzt und als Verbindung zwischen zytoskeletalen -, Membran- und Signalproteinen fungiert.

Abgesehen von der Bindung an Aktin Filamente interagiert es mit einer Vielzahl von Proteinen. Alpha-Aktinin findet sich an der Plasmamembran, wo es kortikales Aktin quervernetzt, an der Ablösung und Versetzung der Membran beteiligt ist und Transmembranproteine mit dem Zytoskelett verbindet. Die Störung von Integrin-Alpha-Aktinin Interaktionen an Fokalen Kontakten macht Osteoblasten anfällig für Apoptose. Alpha-Aktinin ist ein antiparalleles Homodimer, dessen Struktur von den einzelnen Domänen bereits gelöst wurde. Ein Monomer besteht aus einer Aktin bindenden Domäne am N-Terminus, die durch ein 15 Aminosäuren langes Peptid (Neck) mit dem stabförmigen Teil, bestehend aus vier Spektrin-ähnlichen Domänen, verbunden ist. Der C-Terminus wird durch eine Calmodulin-ähnliche Domäne gebildet, die an den Neck der gegenüberliegenden Untereinheit des inaktiven Dimers binden kann. Noch ist es spekulativ, welche Aminosäurereste in der Assemblierung und Bindung der C-terminalen Domäne an den Neck involviert sind und wie sich die molekulare Architektur des gesamten Homodimers darstellt.

Das Ziel der vorliegenden Arbeit war die Untersuchung der Bindung der C-terminalen Calmodulin Domäne einerseits an ein synthetisiertes Peptid des Necks und andererseits an den nativen N-terminalen Teil von Alpha-Aktinin Isoform 2. Bindungsstudien, Analyse der Komplexe als auch Kristallisationsversuche des Komplexes wurden durchgeführt, um die Struktur des Teils des Homodimers aufzulösen, der für die Existenz einer offenen als auch einer geschlossenen Konformation verantwortlich ist.

Weiters wurden Mutationsstudien durchgeführt, in Zuge derer eine künstliche Aminosäure an jene Stellen der Calmodulin-ähnlichen Domäne inkorporiert wurden, die im Verdacht stehen für die Interaktion mit dem Neck ausschlaggebend zu sein. Diese Interaktionsstellen wurden durch frühere Daten über die Bindung der Calmodulin-ähnlichen Domäne an andere Interaktionspartner und durch bioinformatische Methoden, unter der Verwendung der Programme WHAT IF, CHARMM und Pymol, ermittelt. Die künstliche Aminosäure hat die Eigenschaft Aminosäurereste innerhalb eines Radius von

3 Ångström unter UV Bestrahlung kovalent quervernetzen. Durch diese Vorgehensweise wurde sichergestellt, dass beide Komponenten des Komplexes im Kristall vorhanden waren.

Abstract

Alpha-actinin is a cytoskeletal protein that cross-links actin filaments and serves as a connection between the cytoskeleton and signaling and membrane proteins. Apart from binding to actin filaments it interacts with a tremendous number of interaction partners. Alpha-actinin can localize to the plasma membrane, where it cross-links the cortical actin, aids in membrane displacement, and links transmembrane receptors with the cytoskeleton. Disruption of alpha-actinin-integrin interactions at focal adhesions renders osteoblasts susceptible to apoptosis.

Alpha-actinin is an antiparallel homodimer, of which the structures of several domains have already been solved. One monomer consists of an actin binding domain at the N-terminal, which is connected via a 15 amino acid peptide (neck) to a rod shaped moiety composed of four spectrin-like domains. The C-terminal is formed by a calmodulin-like domain which is able to bind to the neck of the opposing subunit of dimer in an uninduced state. It remains putative which residues are involved in assembly and binding of the C-terminal domain to the neck, and what is the molecular architecture of the full-length homodimer.

The aim of this work was to investigate the binding of C-terminal calmodulin domain to a synthesized peptide of the neck as well as to a native N-terminal moiety of alpha-actinin isoform 2. Binding studies, complex analyses as well as crystallization trials of the complex were conducted, in order to solve the structure of the moiety of the homodimer responsible for the existence of an open and a closed conformation.

Moreover, mutation studies were performed, in the course of which an artificial amino acid was incorporated into the part of the calmodulin-like domain known to interact with the neck at putative interaction sites. These interaction sites were determined by comparison with previous data of binding of the calmodulin-like domain to certain interaction partners and by bioinformatics methods using the software CHARMM, WHAT IF and Pymol. The artificial amino acid has the property to crosslink covalently residues within 3 Ångström under UV exposure. By this procedure it was ensured, that the whole complex is present in the crystal.

Table of Contents

DANKSAGUNG	3
ZUSAMMENFASSUNG	4
ABSTRACT	6
TABLE OF CONTENTS	7
LIST OF ABBREVIATIONS	11
TABLE OF FIGURES	13
1.0 INTRODUCTION	16
1.1 Alpha-actinin and the current model of two different states	16
1.2 Isoforms of alpha-actinin	20
1.2.1 Alpha-actinin-1	20
1.2.2 Alpha-actinin-2	20
1.2.3 Alpha-actinin-3	21
1.2.4 Alpha-actinin-4	21
1.3 The Alpha-actinin Interactome	22
1.3.1 Actin	23
1.3.2 FATZ	23
1.3.3 Myopalladin	23
1.3.4 Titin	23
1.3.5 Nebulin	24
1.3.6 Vinculin	24
1.3.7 ZASP	24
1.3.8 Myotilin	24
1.3.9 CRP	24
1.3.10 Integrin β 1	24
1.3.11 ALP	25
1.4 The objectives of this study	25

2.0 MATERIALS	26
2.1 Media	26
2.2 <i>E.coli</i> Cell Strains	28
2.3 Plasmids	29
2.4 Buffer for molecular biology techniques	30
2.5 Buffers for Affinity Chromatography	30
2.6 Buffer for Size Exclusion Chromatography	30
2.7 Buffer for TEV Cleavage	30
2.8 Buffers for TEV Purification	31
2.9 Electrophoresis Buffer	31
2.10 Buffers for Tricine SDS PAGE	32
2.11 Buffers for Western Blotting	32
2.12 Buffers for On-Column Binding Studies	33
2.13 Refolding Buffers	33
2.14 Crystallization Screens	35
3.0 METHODS	36
3.1 Molecular Biology Techniques	36
3.1.1 Constructs	36
3.1.2 Primer Design	37
3.1.3 Standard PCR mixture	38
3.1.4 Standard PCR Program	39
3.1.5 Mutagenesis PCR mixture	39
3.1.6 Vector amplifying mutagenesis PCR	40
3.1.7 Two Step mutagenesis method (Young and Dong 2004)	41
3.1.8 Restriction and Ligation Enzymes	42
3.1.9 Transformation of competent cells	45
3.1.10 Colony PCR	45
3.2 Expression and Purification	46
3.2.1 Expression Screen Protocol	46
3.2.2 Large Scale Expression	47
3.2.3 Refolding Assay	48
3.2.4 Affinity Chromatography	49
3.2.5 Buffer Exchange	50
3.2.6 TEV Cleavage	50
3.2.7 Re-batch	50
3.2.8 Size Exclusion Chromatography	50
3.2.9 Concentration of proteins	51

3.2.10 Complex Formation	52
3.2.10 Preparation of recombinant TEV- protease	52
3.3 Analytical Methods	53
3.3.1 Determination of protein concentration	53
3.3.2 SDS-PAGE	53
3.3.3 Tricine-SDS-PAGE	54
3.3.4 Coomassie- Staining	54
3.3.5 Imidazole- Zink- Staining	54
3.3.6 Western Blot	55
3.3.7 Ni-NTA on-Column Binding Studies	56
3.3.8 Complex analysis	57
3.3.9 Isothermal Tritration Calorimetry	57
3.3.10 Circular Dichroism Spectroscopy	59
3.3.11 ThermoFluor	60
3.3.12 Dynamic Light Scattering	62
3.3.11 Photo Cross-linking	63
3.4 Crystallization	65
3.4.1 Mechanisms of protein crystallization	65
3.4.2 Set up of crystal drops and screening	66
3.4.3 Data collection	67
3.4.4 Cryo-conditions	67
3.5 Nuclear magnetic resonance	68
3.6 Molecular Dynamics Simulation	69
4.0 RESULTS AND DISCUSSION	71
4.1 Wild type CaM and EF34 domains	71
4.1.1 Cloning	71
4.1.2 Expression and Purification of CaM	71
4.1.3 Expression and Purification of EF34	74
4.1.4 Biophysical Analysis of EF34	76
4.1.4.1 Analytical gel filtration	76
4.1.4.2 1D-NMR of EF34	76
4.1.4.3 Circular Dichroism of EF34	77
4.2 Complex formation of EF34 with the neck and its analysis	78
4.2.1 Analytical gel filtration of the EF34/neck complex	78
Complex was formed as described in section 3.2.10.	78
4.2.2 2-Mercaptoethanol studies	81
4.2.2 ThermoFluor measurements of free EF34 and bound to the neck	85
4.2.3 ITC measurement of EF34 and the neck	87
4.3 Crystallization of EF34-neck complex	88
4.4 Complex formation and analysis of CaM/ABD-R1 and EF34/ABD-R1	92
4.4.1 Expression and Purification of ABD-R1	92
4.4.2 On Column binding study of ABD-R1 and EF34	95
4.5 Mutants 834ΔpBpa and 889ΔpBpa	97
4.5.1 Selection of mutation sites	97
4.5.2 Cloning of mutants	99
4.5.3 Expression and purification of mutants	99
4.5.4 Purification of inclusion bodies and refolding assay	102
4.5.5 Complex Formation and Photo cross-linking	103

4.5.6 Experiments on the truncated mutant EF34 Δ 889	104
5.0 CONCLUSIONS AND PERSPECTIVES	106
6.0 REFERENCES	108
CURRICULUM VITAE	113

List of Abbreviations

aa	amino acid
ABD	actin binding domain
ABD-R1	actin binding domain and first spectrin repeat of alpha actinin
Amp	ampicillin
APS	ammonium persulfate
BCIP	5-bromo-4-chloro-3-indoyl phosphate p-toluidine salt
bp	base pair
CaM	calmoduline-like domain of alpha-actinin
Cam	chloramphenicol
cDNA	complementary DNA
CRP	cysteine-rich protein
CV	colume volume
Da	dalton (1/12 of the mass of a C12 atom)
DMSO	dimethylsulfoxid
DNA	desoxy-ribonucleic acid
dNTP	desoxy-nucleotide triphosphate
DTT	dichloro-diphenyl-trichloroethane
EDTA	ethylenediaminetetraacetic acid
EF34	EF-hands 3 and 4 of alpha-actinin
EM	electron microscopy
FATZ	filamin-, actinin-, and telethonin-binding protein of the Z-disc
fw	5'-priming oligo-nukleotide
GST	gluthatione-S-transferase
HEPES	4-(2-hydroxyethyl)-1-piperazineethanesulfonic acid
His ₆ tag	six consecutive histidine residues
Ig	immunglobuline
IPTG	isopropyl-β-D-thiogalactopyranosid
ITC	isothermal titration calorimetry
Kan	kanamycin
kb	kilo base
LB media	Luria-Bertani media
MES	2-(N-morpholino)ethanesulfonic acid

NBT	p-nitro blue tetrazoliumvchloride
NBT	p-nitro blue tetrazoliumvchloride
Ni	nickel
OD ₆₀₀	absorbance at 600 nm
pBpa	p-bezoyl-L-phenylalanine
PCR	polymerase chain reaction
PEG	poly ethylene glycol
PIP ₂	phosphatidylinositol-4,5-biphosphate
ppm	part per million
rpm	rounds per minute
rv	3'-priming oligo-nukleotide
TEMED	N,N,N',N'-tetramethylethylenediamine
TEV	<i>Tobacco Etch Virus</i>
Tm	melting temperature
Tris	trishydroxymethylaminomethane
Trx	thioredoxin A
TrxA	thioredoxin A
U	unit
ZASP	Z-band alternatively spliced PDZ protein

Table of Figures

Fig.1	Actin filaments cross-linked by alpha-actinin (from: Olivier Pelletier, Materials Research Laboratory, University of California)
Fig.2	Crystal structure of alpha-actinin rod (Ylanne, Scheffzek et al. 2001)
Fig.3	Crystal structure of ABD of alpha-actinin 3 in its closed conformation (Franzot, Sjoblom et al. 2005)
Fig.4	Crystal structure of ABD of alpha-actinin 1 in its closed conformation (Borrego-Diaz, Kerff et al. 2006)
Fig.5	Uninduced state of the alpha-actinin dimer
Fig.6	Change of the uninduced into an induced conformation of the alpha-actinin dimer upon binding of PIP2
Fig.7	Structure of EF34 of alpha-actinin 2 bound to Zr7 of titin solved by NMR (Atkinson, Joseph et al. 2001)
Fig.8	Alpha-actinin and its role in the sarcomeric Z-disk in concert with its interaction partners in a myocardial cell (from: Norbert Frey – Ruprecht Karls University, University Hospital, Heidelberg
Fig.9	Scheme of the used constructs of alpha-actinin
Fig.10	Amino acid sequence of alpha-actinin2 with the sequences used in this study
Fig.11	Two step mutagenesis method
Fig.12	Schematized affinity chromatography procedure
Fig.13	Schematized gel filtration (size exclusion) chromatography.
Fig.14	Protocols for SDS-PAGE gel casting
Fig.15	ITC device
Fig.16	Examples for the typical profiles of a “far UV” CD spectra
Fig.17	Standard Thermofluor melting curve (kindly provided by Patrizia Ambrusci)
Fig.18	Thermofluor salt-pH screen set up for complex analysis of EF34/neck
Fig.19	Structure of p-benzoyl-L-phenylalanine.
Fig.20	Vector pSup-MjTyrRS-6TRN
Fig.21	Energy barriers a protein has to overcome on its way to crystallization (from: ‘Crystallography made crystal clear’, Gale Rhodes)
Fig.22	Phase diagram showing the solubility curve of a protein (from: ‘Crystallography made crystal clear’, Gale Rhodes)
Fig.23	Hanging drop vapor diffusion (from: ‘Crystallography made crystal clear’, Gale Rhodes)

Fig.24	Graphic presentation of incomplete factorial screening (from: 'Crystallography made crystal clear', Gale Rhodes)
Fig.25	Graphic presentation of sparse matrix screening (from: 'Crystallography made crystal clear', Gale Rhodes)
Fig.26	Data collection of a protein crystal by exposing it to an X-ray beam (from: 'Crystallography made crystal clear', Gale Rhodes)
Fig.27	Gradient PCR of CaM at temperatures 55°C, 60°C and 65°C
Fig.28	Ni-NTA gravity column of CaM-domain
Fig.29	Size exclusion chromatography diagram of CaM after TEV protease cleavage
Fig.30	SDS-PAGE gel of gel filtration fractions of CaM
Fig.31	Analytical gel filtration of CaM
Fig.32	SDS-PAGE gel of Ni-NTA fractions of EF34
Fig.33	SDS-PAGE gel of Ni-NTA fractions after TEV cleavage
Fig.34	Size exclusion chromatogram of EF34 after TEV cleavage
Fig.35	SDS PAGE analysis of size exclusion fractions of EF34
Fig.36	Analytical gel filtration chromatogram of EF34
Fig.37	EF34 1-NMR spectrum
Fig.38	CD spectrum of EF34
Fig.39	Standard run in 20 mM Tris pH 8, 200 mM NaCl, 2 mM 2-mercaptoethanol
Fig.40	Analytical gel filtration of the neck
Fig.41	Analytical gel filtration of EF34
Fig.42	Analytical gel filtration of the EF34/ neck complex
Fig.43	Analytical size exclusion of EF34-neck complex after 4 days storage at 4 °C
Fig.44	16% Urea-Tricine-SDS PAGE gel of fractions of analytical gel filtrations of EF34/neck
Fig.45	Complex of EF34 and the neck run at pH 6
Fig.46a	Fractions of analytical gel filtration run at pH 6 applied to 18 % SDS PAGE gel. Gel was loaded without reducing agents, using glycerol only.
Fig.46b	Fractions of analytical gel filtration run at pH 6 applied to 18 % SDS PAGE gel. Gel was loaded with 2-mercaptoethanol.
Fig.47	Analytical gel filtration of EF34/neck at pH 6 with reducing agents
Fig.48	Analytical gel filtration of EF34/neck in pH 8 without reducing agents
Fig.49a	Fractions of analytical gel filtration run at pH 6 applied to 18 % SDS PAGE gel. Gel was loaded without loading dye, using glycerol only.
Fig.49b	Fractions of analytical gel filtration run at pH 6 applied to 18 % SDS PAGE gel. Gel was loaded with loading dye containing 1 M 2-mercaptoethanol
Fig.50	Thermofluor measurements of the EF34-neck complex

Fig.51	Thermofluor salt-pH screen of EF34-neck complex
Fig.52	EF34 and neck interaction demonstrated by isothermal calorimetry
Fig.53	Pictures of some crystals obtained from EF34/neck complex
Fig.54	SDS-PAGE of fractions of Ni-NTA column of ABD-R1
Fig.55	Preparative size exclusion chromatogram of co-purified ABD-R1 and Cam
Fig.56	Fractions of preparative size exclusion of co-purified ABD-R1 and Cam
Fig.57	Preparative size exclusion chromatography of co-purified ABD-R1-EF34
Fig.58	Fractions of preparative size exclusion of co-purified ABD-R1 and EF34
Fig.59	SDS-PAGE gel of fractions of on column binding study of EF34 and ABD-R1
Fig.60	Analytical gel filtration of flow through after on column TEV cleavage of ABD-R1/EF34
Fig.61	Fractions of analytical gel filtration of on-column TEV protease digested ABD-R1/EF34
Fig.62	Resulting conformations after molecular dynamics of 1 ns of EF34 bound to the neck
Fig.63	Structure of EF34 (PDB:1H8B)
Fig.64	Sequencing result of 834ΔpBpa
Fig.65	SDS PAGE gel of Ni-NTA fractions of 834ΔpBpa and 889ΔpBpa
Fig.66	Gel filtration profile of EF34Δ889 after TEV protease cleavage
Fig.67	Comparison of EF34 and EF34Δ889 on 15 % SDS PAGE
Fig.68	Cell extract of 889ΔTyr expressed in GMML media
Fig.69a	SDS PAGE gel analysis of the refolding assay of 889ΔpBpa
Fig.69b	SDS PAGE gel fractions of Ni-NTA purification of 889ΔpBpa in inclusion bodies
Fig.70	Tricine gel of photo cross-linked 889ΔpBpa/neck
Fig.71	Analytical gel filtration of EF34Δ889 and the neck

1.0 Introduction

1.1 Alpha-actinin and the current model of two different states

The cytoskeleton consists of a number of filamentous systems, composed of polymers of tubulin, intermediate filament proteins and actin filaments. Formation of antiparallel actin filaments and their anchorage by its crosslinking protein alpha-actinin [*Fig. 1*] is found at many different sites throughout the cell. This is the case in the Z-disk of striated muscle, (Masaki, Endo et al. 1967); (Lazarides and Granger 1978) and the cytoplasmic dense bodies of smooth muscle (Geiger, Dutton et al. 1981), to anchoring points of polar arrays of actin filaments, such as the membrane-associated adhesion plaques of smooth muscle (Geiger, Dutton et al. 1981) (Small 1985) and the focal adhesions of non-muscle cells (Burrige, Nuckolls et al. 1990) as well as to regions of poorly oriented actin filaments in the leading edge of motile cells (Langanger, Moeremans et al. 1986).

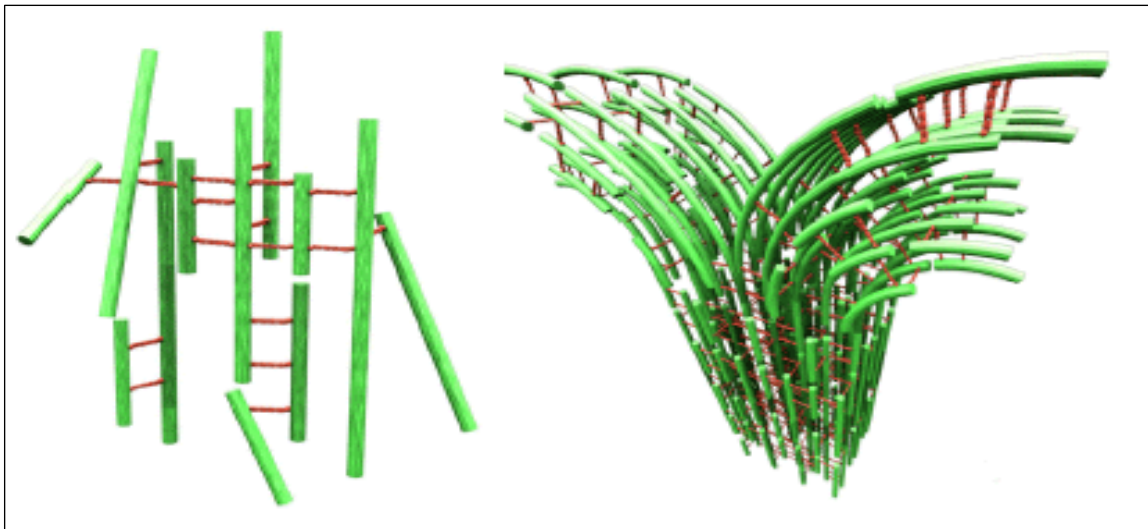


Fig.1 Actin filaments (green) cross-linked by alpha-actinin (red) (from: Olivier Pelletier, Materials Research Laboratory, University of California)

The fact that alpha-actinin is able to crosslink actin filaments in various orientations implies a quite low specificity, whereas it remains unclear whether the arrangement of bipolar or unipolar formations is due to isoform-specific intrinsic crosslinking or to presence or interaction of other cytoskeleton proteins. The functional unit of alpha-actinin is an antiparallel homodimer, with an actin binding domain (ABD) at the N-terminus and a calmodulin-like domain (CaM) at the C-terminus which are connected *via* four spectrin-like repeats (R1, R2, R3, R4) [Fig. 2], which are involved in dimerization of the alpha-actinin homodimer [Fig. 5] (Djinovic-Carugo 1999); Spectrin repeats consist of three-helix bundle structures which serve as a matrix for assembly of cytoskeletal and signaling proteins.

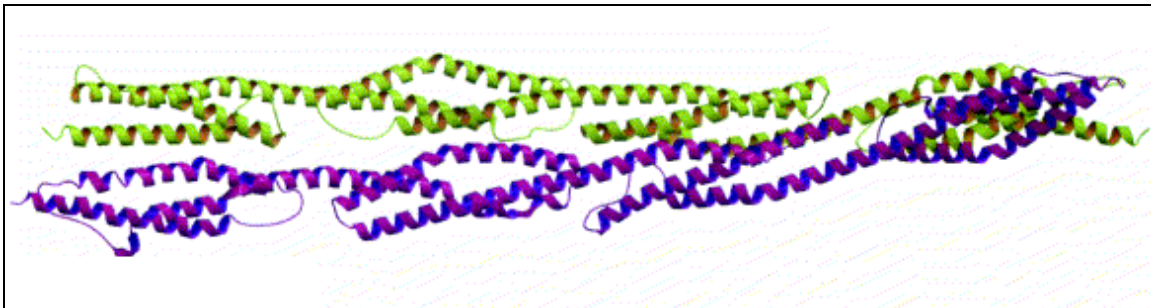
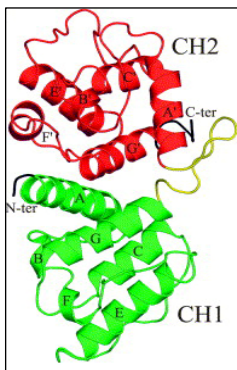


Fig. 2 Crystal structure of alpha-actinin rod (Ylanne, Scheffzek et al. 2001).

The ABD consists of two chalconin homology (CH) domains (Franzot, Sjoblom et al. 2005) [Fig. 3, Fig.4]. Dependent on the isoform of alpha-actinin different actin binding sites exist and it has been proposed that a single ABD is able to bind actin filaments in several conformations (Galkin, Orlova et al. 2002; Litjens, Wilhelmsen et al. 2005). A study of alpha-actinin suggested that at one end of the molecule the two CH domains



were in a compact, closed conformation, while at the other end they were in an open, extended state (Liu et al., 2004).

Fig. 3 Crystal structure of ABD of alpha-actinin 3 in its closed conformation (Franzot, Sjoblom et al. 2005).

This may be also due to the fact, that in EM studies the several particles are picked, merged and averaged. This could of course



Fig. 4 Crystal structure of ABD of alpha-actinin 1 in its closed conformation (Borrego-Diaz, Kerff et al. 2006).

result in an interpretation given by Liu et al.

The current model to explain the mechanism of alpha-actinin regulation was proposed by Young and Gautel (2000); it suggests that in the uninduced state CaM of one monomer is

bound tightly to the region between ABD and the first spectrin-like (R1) domain of the other monomer. This region, known as neck due to its position, consists of 15 amino acids.

Upon binding of phosphatidylinositol-4,5-biphosphate (PIP_2) to ABD in muscle cells, the inactive conformation changes into an active state, enabling the protein now to interact with distinct binding partners. It is proposed, that the fatty acid tail of PIP_2 interferes with the binding of the CaM domain to the neck what results in opening of the structure and activation.

While the phospholipid PIP_2 is triggering these conformational changes in the muscle isoforms, it is proposed that in the non-muscle isoforms calcium is responsible for these changes, since the muscle-isoforms are calcium in-sensitive.

In [Fig.5] the bound, uninduced state is schematized. The conformational change upon binding of PIP_2 to ABD is illustrated in [Fig. 6]. The dissociation of the binding may enable the CaM domain to interact with certain interaction partners, which will be described below.

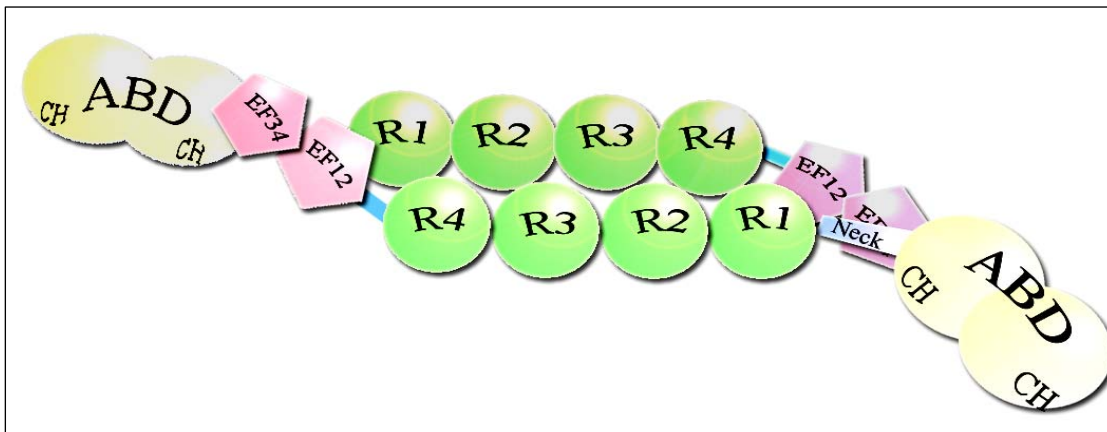


Fig. 5 Uninduced state of the alpha-actinin dimer. The four spectrin-domains (R1, R2, R3, R4) are proposed to mediate the dimerization (Djinovic-Carugo et al., 2001). In the uninduced state the current opinion is, that EF12/EF34 are bound to the neck.

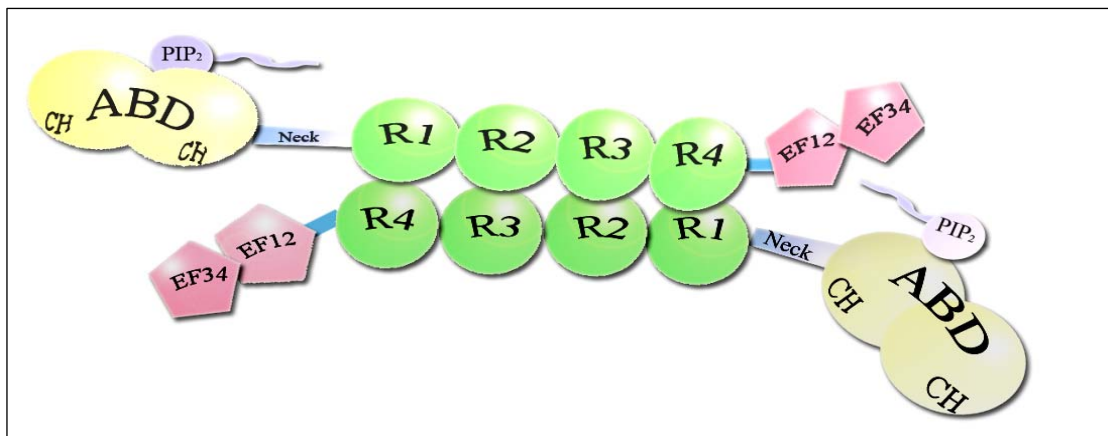


Fig. 6 Change of the uninduced into an induced conformation of the alpha-actinin dimer upon binding of PIP₂. The CaM-domain is now free to bind to distinct interaction partners like the Zr7 repeat of titin.

The CaM domain at the C-terminal of alpha-actinin consists of two pairs of EF hands. EF hands are helix-loop-helix motifs, involved in many different protein-protein interactions and the regulation of cellular processes (Branden C 1999). Usually, pairs of EF-hands form globular domains which have the ability to coordinate up to two calcium ions. Upon binding of calcium ions a conformational change is triggered, whereby proteins showing this motif exist in two different states: an “open” and a “closed” (Ikura 1996). In the open conformation, a hydrophobic region is exposed to the surface which allows binding to designated targets. The two pairs of EF-hands of alpha-actinin of muscle cells diverge, since they show a mutation which made them loose their ability of calcium coordination (Atkinson, Joseph et al. 2001) [Fig. 7].

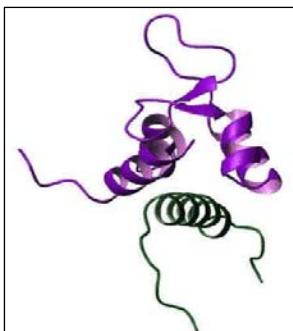


Fig. 7 Structure of EF34 of alpha-actinin 2 bound to Zr7 of titin solved by NMR (Atkinson, Joseph et al. 2001).

The conclusion is therefore, that very similar progressions take place in the several isoforms, resulting always in the two possible states. Nevertheless, the way of triggering and changing this state is very different and isoform specific.

The structure of the alpha-actinin rod domain forming a dimer has already been solved (Djinovic-Carugo 2001; Ylanne, Scheffzek et al. 2001), as well as EF34 in complex with Zr7 of titin (Atkinson, Joseph et al. 2001). Sequence alignment of alpha-actinin and titin shows basically no similarity, but titin Zr7 and the neck of alpha-actinin bind with comparable affinity to the CaM-domain. Therefore it is proposed that the C-terminal of alpha-actinin shows high plasticity, facilitating interaction of CaM either with the neck or with Zr7 of titin.

The following list gives a short overview over the various isoforms of alpha-actinin and their physiological relevance.

1.2 Isoforms of alpha-actinin

1.2.1 Alpha-actinin-1

Non-muscle actinin-1 has been reported to associate with cell adhesion molecules, such as integrin *b1* and *a*-catenin, and is believed to play an important role in stabilizing cell adhesion and regulating cell shape and cell motility. It is found in focal adhesion plaques and adherens junctions (Honda, Yamada et al. 1998). As described above, the active state is triggered by binding of calcium to EF-hands.

1.2.2 Alpha-actinin-2

Alpha-actinin-2 is expressed in all muscle fibers and due to its more general function its expression in human skeletal muscle completely overlaps alpha-actinin-3. These two isoforms (2 and 3) are 80% identical and 90% similar (Beggs, Byers et al. 1992). In addition, alpha-actinin-2 and alpha-actinin-3 form heterodimers *in vitro* and *in vivo*, suggesting structural similarity and lack of significant functional differences between the two skeletal muscle alpha-actinin isoforms (Chan Y. M et al., 1998). Upon binding of PiP_2 to ABD the conformational change into the active state is triggered.

1.2.3 Alpha-actinin-3

Loss of alpha-actinin-3 gene function alters mouse muscle metabolism and shows evidence of positive selection in humans. A deficiency in alpha-actinin-3 in humans is associated with elite athlete status. By virtue of a knockout mouse model it is proposed that this is due to a shift in muscle metabolism toward the more efficient aerobic pathway and an increase in intrinsic endurance performance (Macarthur, Seto et al. 2007). Since we are dealing here again with a muscle-isoform, it is PiP_2 - sensitive, as described above.

1.2.4 Alpha-actinin-4

The regulation of the actin cytoskeleton plays an essential role in cell motility and cancer invasion. Alpha-actinin 4 exhibits tumor suppressor activity. Stable clones containing increased levels of alpha-actinin, isolated from highly malignant neuroblastoma stem after transfection with a full-length alpha-actinin-4 cDNA, show decreased anchorage-independent growth ability, loss of tumorigenicity in nude mice, and decreased expression of the N-myc proto-oncogene (Nikolopoulos, Spengler et al. 2000).

Alpha-actinin-4 is located in the cytoplasm of non muscle cells where cells are sharply extended and migrating. It is absent in focal adhesion plaques and adherent junctions (Honda, Yamada et al. 1998). As described above, this isoform is calcium-sensitive.

Some atypical alpha-actinins were found in early diverging organisms, such as protozoa and yeast (Virel and Backman 2006; Virel, Addario et al. 2007). In these organisms the rod domain consists of one or two spectrin repeats, respectively. This implies that the four spectrin repeats, found in the modern alpha-actinin homodimer, arose from two consecutive intragenic duplications from an ancestral alpha-actinin with a single repeat. The four human isoforms are encoded in at least four distinct genes.

1.3 The Alpha-actinin Interactome

The numerous proteins which interact with alpha-actinin complicate the understanding of alpha-actinin–actin interactions [Fig.8]. These are among others the β -integrins (Otey, Pavalko et al. 1990), vinculin (Wachsstock, Wilkins et al. 1987) intercellular adhesion molecule (ICAM)(Heiska, Kantor et al. 1996), titin (Ohtsuka, Yajima et al. 1997);

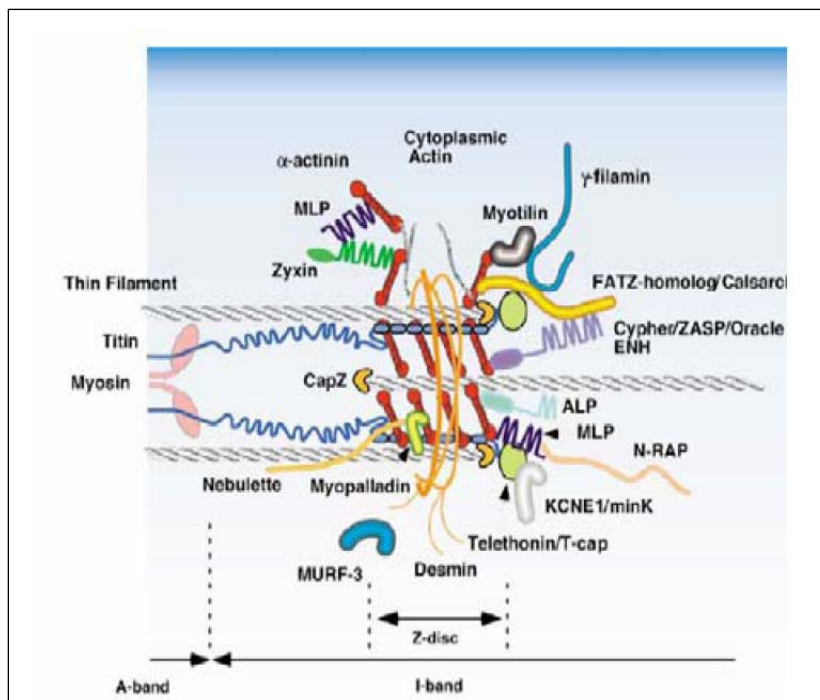


Fig. 8: Alpha-actinin (red) and its role in the sarcomeric Z-disk in concert with its interaction partners in a myocardial cell (from: Norbert Frey – Ruprecht Karls University, University Hospital, Heidelberg

(Sorimachi, Freiburg et al. 1997)), zyxin (Crawford, Michelsen et al. 1992), CLP-36 PDZ-LIM (Vallenius, Luukko et al. 2000), Cysteine-rich protein (Yao, Perez-Alvarado et al. 1999) and nebulin (Nave, Furst et al. 1990).

These proteins, which bind to different

domains of alpha-actinin, may affect its interaction with actin in ways not yet understood. The huge number of interaction partners of alpha-actinin can mainly be divided into three groups: cytoskeletal proteins, signaling proteins and membrane proteins.

The following list shall give a short overview over the interaction partners, emphasizing the cytoskeletal proteins.

1.3.1 Actin

Actin is one of the most conserved proteins in eukaryotic cells; it is the monomeric subunit of microfilaments; its importance in cellular processes ranges from cell motility to muscle contraction (McGough, Way et al. 1994). Actin binding sites are found in alpha-actinin isoforms 1 and 2 at the CH1 domain in the C- and the N-terminal helices, whereas isoform 3 binds actin via the N-terminal helix and the linker part of CH2 (Gimona and Mital 1998). Results indicate that residues 86-117 and 350-375 comprise distinct binding sites for alpha-actinin on adjacent actin monomers (McGough, Way et al. 1994).

1.3.2 FATZ

FATZ stands for filamin-, actinin-, and telethonin-binding protein of the Z-disc of skeletal muscle. From yeast two hybrid experiments it was shown that the spectrin like repeats of alpha-actinin 2 are required to bind the C-terminal region of the FATZ as does gamma-filamin *via* its immunoglobulin-like domain 23 (Faulkner, Pallavicini et al. 2000).

1.3.3 Myopalladin

Myopalladin is a sarcomeric protein with multiple roles in Z-disc and I-band protein assemblies; tethers together the COOH-terminal Src homology 3 domains of nebulin and nebulin with the EF hand motifs of alpha-actinin in vertebrate Z-lines (Bang, Mudry et al. 2001).

1.3.4 Titin

Titin, also known as connectin, is a giant protein connecting muscle fibers within the sarcomere. Single titin molecules emanate from the Z-disk, where their N-terminal is located, and range to the center of the sarcomere in the M-line. Thus both ends of the protein are anchored to the muscle fiber. It is thought that titin plays an essential role in muscle assembly and is implicated in muscle elasticity by conferring passive resistance of the sarcomere to stretching. Z-repeats are localized in the sarcomere Z-disk near the N-terminus of titin and in humans their number varies in different tissues. The N-terminal

Z-repeat 7 of titin binds to EF3/4 of alpha-actinin (Young and Gautel 2000); an additional binding site was described involving the region of titin directly adjacent to the last Z-repeat and the two central spectrin repeats of alpha-actinin (Young, Ferguson et al. 1998).

1.3.5 Nebulin

Nebulin is an actin-binding protein anchored in the sarcomeric Z-disk via its C-terminal end and protrudes into I- and A-band in skeletal muscle wrapped around thin filaments; it is believed to regulate the length of thin filaments during sarcomere assembly (McElhinny, Kazmierski et al. 2003).

1.3.6 Vinculin

Vinculin is a membrane-associated cytoskeletal protein in focal adhesion plaques that is involved in linkage of integrin adhesion molecules to the actin cytoskeleton (Wachsstock, Wilkins et al. 1987).

1.3.7 ZASP

Z-band alternatively spliced PDZ protein; the PDZ domain binds to EF34 of alpha-actinin simultaneously with Zr7-repeat of titin (Faulkner, Pallavicini et al. 1999; Au, Atkinson et al. 2004).

1.3.8 Myotilin

Myotilin is a myofibrillar protein which resides both in the sarcomere, where it localizes within the Z-disk and is bound to spectrin-like repeats of alpha-actinin, as well as along the sarcolemmal membrane. Myotilin contains two C2-type Ig-like domains with considerable homology to certain Ig domains of titin (Salmikangas, Mykkanen et al. 1999).

1.3.9 CRP

CRP is a cysteine-rich protein with a LIM domain, which is involved in muscle differentiation. CRP1 and alpha-actinin are colocalized along the actin stress fibers of cation exchange fibers and smooth muscle cells; the N-terminal moiety of CRP interacts with actin binding domain of alpha-actinin (Pomies, Louis et al. 1997).

1.3.10 Integrin β 1

Integrins are adhesion proteins which built a linkage to the cytoskeleton;

Alpha-actinin binds to the cytoplasmic domain of the beta 1 subunit of integrin, suggesting that alpha-actinin may form a direct link between the actin cytoskeleton and the transmembrane fibronectin receptor (Otey, Pavalko et al. 1990).

1.3.11 ALP

ALP contains an N-terminal PDZ domain and a C-terminal LIM motif; it occurs in association with alpha-actinin-2 at the Z lines of myofibers.

The PDZ domain of ALP binds to the C-terminal region of alpha-actinin-2 (Xia, Winokur et al. 1997).

This list is not exhaustive, but should give an overview over the manifold processes and interactions alpha-actinin is involved in.

1.4 The objectives of this study

The aim of this work was to investigate and verify the current model of the change of the alpha-actinin homodimer from a closed, uninduced state to an open, active state. The following outlines the attempts to solve the described issue.

- (1) Establishment of an expression and purification protocol for wild type proteins EF34, CaM and ABD-R1.
- (2) Complex formation with the wild type EF34 protein with a synthesized peptide of the neck, its analysis and crystallization.
- (3) Complex formation of wild type EF34 or CaM proteins, respectively, with ABD-R1 and its analysis.
- (4) Creation of mutants of EF34 with an incorporated artificial amino acid residue at putative interaction sites, which enables photo cross-linking of mutated EF34 with the neck and its subsequent crystallization.

2.0 Materials

2.1 Media

LB-Media (sigma)

SOB Media (sigma)

GMMML Media

1 % glycerol	900 ml
10 x M9 salts	100 ml
1 M MgSO ₄	1 ml
1 M CaCl ₂	100 µl
5 M NaCl	1,7 ml
0.3 M leucine, dissolved in 100 mM LiOH	1 ml
Biotin	1 mg
1 % Thiamine	100 µl

Autoinduction Media:

(Dubendorff and Studier 1991)

Ingredients for 1L Autoinduction media	
ZY	928 ml
1M MgSO ₄	1 ml
1000 x metal mix	1 ml
50 x 5052	20 ml
20 x NPS	50 ml

Antibiotics as needed:

Kanamycin (100 mg / ml)	1 ml
Chloramphenicol (25 mg/ml)	1 ml
Ampicillin (50 mg / ml)	1 ml

ZY	
Tryptone	10 g
Yeast extract	5 g

20 x NPS (1 L)	
(NH ₄) ₂ SO ₄	66 g (0.5M)
(KH ₂ PO ₄	136 g (1M)
Na ₂ HPO ₄	142 g (1M)
H ₂ O	900ml
Add in sequence in beaker, stir until dissolved, pH should be ~ 6.75, autoclave	

50 x 5052 (1 L)	
Glycerol	250 g
H ₂ O	730 ml
Glucose	25 g
Lactose	100 g
Add in sequence in beaker, stir until dissolved, autoclave	

1000 x trace metals mixture (100ml)	
0.1 M FeCl ₃ – 6 H ₂ O, dissolved in 0.1 M HCL	50 ml
1 M CaCl ₂	2 ml
1 M MnCl ₂	1 ml
1 M ZnSO ₄	1 ml
0.2 M CoCl ₂	1 ml
0.1 M CuCl ₂	2 ml
0.2 M NiCl ₂	1 ml
0.1 M Na ₂ MoO ₄	2 ml
0.1 M Na ₂ SeO ₃	2 ml
0.1 M H ₃ BO ₃	2 ml
Autoclave stock solutions except FeCl ₃	

2.2 *E.coli* Cell Strains

Cell Strains	Genotype	Description
DH5 α	supE44 Δ U169 deoR (f80lacZAM15)hsdR17 recA1 endA1 gyrA96 thi-1 relA1	High copy plasmid cell line
XL1-blue	<i>recA1, lac-, endA1, gyrA96,</i> <i>thi, hsdR17 (rk-, mk+),</i> <i>supE44, relA1, λ-, [F',</i> <i>proAB, lacIqZ, ΔM15, Tn10</i> <i>(tetr)</i>	
BL21 (DE3)	F- ompT hsdSB (rb- mB-) gal dcm (DE3)	The (DE3) cells carry a chromosomal copy of the T7 RNA polymerase gene under control of the lacUV5 promoter. This strain is used for protein expression of pET vectors.
Rosetta (DE3)	F- ompT hsdSB (rb- mB-) gal dcm lacY1 (DE3)	This strain is derived from the Tuner cell and is used to enhance the expression of

	pRARE6 (CmR)	eukaryotic proteins that contain rare codons. This is accomplished by supply tRNAs for AGG, AGA, AUA, CUA, CCC, GGA codons on a compatible chloramphenicol-resistant plasmid.
Rosetta (DE3) pLysS	F ⁻ ompT hsdSB (rb ⁻ mB ⁻) gal dcm lacY1 (DE3) pRARE6 pLysE (CmR)	Same as above but has an additional vector transformed that produce a larger amount of T7 lysozyme than that of pLysS. In Rosetta(DE3)pLysE the rare tRNA genes are carried on the same plasmids that carry the T7 lysozyme.
C41 (DE3)		derived from BL21(DE3)
BL21* (DE3)	F ⁻ ompT hsdS _B (r _B ⁻ m _B ⁻) gal dcm rne131 (DE3)	
BL 21 (DE3) pLysS	Genotype: F ⁻ ompT hsdSB (rb ⁻ mB ⁻) gal dcm (DE3) pLysE (CmR)	Same as above but has an additional vector transformed that produce a small amount of T7 lysozyme that is used to suppress basal expression of T7 RNA polymerase prior to induction and thus reduces leaky expression.

2.3 Plasmids

Plasmid	Resistance	ORI	Cloned By	Tags	Cleavage site
pETM 20	Ampicillin	pBR322	G. Stier	N-His C-His	TEV
pETM 13	Kanamycin	pBR322	G. Stier	C-His	TEV
pETM 30	Kanamycin	pBR322	G. Stier	N-His N-GST C-His	TEV

2.4 Buffer for molecular biology techniques

TAE Buffer	
Tris-Acetate	40 mM
EDTA	1mM
Eisessig	Add to pH 8.0

Loading dye (6x) Agarosegel	
Bromphenol-blue	0.25 % (w/v)
Saccharose	40 % (w/v)

2.5 Buffers for Affinity Chromatography

Binding and Wash Buffer	
Tris -HCl	100 mM pH 8
NaCl	150 mM
Imidazole	10 mM

Elution Buffer	
Tris-HCl	100 mM pH 8
NaCl	150 mM
Imidazole	300 mM

2.6 Buffer for Size Exclusion Chromatography

Gelfiltration Buffer	
Tris-HCl	20 mM pH 8
NaCl	200 mM
2-mercaptoethanol	2 mM

2.7 Buffer for TEV Cleavage

TEV Cleavage Buffer	
Tris-HCl	50 mM pH 8
EDTA	0.25 mM
2-mercaptoethanol	2 mM

2.8 Buffers for TEV Purification

TEV Lysis and Wash Buffer I	
Tris - HCl	20 mM pH 8
Imidazole	10 mM pH 8
NaCl	150 mM
2-mercaptoethanol	2 mM

TEV Wash Buffer II	
Tris - HCl	20 mM pH 8
Imidazole	10 mM pH 8
NaCl	1 M
2-mercaptoethanol	2 mM

TEV Wash Buffer III	
Tris - HCl	20 mM pH 8
Imidazole	50 mM pH 8
NaCl	150 mM
2-mercaptoethanol	2 mM

TEV Elutionbuffer	
Tris - HCl	20 mM pH 8
Imidazole	330 mM pH 8
NaCl	150 mM
2-mercaptoethanol	2 mM

2.9 Electrophoresis Buffer

50 x TAE- Buffer	
Tris	2 M
EDTA-Na	0.05 M
Acetic Acid	1 M
pH 8.5	

SDS – Sample Buffer (5 x)	
Tris pH 6.8	255 mM
EDTA	12.5 mM
SDS	5 %
2-mercaptoethanol	700 mM
Glycerol	50 %
Bromphenolblue	0,35 %

Coomassie Stain	
Methanol	50 %
Acetic acid	10 %
Coomassie blue R250	0.25 %

Destaining Solution	
Ethanol	30 %
Acetic acid	10 %
H ₂ O distilled	60 %

2.10 Buffers for Tricine SDS PAGE

10x Anode Buffer pH 8.9	
Tris pH 8	1 M
HCl	225 mM

10x Cathode Buffer ~ pH 8,25 (pH must not be adjusted)	
Tris pH 8	1 M
Tricine	1 M
SDS	1 %

3x Gel Buffer pH 8.45	
Tris	3 M
HCl	1 M
SDS	0.3 %

2.11 Buffers for Western Blotting

10x Transfer Buffer	
Glycine	29 g
Tris	58 g
SDS	3.7 g

TBPS Buffer (pH must not be adjusted)	
Tris	3 g
NaCl	8 g
KCl	0.2 g

Color-development Buffer	
Tris-HCl pH 9.5	100 mM
NaCl	100 mM
MgCl ₂	3.7 g
5% Nitro Blue Tetrazolium in dimethylformamid	100 µl
5% 5-bromo-4-chloro-3-indolyl-phosphate in dimethylformamid	100 µl

2.12 Buffers for On-Column Binding Studies

Binding Buffer for Ni-on column binding	
K ₂ HPO ₄ /KH ₂ PO ₄ pH 8	50 mM
NaCl	50 mM
Imidazole	5 mM
2-mercaptoethanol	20 mM

Elution Buffer for Ni-on column binding	
K ₂ HPO ₄ /KH ₂ PO ₄ pH 8	50 mM
NaCl	50 mM
Imidazole	300 mM
2-mercaptoethanol	20 mM

2.13 Refolding Buffers

Wash Buffer	
Urea	4 M
NaCl	0.5 M
EDTA	1 mM
Tris-HCl pH 8	50 mM

Solubilization Buffer	
Guanidine-HCl	6 M
DDT	10 mM
Tris-HCl pH 8	50 mM

Buffer 1	
50 mM MES pH 6.0, 9.6 mM NaCl, 0.4 mM KCl, 2 mM MgCl ₂ , 2 mM CaCl ₂ , 0.75 M Guanidine HCl, 0.5% Triton X-100, 1 mM DTT	
Buffer 2	

50 mM MES pH 6.0, 9.6 mM NaCl, 0.4 mM KCl, 2 mM MgCl ₂ , 2 mM CaCl ₂ , 0.5 M arginine, 0.05% polyethylene glycol 3550, 1 mM GSH, 0.1 mM GSSH
Buffer 3
50 mM MES pH 6.0, 9.6 mM NaCl, 0.4 mM KCl, 1 mM EDTA, 0.4 M sucrose, 0.75 M Guanidine HCl, 0.5% Triton X-100, 0.05% polyethylene glycol 3550, 1 mM DTT
Buffer 4
50 mM MES pH 6.0, 240 mM NaCl, 10 mM KCl, 2 mM MgCl ₂ , 2 mM CaCl ₂ , 0.5 M arginine, 0.5% Triton X-100, 1 mM GSH, 0.1 mM GSSH
Buffer 5
50 mM MES pH 6.0, 240 mM NaCl, 10 mM KCl, 1 mM EDTA, 0.4 M sucrose, 0.75 M Guanidine HC, 1 mM DTT
Buffer 6
50 mM MES pH 6.0, 240 mM NaCl, 10 mM KCl, 1 mM EDTA, 0.5 M arginine, 0.4 M sucrose, 0.5% Triton X-100, 0.05% polyethylene glycol 3550, 1 mM GSH, 0.1 mM GSSH
Buffer 7
50 mM MES pH 6.0, 240 mM NaCl, 10 mM KCl, 2 mM MgCl ₂ , 2 mM CaCl ₂ , 0.75 M Guanidine HCl, 0.05% polyethylene glycol 3550, 1 mM DTT
Buffer 8
50 mM Tris-Cl pH 8.5, 9.6 mM NaCl, 0.4 mM KCl, 2 mM MgCl ₂ , 2 mM CaCl ₂ , 0.4 M sucrose, 0.5% Triton X-100, 0.05% polyethylene glycol 3550, 1 mM GSH, 0.1 mM GSSH
Buffer 9
50 mM Tris-Cl pH 8.5, 9.6 mM NaCl, 0.4 mM KCl, 1 mM EDTA, 0.5 M arginine, 0.75 M Guanidine HCl, 0.05% polyethylene glycol 3550, 1 mM DTT
Buffer 10
50 mM Tris-Cl pH 8.5, 9.6 mM NaCl, 0.4 mM KCl, 2 mM MgCl ₂ , 2 mM CaCl ₂ , 0.5 M arginine, 0.4 M sucrose, 0.75 M Guanidine HCl, 1 mM GSH, 0.1 mM GSSH
Buffer 11
50 mM Tris-Cl pH 8.5, 9.6 mM NaCl, 0.4 mM KCl, 1 mM EDTA, 0.5% Triton X-100, 1 mM DTT
Buffer 12
50 mM Tris-Cl pH 8.5, 240 mM NaCl, 10 mM KCl, 1 mM EDTA, 0.05% polyethylene glycol 3,550, 1 mM GSH, 0.1 mM GSSH
Buffer 13
50 mM Tris-Cl pH 8.5, 240 mM NaCl, 10 mM KCl, 1 mM EDTA, 0.5 M arginine, 0.75 M Guanidine HCl, 0.5% Triton X-100, 1 mM DTT
Buffer 14
50 mM Tris-Cl pH 8.5, 240 mM NaCl, 10 mM KCl, 2 mM MgCl ₂ , 2 mM CaCl ₂ , 0.5 M arginine, 0.4 M sucrose, 0.75 M Guanidine HCl, 0.5% Triton X-100, 0.05% polyethylene glycol 3,550, 1 mM GSH, 0.1 mM GSSH
Buffer 15
50 mM Tris-Cl pH 8.5, 240 mM NaCl, 10 mM KCl, 2 mM MgCl ₂ , 2 mM CaCl ₂ , 0.4 M sucrose, 1 mM DTT

DTT
Dissolve contents of vial in 1 ml of deionized water. Store at 4°C.
Glutathione reduced
Dissolve contents of vial in 1 ml of deionized water. Store at -20°C.
Glutathione oxidized
Dissolve contents of vial in 1 ml of deionized water. Store at -20°C.

Buffer Preparation:

Before using the Buffers add 1 ml DTT, GSH or GSSH solutions to 950 ml of the respective buffer as follows:

DTT Solution: Buffers #1, 3, 5, 7, 9, 11, 13, and 15

GSH Solution: Buffers #2, 4, 6, 8, 10, 12, and 14

GSSH Solution: Buffers #2, 4, 6, 8, 10, 12, and 14

2.14 Crystallization Screens

JCSG (Quiagen)
PACT HT96 (molecular dimensions limited)
Wizard I+II (Emerald BioStructrures)
Grid Screen MPD (Hampton research)
JBScreen 9+10 (Hampton Research)

3.0 Methods

3.1 Molecular Biology Techniques

3.1.1 Constructs

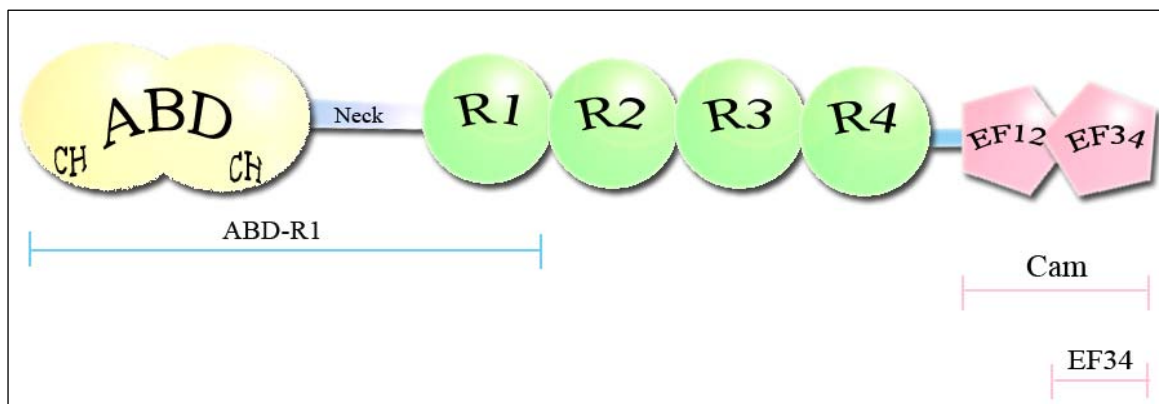


Fig. 9 Scheme of the used constructs of alpha-actinin

Constructs used for this study:

ABD-R1	composed of actin-binding domain, the neck and spectrin repeat R1
CaM	Calmoduline-like C-terminal domain (two pairs of EF hands)
EF34	One pair of EF-hands, which have been found to be sufficient to bind the neck.
Neck	synthesized peptide of the neck (15 residues) plus additional amino acids of the rod domain, resulting in a 28 amino acid peptide(purchased from invitrogen)

MNQIEPGVQYNYVYDEDEYMIQEEEWDRDLLLDPAWEKQQRKTFTAWCNSHLRKAGTQIE
 NIEEDFRNGLKMLLLEVISGERLPKPDRGKMRFHKIANVNKALDYIASKGVKLVSIGAE
 EIVDGNVKMTLGMIIWTIILRFAIQDISVEETSAKEGLLLWCQRKTAPYRNVNIQNFTSW
 KDGLGLCALIHRHRPDLIDYSKLNKDDPIGNINLAMEIAEKHLDIPKMLDAEDIVNTPKP
 DERAIMTYVSCFYHAFAGAEQAETAANRICKVLAVNQENERLMEEYERLASELLEWIRRT
 IPWLENRTPEKTMQAMQKKLEDFRDYRRKHKPKVQEKQLEINFNTLQTKLRISNRPAF
 MPSEGMVSDIAGAWQRLEQAEGYEEWLLNEIRRERLEHLAEKFRQKASTHETWAYGK
 EQILLQKDYESASLTEVRALLRKHEAFESDLAAHQDRVEQIAAIAQELNELDYHDAVNVN
 DRCQKICDQWDRLGTLTQKRREALERMEKLLLETIDQLHLEFAKRAAPFNNWMEGAMEDLQ
 DMFIVHSIEEIQSLITAHEQFKATLPEADGERQSIMAIQNEVEKVIQSYNIRISSNPYS
 TVTMDLRTKWDKVKQLVPIRDQSLQEELARQHANERLRRQFAAQANAIGPWIQNKMEEI
 ARSSIQITGALEDQMNQLKQYEHNIINYKNNIDKLEGDHQLIQEALVFDNKHTNYTMEHI
 RVGWELLTTIARTINEVETQILTRDAKGI TQEQMNEFRASFNHFDRRKNGLMDHEDFRA
 CLISMGYDLGEAEFARIMTLVDPNGQGTVTTFQSFIDFMTRETADTDTAEQVIASFRILAS
 DKPYILAEELRRELPPDQAQYCIKMPAYSGPGSVPGALDYAAFSSALYGESDL

Fig. 10 Amino acid sequence of alpha-actinin2 with the sequences used in this study as fusion proteins highlighted.

CaM= *rosé* and *violet* (two pairs of EF hands)

EF34 = *violet* (one pair of EF hands)

Neck (peptide) = *blue*

3.1.2 Primer Design

Primer with specific overhangs which would introduce the needed restriction sites to the PCR product was designed. When a restriction enzyme is used to cut the very end of a DNA fragment one needs to provide the restriction enzymes additional so called buffer bases to ensure high restriction efficiency. To guarantee the protein is still translated in frame and the ATG in the forward primer is readable two bases were introduced resulting in an additional glycine. Because glycine is a small amino acid which should not influence any regulatory processes, we expected this mutation to have no effect at all. Via GC-rich regions at the 3'-end of the primer and the correlated higher binding affinity due to three hydrogen bonds instead of two which are found between an AT base pair, one ensures a high specific and affine binding of the primer to the template.

$$(A+T)*2 + (G+C)*4 \sim TM$$

The calculated annealing temperature for both was 66 °C. One should avoid annealing temperatures below 55 °C to prevent unspecific annealing as well as above 70 °C, otherwise annealing will be insufficient.

Primers were checked with software available at www.premierbiosoft.com/netprimer/netlaunch/netprlaunch.html to determine their likeliness to form dimers or hairpins.

The primers designed for the mutant studies are listed below.

Primers used for mutant constructs:

9 Q : 5'GACACCGACACTGCCGAGTAGGTCATCGCC 3' 3'CTGTGGCTGTGACGGCTCATCCAGTAGCGG 5'
13 S : 5'CAGGTCATCGCCTAGTTCCGGATCC 3' 3'GTCCAGTAGCGGATCAAGGCCTAGG 5'
40 Y : 5' GGATCAGGCCCAGTAGTGCATCAAGAGG 3' 3' CCTAGTCCGGGTCATCACGTAGTTCTCC 5'
68 Y: 5' GTTCTCTTCCGCACTCTAGGGGGAGAG 3' 3' CAAGAGAAGGCGTGAGATCCCCCTCTC 5'
70 E: 5' GCACTCTACGGGTAGAGCGATCTG 3' 3' CGTGAGATGCCCATCTCGCTAGAC 5'

3.1.3 Standard PCR mixture

1 µl template	1-50 ng
2 µl 10X Taq Pol KCl Buffer	(fermentas)

2 µl dNTP mix	2 mM (fermentas)
1 µl MgCl ₂	25mM (fermentas)
0.5 µl reverse primer	10 pM (sigma)
0.5 µl forward primer	10 pM (sigma)
0.2 µl Taq Polymerase	1u/µl (fermentas)
Add dH ₂ O up to 20 µl final volume	

If necessary, Taq Pol KCl Buffer was exchanged to Taq Pol (NH₂)₄SO₄ buffer, which has a higher MgCl₂ tolerance, to vary the concentration of the latter. For the first trials gradient PCRs were done, to examine the ideal annealing temperature for each primer.

3.1.4 Standard PCR Program

94 °C	00:04:00
94 °C	00:00:30
55 – 65 °C	00:00:30
72 °C	00:01:00
24 cycles	Step 2 to 4
72 °C	00:05:00
4 °C	hold

3.1.5 Mutagenesis PCR mixture

1 µl template	1-10 ng
5 µl 10x Herculase reaction buffer	(stratagene)
1 µl dNTP mix	20 mM (fermentas)
1 µl reverse primer	10 pM (sigma)
1 µl forward primer	10 pM (sigma)

0.5 µl Herculase Polymerase	5U/ µl (stratagene)
Add dH ₂ O up to 50 µl final volume	

3.1.6 Vector amplifying mutagenesis PCR

95 °C	00:03:00
94 °C	00:00:30
60 °C	00:00:30
72 °C	00:09:00
24 cycles	Step 2 to 4
72 °C	00:12:00
4 °C	hold

Directly after PCR 1 µl DpnI was added and incubated 1 h at 37 °C. DpnI cleaves methylated DNA. By this procedure one gets rid of only the template DNA, since the newly synthesized fragments are not methylated, yet. By this methodology nicked, mutated vectors were obtained, which were directly transformed into *E. coli*, where the nick is ligated by the bacterial repair mechanisms.

3.1.7 Two Step mutagenesis method (Young and Dong 2004)

This methodology combines a dual asymmetrical PCR (DA-PCR) (these two reactions were carried out separately) and an overhang extension. For the DA-PCR external T7

primer together with internal primer coding for the mutation were used.

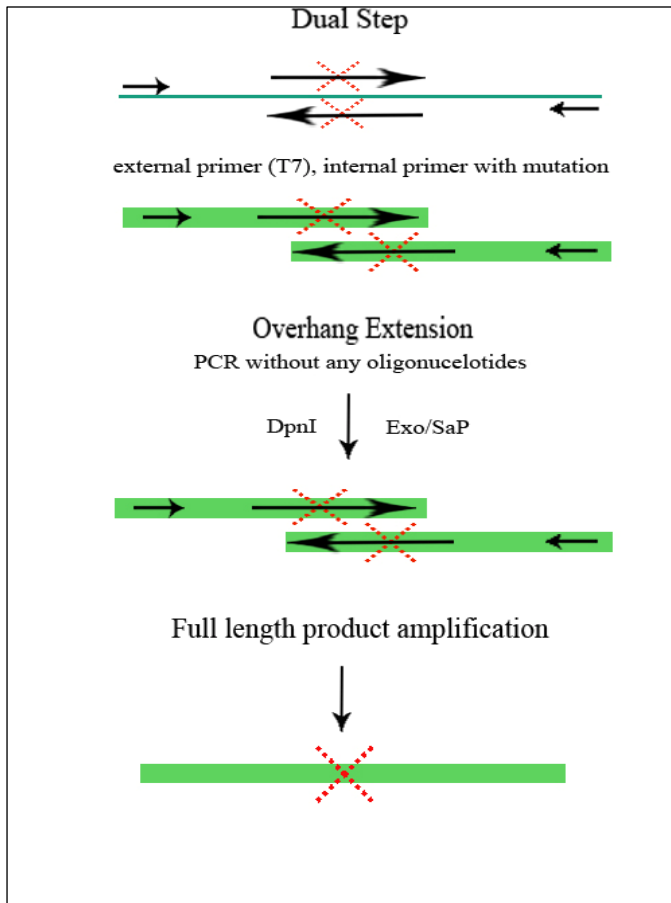


Fig. 11 Two step mutagenesis method

The DA-PCR products were incubated with DpnI to remove methylated DNA, the template. ExonucleaseI and Shrimp Alkaline Phosphatase were used to digest the residual oligo-nucleotides and to dephosphorylate remaining dNTPs. For the overhang extension equal amounts of DA-PCR product were

mixed. The crude overhang extension was amplified by PCR using the two external primers. The full length PCR product was digested with KpnI and NcoI and ligated into restricted pETM30.

Stratagene QuickChange Mutagenesis Kit was also used to produce mutants.

Protocol and procedure was done like in the manual of the kit recommended. The polymerase provided with the kit was substituted with Herculanase Polymerase.

3.1.8 Restriction and Ligation Enzymes (purchased from New England Biolabs and fermentas)

Acc65I	$ \begin{array}{c} 5' \dots \text{GGTACC} \dots 3' \\ 3' \dots \text{CCATGG} \dots 5' \end{array} $
BsaI	$ \begin{array}{c} 5' \dots \text{GGTCTC (N)}_1 \dots 3' \\ 3' \dots \text{CCAGAG (N)}_5 \dots 5' \end{array} $
KpnI	$ \begin{array}{c} 5' \dots \text{GGTACC} \dots 3' \\ 3' \dots \text{CCATGG} \dots 5' \end{array} $
NcoI	$ \begin{array}{c} 5' \dots \text{CCATGG} \dots 3' \\ 3' \dots \text{GGTACC} \dots 5' \end{array} $
DpnI	$ \begin{array}{c} \text{CH}_3 \\ \\ 5' \dots \text{GATC} \dots 3' \\ 3' \dots \text{CTAG} \dots 5' \\ \\ \text{CH}_3 \end{array} $

Classical Restriction Enzyme Reaction Conditions (enzymes and reagents purchased from fermentas)

20 µl PCR product or plasmid (100 -200 ng)	1-10 ng
1 µl restriction enzyme	
3 µl adequate buffer	
6 µl dH2O	

Restrictions were incubated for one hour at adequate temperature and in provided buffer for the corresponding enzyme (purchased for fermentas and New England Biolabs, respectively).

If a double digest was not possible, after each restriction the mixture was purified with PCR- Purification Kit (Quiagen) and eluted in 25 µl dH2O. The same was done before ligation. To check the DNA content the absorbance at 280 nm was measured and verified on a 0.8 % agarose gel.

For a 0.8 % agarose gel the following protocol was used.

0.16 g Agarose
20 ml 1x TAE buffer
2 μ l ethidium bromide

Sample preparation

1 μ l PCR product
1 μ l 6x Loading Dye
4 μ l dH ₂ O

To estimate the size a 1kbp Marker (Fermentas; O'Gene Ruler 1kbp DNA Ladder ready-to use) was used.

The gel was run at 90-100 Volts.

Fast Digest Restriction Enzyme Conditions (enzymes and reagents purchased from fermentas)

10 μ l PCR product or plasmid (100 -200 ng)	1-10 ng
1 μ l restriction enzyme	10U/ μ l
2 μ l adequate buffer	
17 μ l dH ₂ O	

The digests were performed at 37 °C for 5 min.

Standard Ligation Conditions (fermentas)

Vector : fragment ratio; Total volume 6 µl	1:2 to 1:8 (vector : 10-100 ng)
1 µl T4 ligase	5 Weiss U/ µl
1 µl buffer suppl. with 10 mM ATP	
2 µl dH ₂ O	

The ligation reaction was incubated at 16 °C over night and inactivated at 65 °C for 10 min if necessary.

Fast Ligation Conditions (fermentas)

Vector : fragment ratio; Total volume 6 µl	1:2 to 1:8 (vector : 10-100 ng)
1 µl T4 ligase	
4 µl 5x Rapid Ligation Buffer	
4 µl dH ₂ O	

The ligation reaction was incubated at 22 °C for 5 min and inactivated at 65 °C for 10 min if necessary. 2-5 µl of ligation mixture were used for transformation.

All plasmids were constructed in *E.coli* strains DH5α and XL1-blue. Plasmids were recovered by DNA extraction with fermentas MiniPrep kit.

3.1.9 Transformation of competent cells

Competent cells were transformed by heat shock transformation.

For the standard protocol 1 µl of plasmid (conc. 150 to 200 ng/ml) was incubated 30 minutes on ice with 50 µl competent cells. After incubation a 90 seconds heat shock was performed, followed by another 2 minutes on ice. 500 µl LB Media were added and incubated for 1 h at 37 °C. If needed 0.5 µl 40 % PEG8000 was added to transformation mix to increase efficiency. Depending on the transformation efficiency obtained either 120 µl were plated on agar PDs or the whole incubation mixture was spun down, 400 µl were discarded and the pellet was re-suspended in the remaining media and plated. Agar plates were incubated over night at 37 °C.

For the modified protocol to transform the mutated constructs the whole PCR mixture was reduced with speed vac to approximately 3 µl for transformation. SOC Media was used for 1 h incubation at 37 °C.

Cloning was verified by colony PCR and sequencing (carried out by VBC Genomics)

3.1.10 Colony PCR

Colony was picked from agar plate and re-suspended in 100 µl dH₂O. If necessary, colony was re-plated before picking.

Solution was incubated for 5 min at 100 °C and spun down for 5 min at 3000 rpm. 1 µl supernatant was used as template together with primers used prior for cloning.

3.2 Expression and Purification

3.2.1 Expression Screen Protocol

Plasmids and *E.coli* strains as listed in section 23345345 were used to test for the optimal expression conditions for each protein.

Protocol:

- Add into 24 well plate (optional: 96 well plate) per well 50 μ l cells (various cell lines) + 2 μ l DNA
- Mix
- Incubate for 30 min on ice
- Heat shock by floating on 42 °C water bath for 90 seconds
- Incubate samples for 5 min on ice
- Add 1 ml of Auto Induction media, add antibiotics after 1 h, incubate at 37 °C over night
- Check visually for culture growth
- Test for expression by loading culture on a SDS gel (take 3 μ l culture and dilute by adding 12 μ l water and 5 μ l 4x SDS loading dye

Protein expression was analyzed by Coomassie stain or western blot

Three 24 well plates were used at temperatures 20, 30 and 37 °C to determine the best expression conditions.

Testing soluble/insoluble fraction:

- After 16 h growth at 37 °C (temperature can be individually chosen) spin down cells (multiwell plates sealed with oxygen permeable tape)
- Re-suspend in 100 µl Bug Buster (Novagen)
- Spin suspension at 4000 rpm for 30 min
- Test soluble fraction by SDS-PAGE
- Wash pellet with water, re-suspend in 500 µl water to test for insoluble protein
- Test insoluble fraction by SDS-PAGE

Once a promising condition was found one can go into large scale expression.

3.2.2 Large Scale Expression

The *E.coli* strain Rosetta pLysS was used as expression host for native alpha-actinin constructs.

Standard protein expression was done in LB media at 37 °C. O/n 10 ml pre-cultures were diluted to 1 l with LB media, supplemented with adequate antibiotics (1 mg/100ml) and grown to OD600 0.6-0.8. Expression was induced with 0.5 mM IPTG, cells were harvested after 4-6 hours and re-suspended in Binding and Wash Buffer.

Mutated alpha-actinin constructs were expressed in the *E.coli* strain Rosetta.

Expression of mutant proteins was carried out starting from o/n pre-culture in LB media supplemented with adequate antibiotics (0.5 mg/100 ml) and 1mM pBpa. Pre-culture was spun down and re-suspended in pre-warmed GMML media supplemented with adequate antibiotics (0.5 mg/100 ml) and 1mM pBpa. Expression was induced with 0.5 mM IPTG, cells were harvested after 25-30 h grown at 25 – 30 °C and resuspended in Binding and Wash Buffer containing 20 mM 2-mercaptoethanol.

3.2.3 Refolding Assay

In order to refold insoluble mutant protein refolding assays were performed. After lysis by sonication the cell extract was spun down with 20500 rpm for 30 min at 4 °C. The obtained pellet was washed twice with Refolding Wash Buffer, followed by another centrifugation step with 20500 rpm for 15 min. The pellet was resuspended in Solubilization Buffer at 2 ml/g and heated 15 min at 50 °C. The solution was clarified by centrifuging at 20500 rpm for 30 min. The mutant proteins were purified in inclusion bodies via Ni-NTA, using buffer as described, supplemented with 4 M urea.

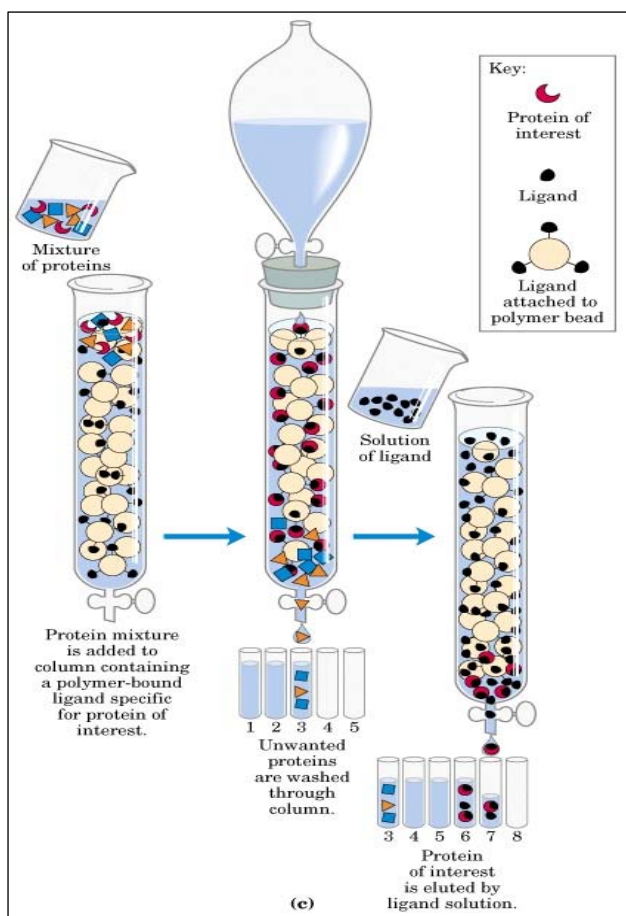
50 µl of the supernatant were added to 15 different refolding buffers provided by Athena™ refolding kit.

In another refolding attempt the neck as the binding partner of 889ΔpBpa was used as scaffold to refold the partially unfolded mutant protein. For this purpose the Refolding buffer #14, which was found to work best for EF34 mutant refolding, was supplemented with 6M, 5M, 4M, 3M, 2M and 1M Guanidine-HCl. The protein was dialyzed in 1 h steps in an iterative approach into the refolding buffer with the next lower Guanidine-HCl concentration. At 4M Guanidine-HCl the neck was added to provide a scaffold for the mutant EF34 to refold.

The success of the refolding attempts was determined by absorbance measurement at 320 nm and analytical gel filtration.

3.2.4 Affinity Chromatography

Proteins expressed as a fusion proteins with a repetition of 6x histidine the first purification step is usually done by a Nickel-NTA-Sepharose chromatography. The principle of this method is a non-covalent and reversible binding of His-tagged protein to



nickel. The nickel ion in turn is bound to a matrix. A buffer containing high imidazole is utilized to elute the protein after several washing steps. Imidazole competes with nickel for the binding to the histidine tagged protein.

Fig. 12 Schematized affinity chromatography procedure.

After a freeze-thaw cycle the cells were broken by sonication. If needed a protease inhibitor cocktail was added. The cell lysate was spun down with 18000 rpm for 30 min at 4 °C, followed by ultracentrifugation if needed.

The supernatant was loaded on a gravity His-trap (biorad), which has been equilibrated before with [Binding and Wash Buffer](#). For one liter expression volume approximately 1 ml resin was used. The Flow-through was loaded twice onto the column, followed by a washing step with at least 5 column volumes Binding and Wash Buffer. Bound proteins were eluted in 5-10 ml [Elution Buffer](#).

3.2.5 Buffer Exchange

Depending on the amount of protein for the buffer exchange into TEV Cleavage Buffer either HiLoad Desalting (Amersham Bioscience) column on ÄKTApurifier or dialysis was used.

Dialysis of 5-10 ml protein sample was performed in SpectraPor dialysis tubes Mw12-14 for 1 h at 4 °C against 1 l TEV Cleavage Buffer.

3.2.6 TEV Cleavage

The tags were removed by tobacco etch virus protease (TEV protease). The cleavage was performed at RT for 4 h or at 4°C o/n. The cleavage was performed with in-house expressed and purified TEV protease, see TEV preparation. Depending on the protein concentration 1-2 % w/w were used for cleavage.

3.2.7 Re-batch

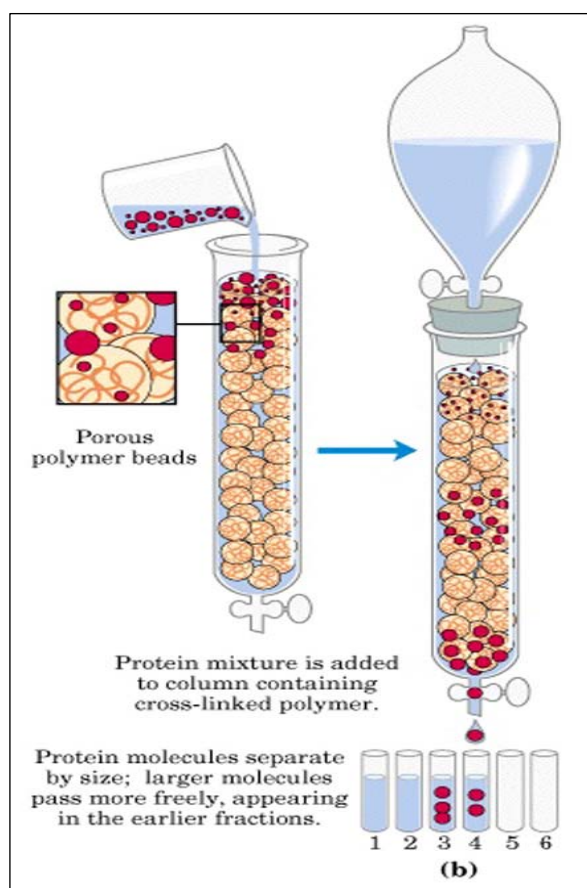
To separate the cleaved protein from the uncleaved plus TEV protease, the solution was run again over a nickel chelating column. His-tagged TEV protease and uncleaved target proteins remain bound while cleaved proteins can be collected in the flow through.

The column was recovered with 5 column volumes Binding and Wash Buffer

Procedure was as described in section 4324243.

3.2.8 Size Exclusion Chromatography

Gel filtration chromatography separates proteins by molecular radii. The sample is applied to a column, packed with porous beads made of hydrated, insoluble polymers, such as dextran or agarose.



Small molecules infiltrate the beads, whereas large molecules stay in the aqueous environment. Large molecules have a smaller volume to pass and consequently exit the column earlier than small molecules.

Fig. 13 Schematized gel filtration (size exclusion) chromatography.

The cleaved protein was either loaded on gel filtration column directly after TEV cleavage, or if needed, on a His-trap before. The flow through of the Ni-NTA or the TEV cleavage mixture was applied to size exclusion column (Superdex75 26/60, Amersham Bioscience, on

ÄKTApurifier).

Analytical size exclusion runs were done to analyze the folding of the proteins and the complexes with the peptide, as well as its behavior in different buffers. Analytical size exclusion chromatography gives information about the solvation radius from which one can deduce the oligomerization state and the monodispersity of the sample.

3.2.9 Concentration of proteins

Proteins were concentrated in millipore concentrators or dialysis, respectively.

Dialysis tubes were incubated several minutes in dH₂O. The filled dialysis tube was placed in a plastic tray filled with PEG20000. Both, Millipore concentrator membranes as well as dialysis tubes were rinsed with 20 % galactose prior usage to prevent binding of highly sticky proteins to the membranes.

3.2.10 Complex Formation

Fractions from preparative gel filtration containing pure fusion protein were collected and pooled, having a approximate concentration of 0.1 mM. The lyophilized peptide of the neck was added directly into the solution of the fusion protein EF34 in molar ratios 1:2 (EF34:neck). The complex was incubated 30 min at 4 °C prior to further analysis.

3.2.10 Preparation of recombinant TEV- protease

TEV plasmid was transformed via heat shock transformation into BL21 [pLysS].

It was started with a 5 ml o/n culture in Kan/Cam LB 1% glucose.

1l Kan/Cam LB were inoculated with o/n culture and grown to OD600 0.6 at 37°C.

The culture was chilled to 25 °C and induced with a final concentration of 0.5 mM IPTG.

Cells were harvested after 6-12 h and re-suspended in TEV Lysis Buffer 10 ml per 1g wet weight.

Re-suspended cells were frozen at -20 °C and sonicated after thawing until a reduced viscosity was obtained.

Cell lysate was centrifuged at 20500 rpm for 30 min at 4 °C.

Supernatant was decanted on with TEV Lysis Buffer equilibrated Ni-chelate column with around 1.5 ml of resin.

The flow-through was reloaded twice in the column before the washing steps have been carried out with 10 column volumes of TEV Wash Buffer I/II/III.

It was eluted with 5 column volumes of TEV Elution Buffer.

Protein concentration was assessed by spectro-photometry at 280nm

The sample was diluted with 50 % glycerol to a final concentration of 1 mg/ml, shock frozen in liquid nitrogen and stored at -20 °C.

3.3 Analytical Methods

3.3.1 Determination of protein concentration

Protein concentration was determined by measuring the absorbance of the in 6 M Guanidine-HCl denatured protein at 280 nm.

Alternatively Lowry method was used (Lowry, Rosebrough et al. 1951).

3.3.2 SDS-PAGE

The gels were run at 150-200V for 30-45min. Visualization of proteins was done with Coomassie Stain or the more sensitive Zn- Imidazole- Staining or they were used for Western Blotting.

TABLE A8-9 Solutions for Preparing Resolving Gels for Tris-glycine SDS-Polyacrylamide Gel Electrophoresis									
		VOLUME (ml) OF COMPONENTS REQUIRED TO CAST GELS OF INDICATED VOLUMES AND CONCENTRATIONS							
↓ COMPONENTS	GEL VOLUME ⇒	5 ml	10 ml	15 ml	20 ml	25 ml	30 ml	40 ml	50 ml
6% gel									
H ₂ O		2.6	5.3	7.9	10.6	13.2	15.9	21.2	26.5
30% acrylamide mix <1>		1.0	2.0	3.0	4.0	5.0	6.0	8.0	10.0
1.5 M Tris (pH 8.8)		1.3	2.5	3.8	5.0	6.3	7.5	10.0	12.5
10% SDS		0.05	0.1	0.15	0.2	0.25	0.3	0.4	0.5
10% ammonium persulfate <1>		0.05	0.1	0.15	0.2	0.25	0.3	0.4	0.5
TEMED <1>		0.004	0.008	0.012	0.016	0.02	0.024	0.032	0.04
8% gel									
H ₂ O		2.3	4.6	6.9	9.3	11.5	13.9	18.5	23.2
30% acrylamide mix <1>		1.3	2.7	4.0	5.3	6.7	8.0	10.7	13.3
1.5 M Tris (pH 8.8)		1.3	2.5	3.8	5.0	6.3	7.5	10.0	12.5
10% SDS		0.05	0.1	0.15	0.2	0.25	0.3	0.4	0.5
10% ammonium persulfate <1>		0.05	0.1	0.15	0.2	0.25	0.3	0.4	0.5
TEMED <1>		0.003	0.006	0.009	0.012	0.015	0.018	0.024	0.03
10% gel									
H ₂ O		1.9	4.0	5.9	7.9	9.9	11.9	15.9	19.8
30% acrylamide mix <1>		1.7	3.3	5.0	6.7	8.3	10.0	13.3	16.7
1.5 M Tris (pH 8.8)		1.3	2.5	3.8	5.0	6.3	7.5	10.0	12.5
10% SDS		0.05	0.1	0.15	0.2	0.25	0.3	0.4	0.5
10% ammonium persulfate <1>		0.05	0.1	0.15	0.2	0.25	0.3	0.4	0.5
TEMED <1>		0.002	0.004	0.006	0.008	0.01	0.012	0.016	0.02
12% gel									
H ₂ O		1.6	3.3	4.9	6.6	8.2	9.9	13.2	16.5
30% acrylamide mix <1>		2.0	4.0	6.0	8.0	10.0	12.0	16.0	20.0
1.5 M Tris (pH 8.8)		1.3	2.5	3.8	5.0	6.3	7.5	10.0	12.5
10% SDS		0.05	0.1	0.15	0.2	0.25	0.3	0.4	0.5
10% ammonium persulfate <1>		0.05	0.1	0.15	0.2	0.25	0.3	0.4	0.5
TEMED <1>		0.002	0.004	0.006	0.008	0.01	0.012	0.016	0.02
15% gel									
H ₂ O		1.1	2.3	3.4	4.6	5.7	6.9	9.2	11.5
30% acrylamide mix <1>		2.5	5.0	7.5	10.0	12.5	15.0	20.0	25.0
1.5 M Tris (pH 8.8)		1.3	2.5	3.8	5.0	6.3	7.5	10.0	12.5
10% SDS		0.05	0.1	0.15	0.2	0.25	0.3	0.4	0.5
10% ammonium persulfate <1>		0.05	0.1	0.15	0.2	0.25	0.3	0.4	0.5
TEMED <1>		0.002	0.004	0.006	0.008	0.01	0.012	0.016	0.02
Modified from Harlow and Lane (1988).									
TABLE A8-10 Solutions for Preparing 5% Stacking Gels for Tris-glycine SDS-polyacrylamide Gel Electrophoresis									
		VOLUME (ml) OF COMPONENTS REQUIRED TO CAST GELS OF INDICATED VOLUMES							
↓ COMPONENTS	GEL VOLUME ⇒	1 ml	2 ml	3 ml	4 ml	5 ml	6 ml	8 ml	10 ml
H ₂ O		0.68	1.4	2.1	2.7	3.4	4.1	5.5	6.8
30% acrylamide mix <1>		0.17	0.33	0.5	0.67	0.83	1.0	1.3	1.7
1.0 M Tris (pH 6.8)		0.13	0.25	0.38	0.5	0.63	0.75	1.0	1.25
10% SDS		0.01	0.02	0.03	0.04	0.05	0.06	0.08	0.1
10% ammonium persulfate <1>		0.01	0.02	0.03	0.04	0.05	0.06	0.08	0.1
TEMED <1>		0.001	0.002	0.003	0.004	0.005	0.006	0.008	0.01
Modified from Harlow and Lane (1988).									

Fig. 14 Protocols for SDS-PAGE gel casting

3.3.3 Tricine-SDS-PAGE

This special kind of SDS-PAGE is commonly used for separating proteins in the mass range of 1-100 kDa. This can be extremely useful for analyzing complexes containing small peptides. For separating EF34 (8 kDa) and the bound neck (3 kDa) a 16 % separation gel supplemented with urea overlaid with 10 % spacer gel was used.

An initial voltage of 30 V was used until the whole sample had entered the stacking gel; the remaining run was done with 90 V. (Schagger 2006)

The gel was washed several times with dH₂O to remove SDS which prevents proper Coomassie staining. The tricine gel was fixed in a solution containing 50 % methanol, 10% acetic acid, 100 mM ammonium acetate, stained and de-stained with solutions without methanol to increase the sensitivity of the Coomassie staining.

3.3.4 Coomassie- Staining

Coomassie binds at acidic environment to the positive charged amino acids lysine, histidine and arginine. In the rest of the gel Coomassie diffuses out when treated with de-staining solution. Around 100ng /band can be detected.

For buffers and solutions see section 2.4.

Gel was rinsed a few seconds with water, stained 5-10 min and treated with de-staining solution for 20-50 min.

3.3.5 Imidazole- Zink- Staining

This reverse staining method is around 10× times more sensitive than Coomassie staining and much less time consuming than silver staining.

The method exploits the ability of proteins to bind Zn²⁺ and of imidazole to react with unbound Zn²⁺ to produce insoluble zinc- imidazolate.

The background of the gel is therefore deep- white while the protein bands are transparent.

The gel was rinsed in dH₂O for a few seconds and equilibrated in 100 ml 0.2 M imidazole solution for about 30 min for a 15 % SDS PAGE. The solution was discarded and the gel was stained in 100 ml 0.3M ZnCl₂ solution. Stained gel was stored in dH₂O.

3.3.6 Western Blot

Western blotting is a method to detect a specific protein within a protein mixture.

It possesses incredible sensitivity. In fact it is possible to detect 0.5-1 ng protein by immunoblotting!

Before blotting the protein mixture is separated by SDS PAGE. Subsequently the protein is transferred onto a nitrocellulose membrane. For this procedure, an electric current is applied to the gel so that the separated, negatively charged proteins transfer through the gel onto the membrane (stationary phase). The pattern stays the same as on the poly-acrylamide gel. Proteins are bound through hydrophobic interactions to the nitrocellulose membrane

A SDS PAGE is blotted on a nitrocellulose- membrane. With antibodies a special protein or a part of it can be detected.

1. Run one gel for Western blotting and one for Coomassie- staining
2. Equilibrate a suitable size of membrane and soak 2 sponges and 2 pieces of filterpaper in Transfer Buffer (Touch the membrane only with tweezers)
3. Now build the Transfer- “Sandwich” beginning from the anode in the following order together:
 - a. Sponge
 - b. Filter
 - c. Gel
 - d. Membrane
 - e. Filter
 - f. Sponge

The proteins travel from the cathode (black) to Anode (red).

4. Place the cassette in the holder with ice cold Transfer Buffer and run the blot for 1h at 100V while stirring; disassemble the sandwich and stain the gel as a transfer control
5. Block the membrane at least for one hour in 10-20ml in Blocking Solution
6. Wash 3×10min. in 20ml TBST
7. Incubate for 1h with 1st antibody (anti- his- tag antibody)
8. Wash 3×10min. in 20ml TBST
9. Incubate for 1h with 2nd antibody
10. Wash 3×10min. in 20ml TBST
11. Develop the blot in 10ml Development Buffer containing 100µl NBT (stored on – 20°C) and 100µl BCIP (stored on –80°C)
12. Shake gently till the colour develops and the wash with water to stop the reaction

3.3.7 Ni-NTA on-Column Binding Studies

In order to investigate complex formation between two putative interaction partners, binding studies were carried out.

A histidine-tagged protein, thought to complex with a certain interaction partner was loaded to a gravity Ni-NTA equilibrated with Binding Buffer. After a washing step with 5 column volumes of this buffer the putative interaction partner (untagged) was loaded on the column. After 1 h incubation at room temperature or 4 °C, the flow through was collected and another washing step was carried out. The on-column formed complex was eluted with Elution Buffer, collected and analyzed. Alternatively, instead of eluting the complex an on-column TEV protease cleavage was performed. For this purpose 1 % w/w of TEV protease was added, incubated 4 h at room temperature, before the flow through was collected.

All fractions were collected and analyzed by 15 % SDS PAGE gels.

3.3.8 Complex analysis

The complex was freshly formed as described in section

After 30 min incubation at 4 °C, the complex was applied to analytical gel filtration.

This was done at pH 6 (20 mM Bis-Tris buffer pH 6, 50 mM NaCl), at pH 7.5 (20 mM Tris pH 7.5, 50 mM NaCl) and at pH 8 (20 mM K-Phosphate pH 8, 50 mM NaCl) and with varying salt concentrations from 20 mM to 200 mM NaCl. In all these conditions also the single components of the complex were tested to run on analytical gel filtration. This was done to analyze the complex in terms of which conditions are stabilizing it which may allow conclusions about the binding mechanisms.

The procedure was repeated with buffers as described above but supplemented with 5 mM 2-mercaptoethanol. The sample of the complex itself was incubated 15 min on 4 °C after 10 mM 2-mercaptoethanol was added. An aliquot was taken and immediately tested on analytical gel filtration. The rest of the sample was incubated for 1 hour, 2 hours, and over night, respectively, and tested again.

The fractions of analytical gel filtration were collected and were loaded twice to an 18 % SDS PAGE diverging in the sample preparation. One aliquot was mixed with SDS loading dye, the other one with 6 % glycerol.

3.3.9 Isothermal Titration Calorimetry

ITC is a technique to study molecular interactions – it can be used to get information about stoichiometry (n), binding affinity (K_a), heat of binding (ΔH), entropy (ΔS) and free energy (ΔG). It is also possible to find out the heat capacity of binding (ΔC) by running three or more measurements at different temperatures:

$$\Delta C = (\Delta H(T_2) - \Delta H(T_1)) / (T_2 - T_1)$$

Negative numbers of heat capacity indicate hydrophobic contact formation (energy release) and positive numbers for hydrophobic contact breaking. Another interesting assay to study is the involvement of protonation in molecular interactions. The principle of ITC is based upon heat measurements which evolves or absorbs when the protein and a hypothetical ligand are mixed.

The experimental set up exists of two equal cells, a discoid and a reference cell. The reference cell is filled with a buffer; the discoid cell contains the protein solution in the same volume and buffer. Before titration the temperature of the two cells is equilibrated. The ligand concentration should be between 100-1000 μM in a volume which is enough to fill the syringe and carry out 30-40 injections (minimum 320 μl) while the sample solution must have a volume of 1.8 ml and a concentration of 10-100 μM . Important to know is the exact ligand and protein concentration before starting the experiment. The ratio in terms of molar concentration between protein and ligand should be around 1:10. An additional requirement is that both components are in the same buffer

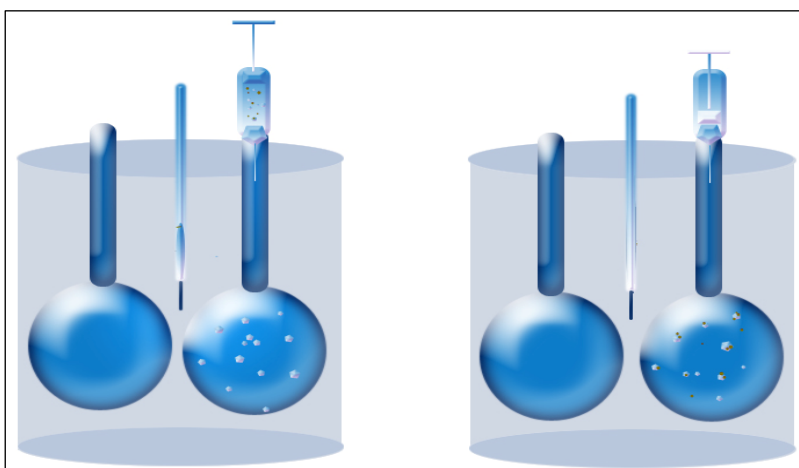


Fig. 15 ITC device

(left) sample cell is filled and is equilibrated to working temperature. (right) ligand is titrated to the macromolecule in the sample cell and temperature changes due to heat of dilution and exothermic or endothermic complex formation reaction are measured.

to avoid high signals due to high heat of dilution.

The ITC machine [Fig.15] measures temperature differences during titration between equilibrated cells. A so called cell feedback (differential power) is applied to maintain identical temperatures

between the cells; therefore a positive feedback is a sign for an endothermic reaction (ligand binding requires energy) while a negative feedback allows the conclusion of an exothermic reaction. Thus absorption of heat is counterbalanced by an input of cell feedback power and the evolvement of heat leads to cooling the system. The thermal energy, ΔH is measured in $\mu\text{calorie}$.

Buffer exchange of EF34 and the neck was done on HiPrep Desalting column (AmershamBioScience) into ITC buffer (50 mM K-phosphate, 50 mM NaCl). The neck at a concentration of 0.125 mM was titrated into a 0.025 mM EF34 solution.

3.3.10 Circular Dichroism Spectroscopy

This spectroscopy method measures the differences in absorption of left-handed and right-handed polarized light. By usage of the “near-UV” spectral region (190-250 nm) information about the tertiary structure of a protein or conformational changes upon protein-protein interaction, respectively, can be obtained. The chromophores at these wavelengths are aromatic amino acids and disulfide bonds. The signal is much weaker compared to “far-UV” measurements, therefore around 1 ml of protein sample with a concentration from 0.25- 2.5 mg/ml is needed.

The secondary structure of a protein can be analyzed by “far-UV” spectra (250-350 nm).

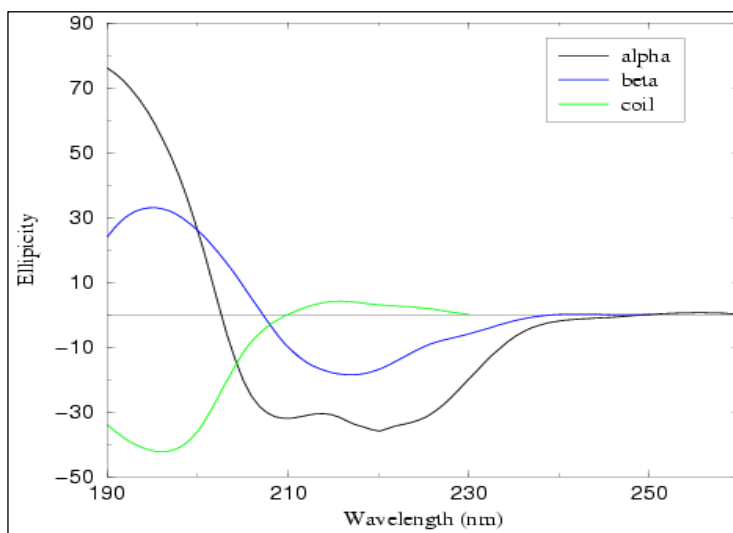


Fig. 16 Examples for the typical profiles of a “far UV” CD spectra of alpha-helix (black), beta-strand (blue) and

At these wavelengths the signal obtained is due to the absorption of the peptide bond.

By virtue of the shape and magnitude of the obtained CD spectrum it can be concluded, whether the protein is well folded and if it contains alpha helices, beta sheets or random coils and to which extent.

To record a far UV CD spectrum 20-200 μ l solution

containing protein 50 μ g/ml – 1 mg/ml are needed. One should avoid using buffers with high absorbance at the used wavelength like imidazole, DDT or histidine. Tris - buffers can cause low signal to noise ratios and therefore their usage is now recommended (Berova 2000).

EF34 was dialyzed into CD buffer (50 mM K-phosphate, 50 mM NaCl) and measurements were done at a concentration of 0.03 mM.

3.3.11 Thermofluor

Thermofluor is a methodology which provides the possibility to investigate a buffer system in which a protein is most stable.

This is done by the use of a special fluorescence dye (Sypro Orange), which is quenched by water molecules when unbound. It is added to a protein solution which is heated iteratively, resulting in successive unfolding of the protein and the exposure of its hydrophobic patches. The dye binds to these patches whereby its fluorescence signal

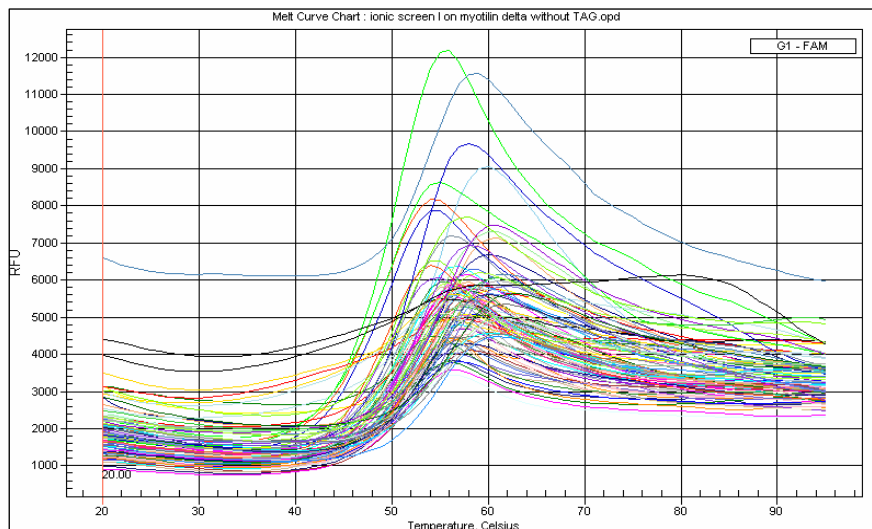


Fig. 17 Standard Thermofluor melting curve (kindly provided by Patrizia Ambrusci)

increases. The more stable a protein behaves in a certain buffer condition, the later it will start to unfold in the heating process and the later a rise of the fluorescence signal will be

observed. Therefore it can be stated, that the most right shifted curve in the thermofluor spectrum corresponds to the buffer stabilizing the protein analyzed best. (Ericsson, Hallberg et al. 2006).

This experiment was done in a Bio Rad Real time PCR machine in 96 well plates. Water was added instead of protein in the control samples. Every condition was done in three replicates to cancel pipeting mistakes. Each well was set up as follows, performing the experiment either in 25 μ l or 15 μ l.

<u>25 µl set up</u> 12.5 µl buffer 5 µl protein (2 -3.5 mg/ml) 7.5 µl dye solution
<u>15 µl set up</u> 7.5 µl buffer 3 µl protein (2 -3.5 mg/ml) 4.5 µl dye solution

The first experiments run were dye:protein titration studies, to determine the ideal ratio between dye- and protein concentration.

The next step was a salt-pH screen [Fig. 18] with free EF34 as well as EF34 in complex with the neck. The screen with free EF34 should suggest the best buffer conditions to keep EF34 as well as first hints concerning crystallization conditions. By a thermofluor screen with the complex one should be able to determine the same

parameters as for the free protein. Moreover it can provide information about the stability of the complex, and maybe also about the way, the complex is formed.

20 mM Tris, 20mM NaCl, 2 mM bME pH 7.5	20 mM Tris, 20mM NaCl, 2 mM bME pH 7.5	20 mM Tris, 20mM NaCl, 2 mM bME pH 7.5	20 mM Tris, 40 mM NaCl, 2 mM bME pH 7.5	20 mM Tris, 40 mM NaCl, 2 mM bME pH 7.5	20 mM Tris, 40 mM NaCl, 2 mM bME pH 7.5
20 mM Tris, 20mM NaCl, 2 mM bME pH 8	20 mM Tris, 20mM NaCl, 2 mM bME pH 8	20 mM Tris, 20mM NaCl, 2 mM bME pH 8	20 mM Tris, 40 mM NaCl, 2 mM bME pH 8	20 mM Tris, 40 mM NaCl, 2 mM bME pH 8	20 mM Tris, 40 mM NaCl, 2 mM bME pH 8
20 mM Tris, 20mM NaCl, 2 mM bME pH 8.5	20 mM Tris, 20mM NaCl, 2 mM bME pH 8.5	20 mM Tris, 20mM NaCl, 2 mM bME pH 8.5	20 mM Tris, 40 mM NaCl, 2 mM bME pH 8.5	20 mM Tris, 40 mM NaCl, 2 mM bME pH 8.5	20 mM Tris, 40 mM NaCl, 2 mM bME pH 8.5
20 mM Tris, 100 mM NaCl, 2 mM bME pH 7.5	20 mM Tris, 100 mM NaCl, 2 mM bME pH 7.5	20 mM Tris, 100 mM NaCl, 2 mM bME pH 7.5	20 mM Tris, 200 mM NaCl, 2 mM bME pH 7.5	20 mM Tris, 200 mM NaCl, 2 mM bME pH 7.5	20 mM Tris, 200 mM NaCl, 2 mM bME pH 7.5
20 mM Tris, 100 mM NaCl, 2 mM bME pH 8	20 mM Tris, 100 mM NaCl, 2 mM bME pH 8	20 mM Tris, 100 mM NaCl, 2 mM bME pH 8	20 mM Tris, 200 mM NaCl, 2 mM bME pH 8	20 mM Tris, 200 mM NaCl, 2 mM bME pH 8	20 mM Tris, 200 mM NaCl, 2 mM bME pH 8
20 mM Tris, 100 mM NaCl, 2 mM bME pH 8	20 mM Tris, 100 mM NaCl, 2 mM bME pH 8.5	20 mM Tris, 100 mM NaCl, 2 mM bME pH 8.5	20 mM Tris, 200 mM NaCl, 2 mM bME pH 8.5	20 mM Tris, 200 mM NaCl, 2 mM bME pH 8.5	20 mM Tris, 200 mM NaCl, 2 mM bME pH 8.5

Fig.18 Thermofluor salt-pH screen set up for complex analysis of EF34/neck

3.3.12 Dynamic Light Scattering

This technique is used to determine molecular particles size.

It is based on detecting random diffusive motion of particles (Gillespie 1996) suspended in liquid. In principle DLS measures how fast particles move (diffuse) through solution.

The sample is illuminated by a laser beam (monochromatic beam of light) and in the manner the light is scattered it reveals average particle radius. A very important parameter is the change in momentum (including speed and direction) of the particles. The radiation of the laser-illuminated particles is scattered to a detector and as a consequence of different particle detector distances within time the intensity of arriving photons will fluctuate. The intensity of all the scattered wavelets have a value $I(t)$ at time t . A little time later- delay of time (τ)- the value will be $I(t + \tau)$ because the intensity on the detector will be different when the particles have a new position. The general form of the function for monodisperse particles is

$$g(1)^{(\tau)} = e^{-DQ^2\tau}$$

D stands for the diffusion coefficient, from which particle sizes can be determined after Stokes-Einstein equation: $D = K_B T / 6\pi\eta a$

K_B = Boltzmann constant, T = temperature in Kelvin, η = viscosity of the solvent, a = radius of the beads.

Before starting the experiment the samples must be prepared to have a concentration between 0.1-1 mg/ml. The concentration is important because too many molecules in solution may interact with each other and show aggregation pattern even if there is none while lower concentrations will not scatter enough.

The count rate panel displays a graph in which the y-axis shows the count rate in kcounts/sec and the x-axis shows the seconds since the start of measurements. The counts should not be above 8000 kcounts/sec, if so, the sample must be further diluted.

The measurement panel displays a graph in which the y-axis displays the hydrodynamic radius in nm and the x-axis the seconds since the start of measurements. Approximately 20-30 measurements should be taken for accurate data. If many bars become red the sample might be not clean enough or it is an indication for the baseline of the measurement exceeds the data collection tolerance. That indicates that the protein is

aggregated and not useful for crystallization. Be aware that dust or other impurities will affect your data. Clean each time before starting the experiment cuvettes thoroughly and if necessary filter the protein solution before applying it to the measurements. Avoid air bubbles when filling the protein into the cuvette.

3.3.11 Photo Cross-linking

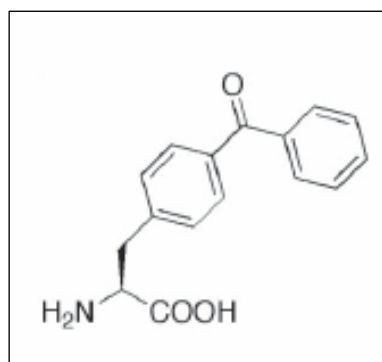
One of the most useful photo cross-linking agents in biology are benzophenones (Chin, Martin et al. 2002). Upon excitation at 350-360 nm, wavelengths that avoid protein damage, they react with otherwise inactivated carbon-hydrogen bonds (Galardy, Craig et al. 1973). An orthogonal aminoacyl-tRNA Synthetase/tRNA pair was evolved, which allows the *in vivo* incorporation of p-benzoyl-L-phenylalanine (pBpa) into *E.coli* proteins in response to the amber stop codon TAG. Together with a vector providing this mutated construct another vector containing several repeats coding for an adequate tRNA and *Methanococcus jannaschii* tyrosyl-Bpa-tRNA synthetase are co-transformed into an *E. coli* strain of choice.

Fig. 19 Structure of p-benzoyl-L-phenylalanine

The residues of choice were mutated to coding for the artificial amino acid pBpa by stop codon UAG in four different residues containing one mutation (Xie and Schultz Xie et al. 2006). These constructs were co-

together with pSup-BpaRS-6TRN, which is coding for tRNA and tRNA-synthetase for incorporation of pBpa into Rosetta.

For positive control the same was done with the vector pSup-MjTyrRS-6TRN [Fig. 20], which results in incorporation of tyrosine at the mutated site (Chin, Martin et al. 2002; Ryu and Schultz 2006).



triplets
the amber
each
2005; Wang,
transformed

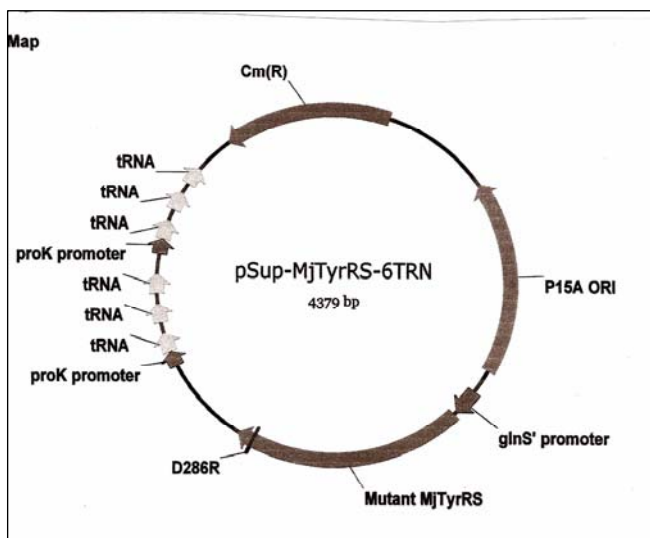


Fig. 20 Vector pSup-MjTyrRS-6TRN, providing tRNAs for translation of amber stop codons to tyrosine and adequate tRNA synthetase

Expression screen were done in GMML and LB media containing 1 mM pBpa, at different temperatures

and varying IPTG concentrations. It was found that LB media at 30 °C o/n gave the best results. Expression and cross-linking studies were performed according to (Farrell, Toroney et al. 2005).

Within this study the optimal way of photo cross-linking for the present complex was investigated. Two different devices, BioDoc IT-Sytem UV Transilluminator UVP and BLAK-Ray UVP Model B100 AP were used for cross-linking and compared. Due to the construction of the facility, for BioDoc IT-Sytem UV Transilluminator UVP it was not possible to use a cooling system. For BLAK-Ray UVP Model B100 AP a thermo-cycler was used for cooling the sample down to ~ 12 °C. UV exposure was accomplished in 2 ml eppendorf tubes and, in order to minimize damaging effects of short-wavelength UV, polystyrene Petri dish lids or Pyrex glass was used as filter (Farrell, Toroney et al. 2005).

3.4 Crystallization

3.4.1 Mechanisms of protein crystallization

Under certain circumstances protein solidify to form crystals. Crystals are formed as the conditions in a supersaturated solution slowly change. A protein to crystallize must overcome an energy barrier [Fig.21] analogous to that for conventional chemical reactions.

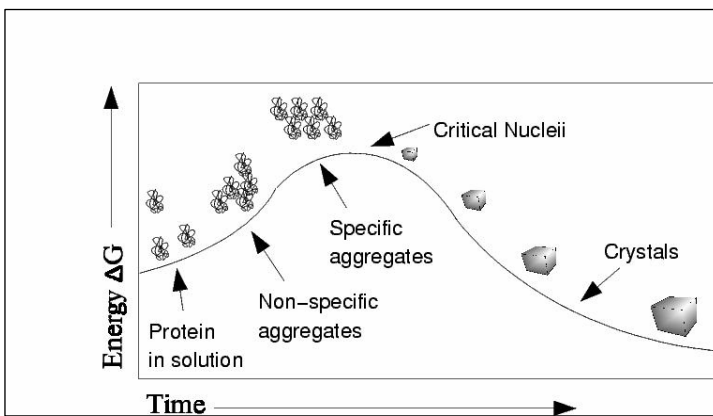


Fig.21 Energy barriers a protein has to overcome on its way to crystallization. (from: 'Crystallography made crystal clear', Gale Rhodes)

In any case, if changes in the crystal drop are observable, like phase separation, precipitant formation et cetera, one can conclude, that the protein is about by some means ore other to overcome an energy barrier.

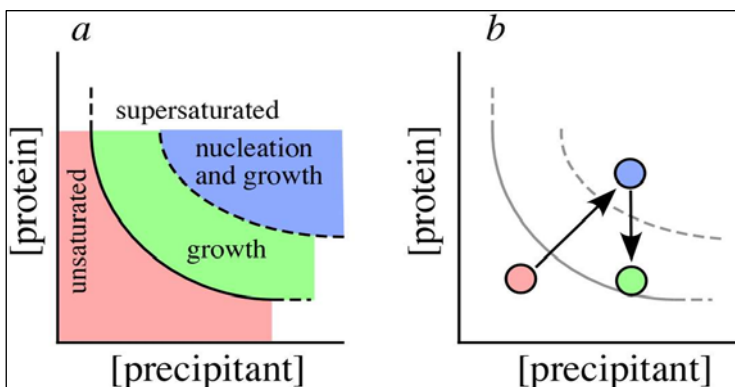


Fig 22 Phase diagram showing the solubility curve of a protein (from: 'Crystallography made crystal clear', Gale Rhodes)

The solubility of proteins can be represented in phase diagrams. The phase diagram plots the solubility curve of a protein. The horizontal axis shows the parameter being varied (usually precipitant concentration) and the vertical axis shows the protein concentration.

Saturation occurs when the rate of loss and gain of both the solid and solution phases of the protein are equal, and the system is in equilibrium.

Salting-out is seen in [Fig. 22] on the right hand side of the diagram where there is a reduction in protein solubility as the concentration of salt increases. Salting-in is seen on the left hand side of the diagram where there is an increase in protein solubility as the concentration of salt increases.

3.4.2 Set up of crystal drops and screening

There are several ways to grow crystals of proteins. The one which was used in this work is vapor diffusion.

In a vapor diffusion experiment, small volumes of precipitant and protein mixed together and the drop equilibrated against a larger reservoir of solution containing precipitant or another dehydrating agent [Fig. 23].

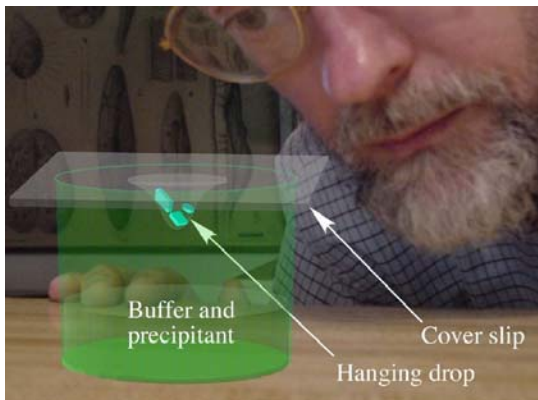


Fig. 23 Hanging drop vapor diffusion (from: 'Crystallography made crystal clear', Gale Rhodes)

The main bottleneck a crystallographer has to struggle with is to grow crystals of the protein of interest. Therefore one has to screen a lot of conditions in order to find the ones which yield crystals.

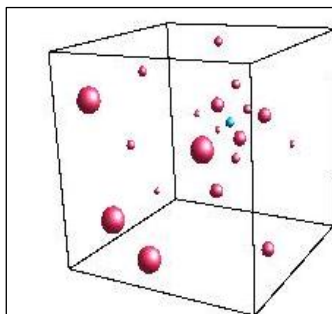
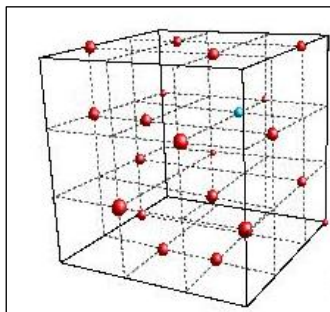


Fig. 24 Graphic presentation of incomplete factorial screening (from: 'Crystallography made crystal clear', Gale Rhodes)

Incomplete factorial screening [Fig.24] is a method of sampling parameter space evenly and efficiently. Factor levels are chosen randomly and then balanced to achieve uniform sampling.

All two-factor interactions are sampled as uniformly as possible. Sparse Matrix screens [Fig. 25] involve an intentional bias towards combinations of conditions that have worked



previously.

Fig. 25 Graphic presentation of sparse matrix screening (from: 'Crystallography made crystal clear', Gale Rhodes)

3.4.3 Data collection

When X-rays are beamed at the crystal, electrons diffract the X-rays, which causes a diffraction pattern. Using the mathematical Fourier transform these patterns can be

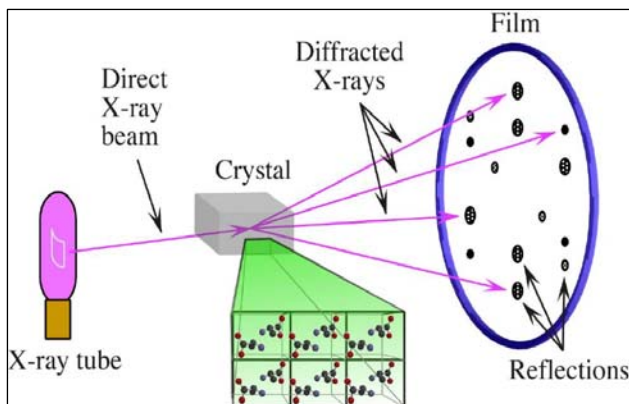


Fig. 26 Data collection of a protein crystal by exposing it to an X-ray beam (from: 'Crystallography made crystal clear', Gale Rhodes)

converted into electron density maps.

These maps show contour lines of electron density. Since electrons more or less surround atoms uniformly, it is possible to determine where atoms are located [Fig.26].

To get a three dimensional picture, the crystal is rotated while a computerized detector produces two dimensional electron density maps for

each angle of rotation. The third dimension comes from comparing the rotation of the crystal with the series of images. Computer programs use this method to come up with three dimensional spatial coordinates.

3.4.4 Cryo-conditions

In order to avoid extensive radiation damage, the crystals need to be frozen upon exposure to the X-ray beam. To prevent the crystal to crack and the formation of ice

rings, the crystal has to be in a suitable cryo-solution. The optimal case is, if the mother liquid of the crystal contains already substances preventing formation of ice crystals, like MDP, PEG <3000, or glycerol. If one of these substances or something comparable is not present in the mother liquid, it has to be added into the cryo-solution.

3.5 Nuclear magnetic resonance

Here we stray from analogy with our senses. NMR uses much more indirect methods to determine 3D structure. It is based on the quantum mechanical properties of atoms, particularly spin, and it determines information about atoms from the fact that their local environment influences how they respond to applied magnetic fields. The kind of information that can be obtained includes the measurement of inter-atomic distances, and features of the spectrum (coupling constants) that can be interpreted in terms of torsion angles.

One dimensional NMR is the most used structural determination methodology in chemistry. It is a fast and efficient way to investigate whether a protein is well folded or not. The chemical shift is measured in comparison to a reference substance. The spectra are recorded in a way, that coupling over three bonds at maximum are visible (which corresponds to a leap from one CH-bond to the adjacent). The atom in the protein shows a characteristic shift. The outcome of this is a separation of the signal characteristic for the atom's environment in the protein. The distance between the smaller peaks corresponds to the coupling constants. Via coupling constants one can assess information about molecular structures. It should be mentioned, that these couplings are visible between C-H bonds only and are interrupted by heteroatoms like nitrogen or oxygen.

For recording a 1D NMR-spectra at least 500 μ l of 300 μ M protein solution in phosphate buffer is needed.

3.6 Molecular Dynamics Simulation

A principal tool in the theoretical study of biological molecules is the method of molecular dynamics simulations (MD). This computational method calculates the time dependent behavior of a molecular system by applying Newton's equation of motion to the movement of proteins. MD simulations have provided detailed information on the fluctuations and conformational changes of proteins and nucleic acids. These methods are now routinely used to investigate the structure, dynamics and thermodynamics of biological molecules and their complexes. They are also used in the determination of structures from x-ray crystallography and from NMR experiments.

Energy minimization is necessary whenever the protein is changed and/or distorted manually. It can repair distorted geometries by moving atoms to release internal constraints.

In order to obtain mean distances between the C-beta atoms of the neck helix structure and 1H8B, molecular dynamics (MD) simulations were carried out with the CHARMM19 all hydrogen protein force field (MacKerell, Bashford et al. 1998) in CHARMM version c32a2 (Brooks, R. Bruccoleri et al. 1983). The initial structure was obtained by creating an ideal helix with the amino acid sequence of the neck protein utilizing WHAT IF 6.0. Following an energy-minimization, a MD of 200 ps was performed. Based on the positions of the C-alpha atoms, the neck peptide was superposed (Maiti, Domselaar et al. 2004) with Zr-7 of titin in PDB-Structure 1H8B, which was deleted thereafter to yield the receptor with the inserted neck peptide only. The following simulations were set up based on this complex in two stages: In the first stage, the initial system was heated to 900 k for a short while (20ps) in order to overcome local minima, while still conserving the general structure. In the following production phase, a 10 ns trajectory was written. The whole process was performed eight times from the initial structure with different random seeds for the generation of initial velocities. Distance matrices between the C-beta atoms were calculated for the endpoints of each trajectory and weighted according to their total energy. The simulations of the complex were

carried out with Langevin dynamics, thus granting control over the temperature. The friction coefficient was 25 ps^{-1} for all atoms and random forces were applied according to the target temperature of 300 K. To justify the time step of 2fs, the mass of all hydrogens was set to 10 amu. To include the effects of solvation, the EEF1 as solvation model was used (Lazaridis and Karplus 1999) and all energy parameters and modifications to the force field were set in accordance with this protocol. Molecular dynamics simulations were done by Gerhard König.

4.0 Results and Discussion

4.1 Wild type CaM and EF34 domains

4.1.1 Cloning

The constructs of ABD-R1, as well as EF34 and CaM were a generous gift of Anita Salmazo. CaM and ABD-R1 were cloned in pETM20 (TrxA-His₆, EF34 in pETM13 (GST-His₆). As it turned out to be impossible to separate cleaved TrxA from CaM, it was recloned into pETM30 (GST-His₆).

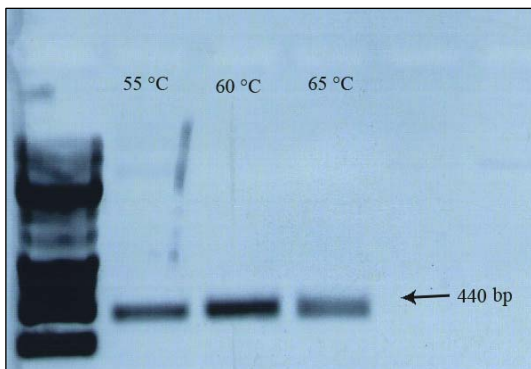


Fig. 27 Gradient PCR of CaM at temperatures 55°C, 60°C and 65°C

Gradient PCR of CaM was performed at temperatures 55°C, 60°C and 65°C. As the agarose gel shows [Fig. 27], 60 °C is the optimal annealing temperature for the primer used.

4.1.2 Expression and Purification of CaM

The native C-terminal alpha-actinin constructs were transformed and expressed in *E.coli* strain Rosetta pLysS, since it was found, that the constructs contain rare codons, which is served best in this strain of choice. EF34 and CaM fusion proteins were expressed and

cells were harvested as described in section [3.2.2](#).

Purification of CaM

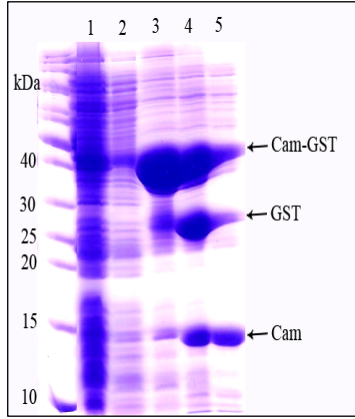


Fig. 28 Ni-NTA gravity column of CaM-domain.

- (1) Flow through
- (2) Wash with Binding and Wash Buffer
- (3) Elution
- (4) TEV cleaved fraction
- (5) Flow through of TEV cleaved fraction

The eluate from Ni-NTA purified CaM was subsequently dialyzed against TEV Cleavage Buffer. 1% v/v TEV protease was added to the dialyzed sample and left to incubate overnight at 4°C or 4 h at room temperature. After TEV digestion the sample was either re-applied to Ni-NTA resin in a re-batch protocol or directly loaded on gel filtration column. The flow-through from the re-batch was applied to gel filtration column.

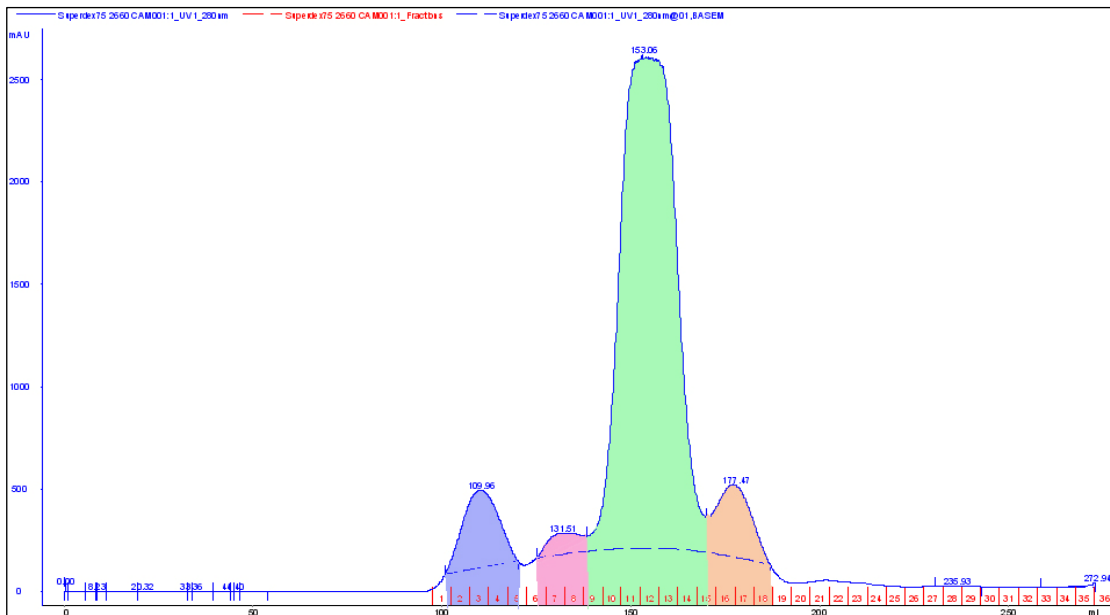
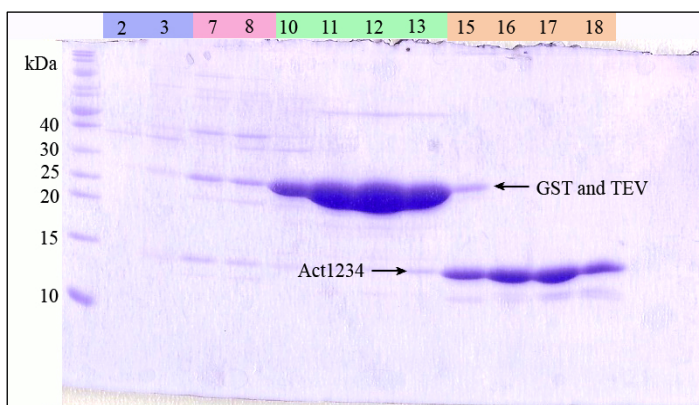


Fig. 29 Size exclusion chromatography diagram of CaM after TEV cleavage run on Superdex75 26/60. The abscissa shows the elution volume in ml and the ordinate the absorption at 280 nm in mAu



The fractions of gel filtration [Fig 29] were collected and analyzed on 15 % SDS PAGE gel.

Fig. 30 SDS-PAGE gel of gel filtration fractions of CaM.

The pure protein was collected. As shown on the gel [Fig. 30] CaM degrades very easily. Since it was found that the C-terminal domain of alpha-actinin attaches strongly to any kind of membrane or surface, protein concentration was avoided if possible to prevent loss of protein. If protein concentration was necessary, membranes used were treated as described in method section [3.2.9](#). The yield of 1 l expression culture was around 20 mg of pure CaM.

Purity and behavior of the protein was tested on analytical gel filtration Superdex 75 10/300 GL [Fig. 31].

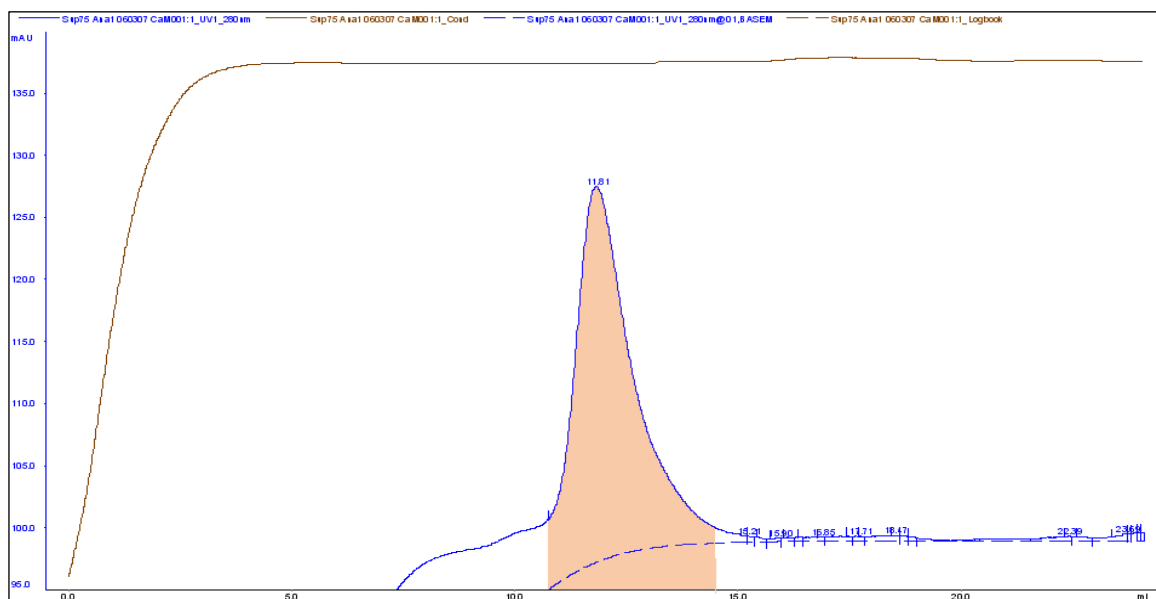


Fig. 31 Analytical gel filtration of CaM. The abscissa shows the elution volume in ml and the ordinate the absorption at 280 nm in mAu.

Due to the fast degradation of CaM, we focused our work on generation of EF34 construct.

4.1.3 Expression and Purification of EF34

Expression and purification procedure was the same as described before for CaM.

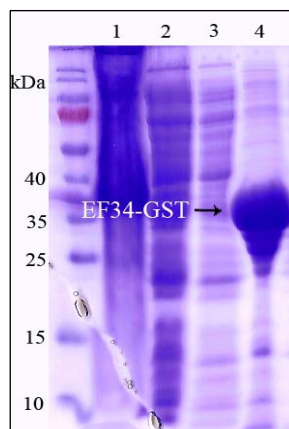


Fig. 32 SDS-PAGE gel of Ni-NTA fractions of EF34

- (1) Insoluble fraction
- (2) Flow through
- (3) Wash
- (4) Elution

The yield of expressed protein was around 8 mg/l culture volume. TEV protease cleavage conditions were found the best over night at room temperature. A reasonable amount of reducing agent turned out to be crucial. Later on in this study evidence was found that EF34 dimerizes via disulfide bonds. The dimerization seems to result in a steric hindrance for the TEV protease cleavage, since the yield of cleaved protein was very poor in the absence of reducing agents. Of course the GST tag and the disulfide bonds within the TEV protease enhance this effect.

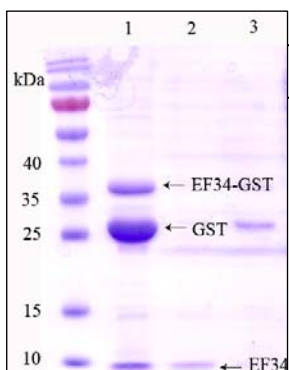


Fig. 33 SDS-PAGE gel of Ni-NTA fractions after TEV cleavage

- (1) Control (before column)
- (2) Flow through
- (3) Elution

It is clearly visible in [Fig. 33] comparing lane (1) before the column and lanes (2) and (3), that a high fraction of protein is lost in the affinity column. For this reason, this step was skipped and the sample was applied to gel filtration right after TEV protease cleavage [Fig. 34].

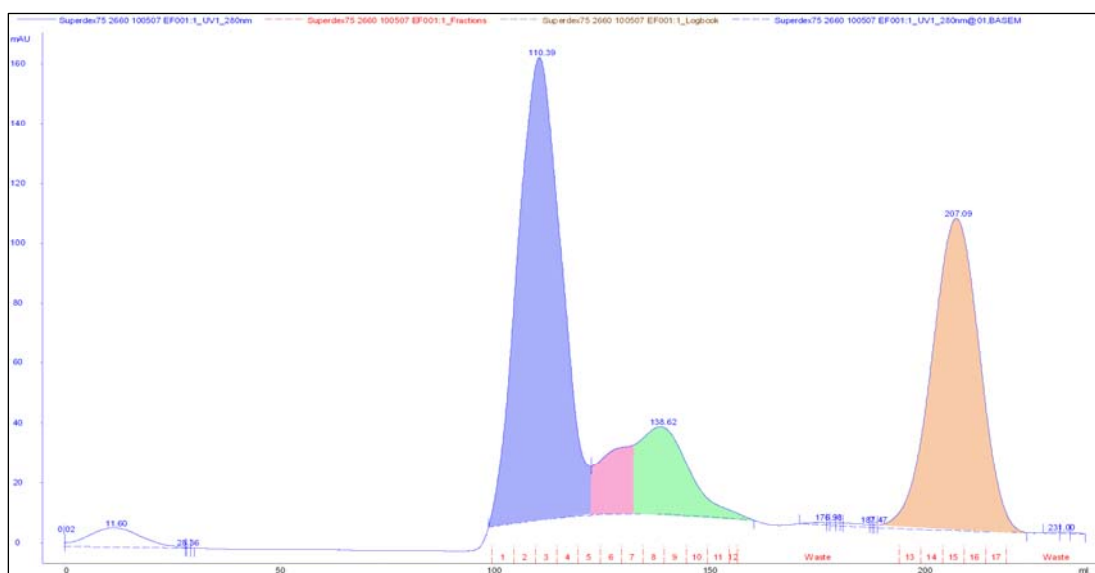


Fig.34 Size exclusion chromatogram of EF34 after TEV cleavage. The abscissa shows the elution volume in ml and the ordinate the absorption at 280 nm in mAu.

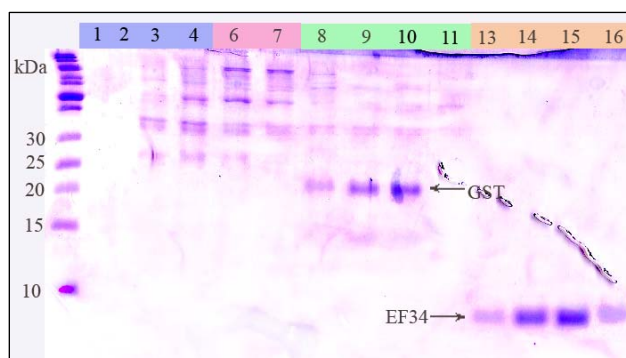


Fig. 35 SDS PAGE analysis of size exclusion fractions of EF34.

Fractions of the analytical gel filtration were loaded on 15 % SDS

PAGE gel for analysis [Fig. 35]

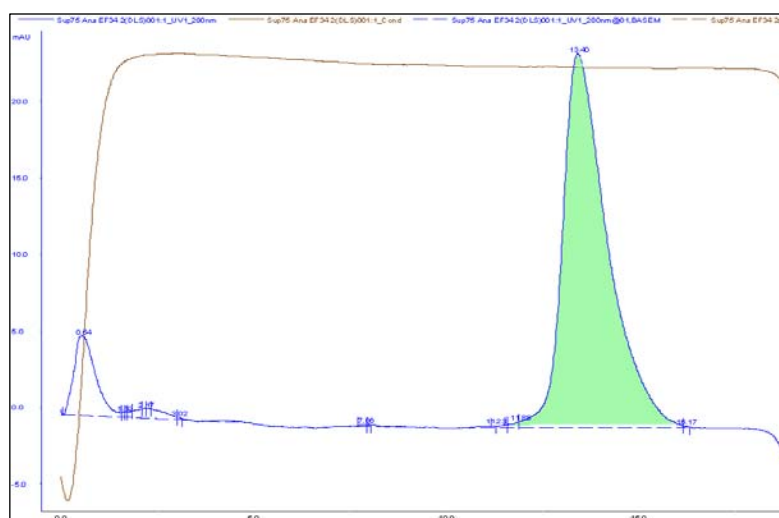
Lanes (1-7) contain mainly contaminants and rest of the uncleaved fusion-protein. GST eluted in the fractions (8-11). The pure fusion protein was collected from fractions (13) – (16).

As described above, also EF34 was only concentrated if it could not be avoided, since we experienced an extreme loss of protein during concentration procedures due to EF34's high affinity to any surfaces.

4.1.4 Biophysical Analysis of EF34

4.1.4.1 Analytical gel filtration

For preliminary analysis pure EF34 was applied on analytical size exclusion column Superdex75 10/300 GL [Fig. 36]. On the base of the shape of the peak conclusions can be drawn concerning the folded state of the protein. Moreover it may be visible if the protein



existed in different

Fig. 36 Analytical gel filtration chromatogram of EF34. The abscissa shows the elution volume in ml and the ordinate the absorption at 280 nm in mAu.

structural species by means of shoulders of a peak.

4.1.4.2 1D-NMR of EF34

A 1D-NMR spectrum of EF34 was recorded to assess whether the protein is in a well folded state. Generally speaking, the spectra [Fig. 37] show all characteristics of a well folded protein. Nevertheless the amide bonds should be visible in much higher peaks than obtained in this spectrum. Additionally, peaks caused by the methyl groups which was expected as well, is lacking. Interpretation of this spectrum is quite delicate since the rest of it argues for a well folded protein. Therefore this spectrum should be regarded as a preliminary result, further analysis would be necessary

The signal of PEG is present in the spectrum due to the fact, that the protein has been concentrated via dialysis against PEG, as described in section 3.2.9.

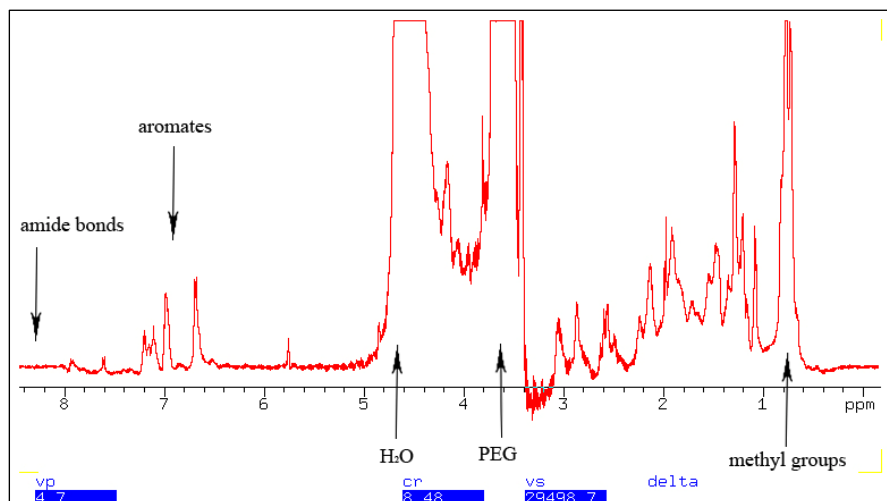


Fig. 37 EF34 1-NMR spectrum. The chemical shift is shown on the abscissa in ppm.

4.1.4.3 Circular Dichroism of EF34

Since the 1-D NMR spectrum did not give unequivocally information on the folded state of EF34, a “far UV” CD spectrum was recorded [Fig. 38].

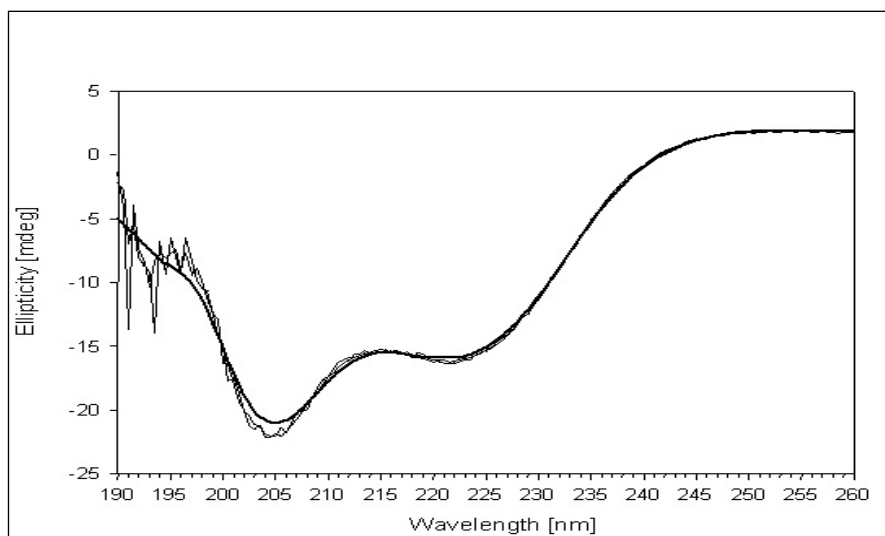


Fig. 38 CD spectrum of EF34. The ellipticity in mdeg is shown on the ordinate versus the wavelength in nm on the abscissa.

CD measurements were repeated 5 times and averaged, resulting in a spectrum confirming the expected helical secondary structure content of EF34.

4.2 Complex formation of EF34 with the neck and its analysis

4.2.1 Analytical gel filtration of the EF34/neck complex

Complex was formed as described in section [3.2.10](#).

Analytical size exclusion chromatography was performed to investigate the complex, its formation and behavior, respectively. As standards ovalbumin, chymotrypsinogen and RNaseA were used [Fig. 39].

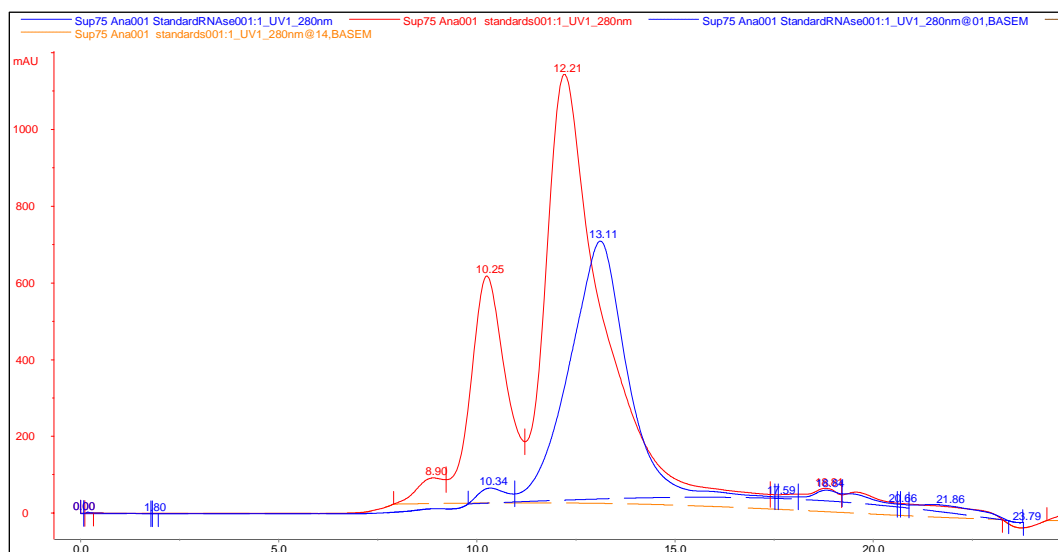


*Fig. 39 Standard run in 20 mM Tris pH 8, 200 mM NaCl, 2 mM 2-mercaptoethanol;
(red) Ovalbumin 43 kDa (10.25 ml elution volume)
Chymotrypsinogen 25 kDa (12.21 ml elution volume)
(blue) RNaseA 13.7 kDa (13.11 ml elution volume)
The abscissa shows the elution volume in ml and the ordinate the absorption at 280 nm in mAu.*

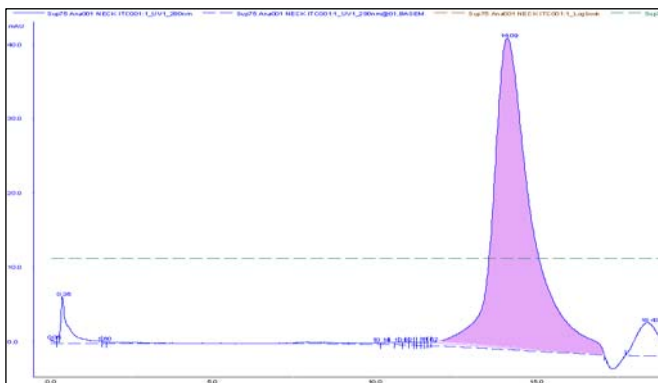


Fig. 40 Analytical gel filtration of the neck. The abscissa shows the elution volume in ml and the ordinate the absorption at 280 nm in mAu.

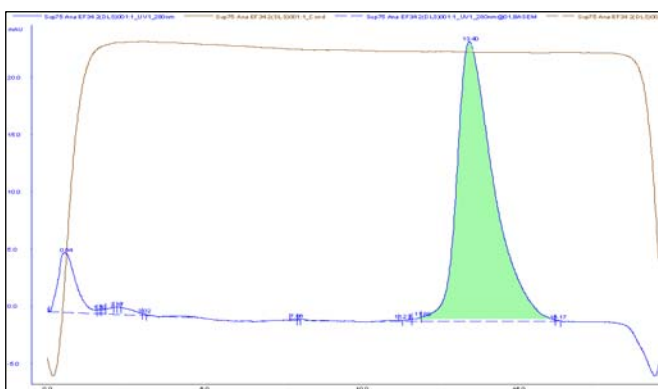


Fig. 41 Analytical gel filtration of EF34. The abscissa shows the elution volume in ml and the ordinate the absorption at 280 nm in mAu.

First, the single components of the complex were applied to analytical gel filtration to provide comparison data [Fig. 40], [Fig. 41].

According to elution volumes compared to those of the standards, 13.43 ml for EF34 and 14.0 ml for the neck, none of the components runs as a monomer. EF34 seems to form a dimer [Fig. 41], the neck even a tetramer [Fig. 40].

These findings were confirmed later on in this work with the 2-mercaptoethanol study.

Nevertheless, the two components are forming a 1:1 complex according to their gel filtration profile when mixed, eluting with 11.99 ml [Fig. 42], which corresponds to the molecular weight of a dimer of EF34 in complex with the neck (19 kDa).

The gel filtration was repeated with varying salt concentrations (20 mM, 50 mM, 100 mM and 200 mM NaCl) which did not have any visible effect on the complex.

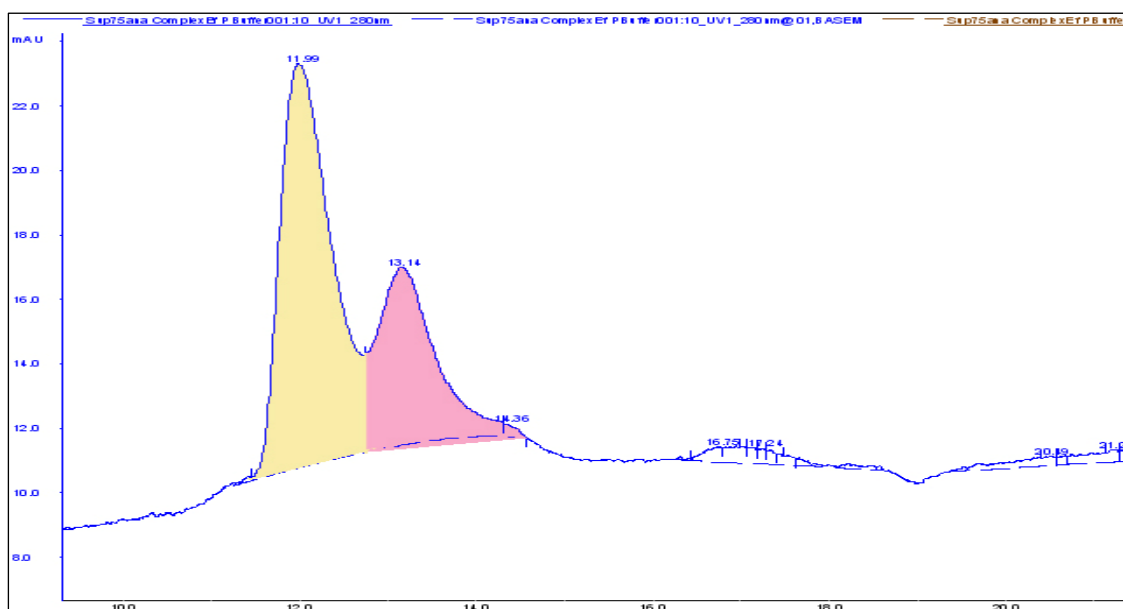


Fig. 42 Analytical gel filtration of the EF34/neck complex. The abscissa shows the elution volume in ml and the ordinate the absorption at 280 nm in mAu.

Moreover, when this complex is stored at 4 °C for a couple of days, an additional peak in analytical gel filtration arises at 10.39 ml [Fig. 43], which implies that an additional

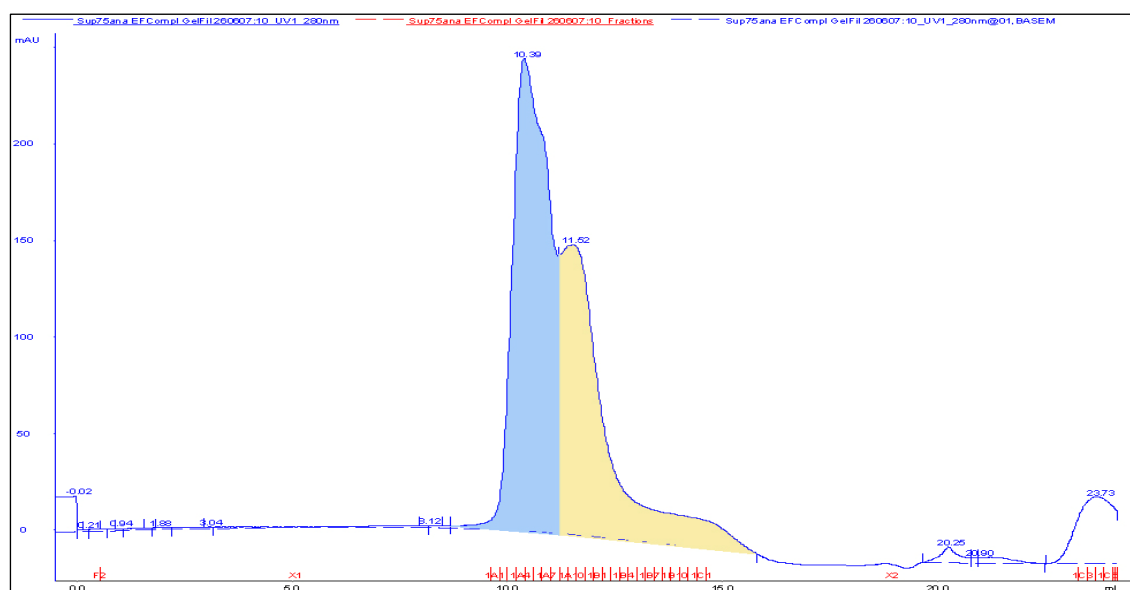


Fig. 43 Analytical size exclusion of EF34-neck complex after 4 days storage at 4 °C. The abscissa shows the elution volume in ml and the ordinate the absorption at 280 nm in mAu

structural species is formed in the sample, which might be a dimer of the complex formed before, in other words a tetramer of EF34 bound to a dimer of the neck.

The peak of unbound EF34 is not visible anymore. The additional peak after storage is not observed if EF34 alone is stored at 4 °C. The contrary is the case, when pure EF34 is stored at 4 °C - it degrades within a few days.

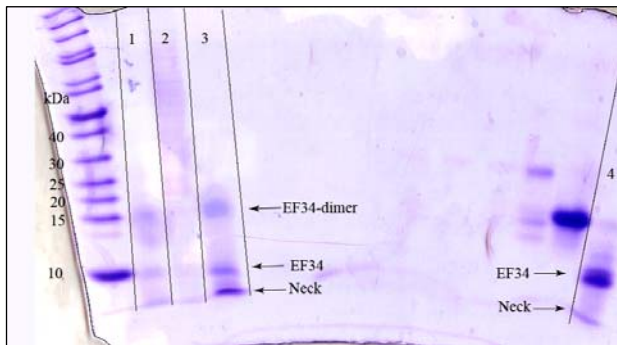


Fig. 44 16% Urea-Tricine-SDS PAGE gel of fractions of analytical gel filtrations of EF34/neck

The fractions loaded on 16 % Tricine SDS-Page gel enlightened the processes going on [Fig. 44]. It becomes obvious, that the additional peak contains a dimer of EF34 complexed with the neck.

(1) Pooled fractions A10-B3 (11.52 ml)

(2) Neck

(3) Pooled fractions A1-A9 (10.39ml)

(4) Sample of EF34-neck complex used for crystallization

It was also found, that upon treatment with 10 mM 2-mercaptoethanol the dimer formation of the complex after storage can be reversibly disrupted.

This fact also explains why 2-mercaptoethanol is essential during purification procedures of EF34. When no 2-mercaptoethanol is added in gel filtration buffers, for example, it is not possible to separate EF34-GST and the cleaved fusion protein.

4.2.2 2-Mercaptoethanol studies

For further investigation of the effect of reducing agents on dimer or tetramer formation of the single components and on the complex, a 2-mercaptoethanol assay was performed (see section 3.3.8). EF34 and the neck were run separately at pH 6 in analytical gel filtration.

The complex between the two interaction partners was formed and loaded on analytical gel filtration after 30 min of incubation at 4 °C and were run at pH 6, which gave the

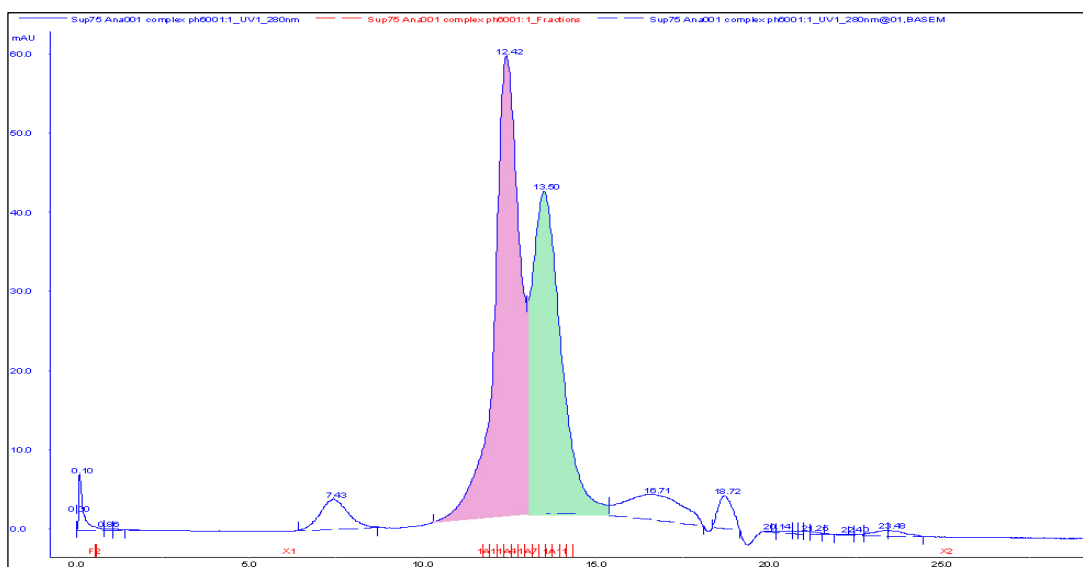


Fig.45 Complex of EF34 and the neck run at pH 6. The abscissa shows the elution volume in ml and the ordinate the absorption at 280 nm in mAu.

elution profile in [Fig. 45]. The fractions were loaded twice on 18 % SDS PAGE gel, once without reducing agent [Fig. 46a] and once with 2-mercaptoethanol [Fig. 46b] in the loading dye.

Apparently, the reducing environment of 1 M 2-mercaptoethanol in the loading dye breaks certain bondings which makes the upper bands in the SDS PAGE gel vanish. To lane (13) and (14) the neck alone has been applied. Strikingly, on the gel it seems to form a tetramer of approximately 12 kDa. This fact is quite surprising, since the present results

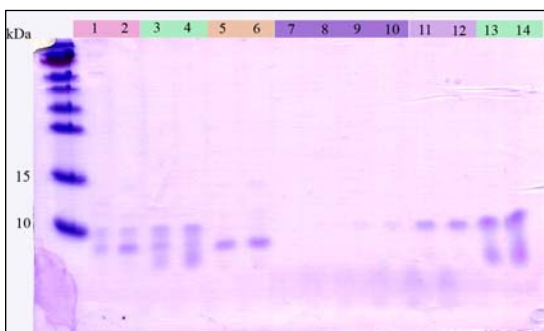


Fig. 46a Fractions of analytical gel filtration run at pH 6 applied to 18 % SDS PAGE gel. Gel was loaded without reducing agents, using glycerol only.

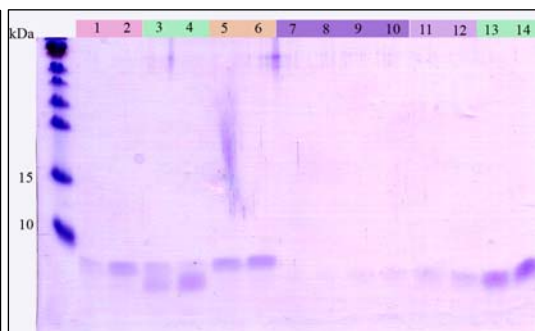


Fig. 46b Fractions of analytical gel filtration run at pH 6 applied to 18 % SDS PAGE gel. Gel was loaded with 2-mercaptoethanol.

imply an interaction via disulfide bonds, but the neck contains only one cysteine. Also the lanes (1), (2) and (3), (4), where the size exclusion fractions of the supposed complex were applied are hard to interpret. On the one hand, it could be again a tetramer of the neck (12 kDa) but also the complex of EF34 and the neck (11 kDa). To identify these bands, they were sent to mass spectroscopy analysis. Dimers of EF34, which also contains one cysteine residue, are found for sure at around 16 kDa.

The next step was an analytical gel filtration run at pH 6 including reducing agents [Fig. 47]. The dimers and tetramers disappear, and so does the complex. After 30 min incubation the unbound binding partners are found in the fractions. Significantly, upon dissociation of the complex two other peaks arise, which do not give any bands when loaded on SDS PAGE gel and are therefore not yet identified (elution volumes 17.47 ml and 19.01 ml which would approximately correspond to 4 and 2 kDa).

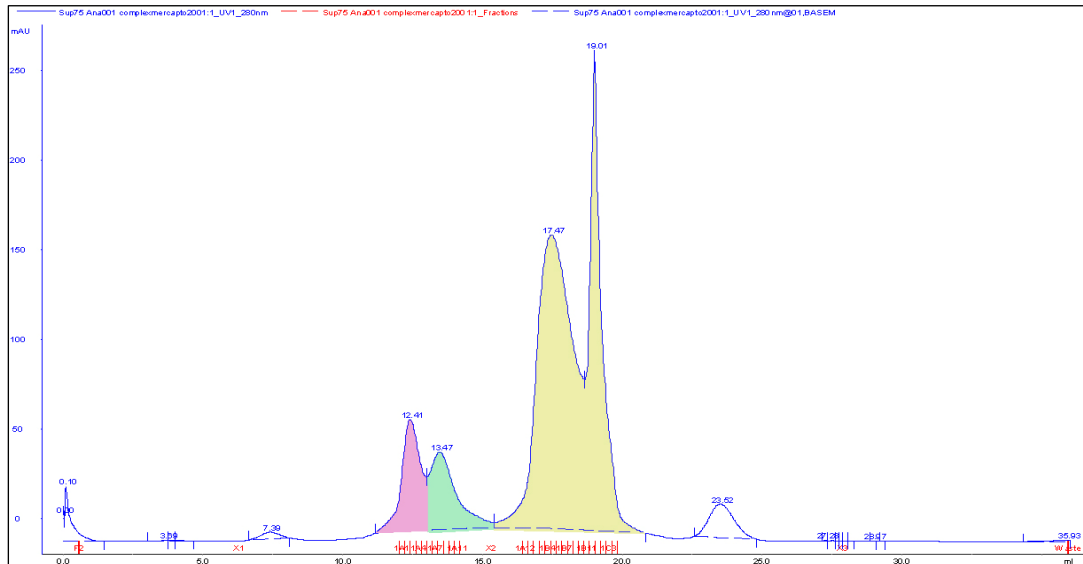


Fig. 47 Analytical gel filtration of EF34/neck at pH 6 with reducing agents. The abscissa shows the elution volume in ml and the ordinate the absorption at 280 nm in mAu.

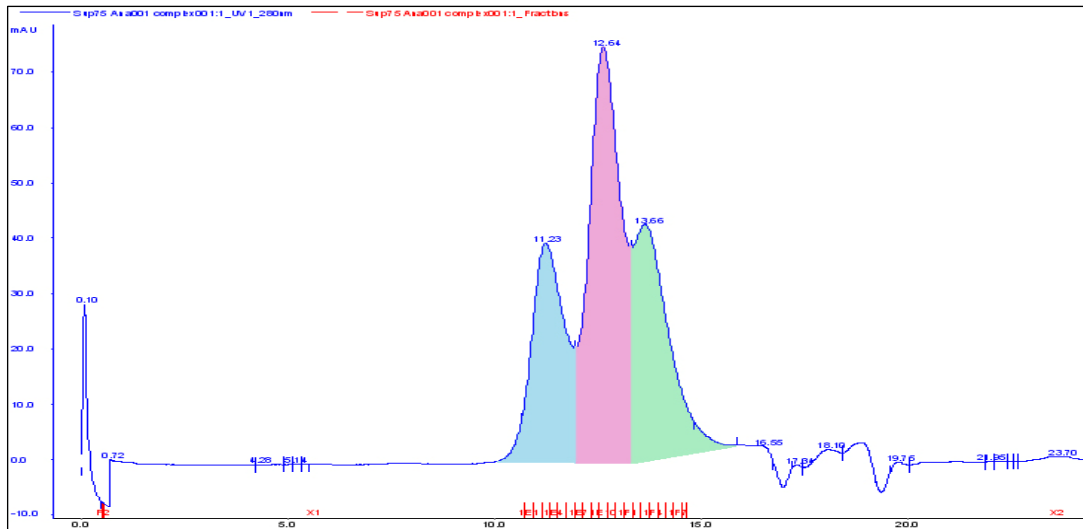


Fig.48 Analytical gel filtration of EF34/neck in pH 8 without reducing agents. The abscissa shows the elution volume in ml and the ordinate the absorbation at 280 nm in mAu.

The procedure has been repeated in pH 8 [Fig. 48]. Remarkably another peak arises at pH 8 at 11.23 ml (corresponds to ~20 kDa), which is absent at pH 6 (lanes (1) and (2) in [Fig. 49]. Upon addition of 2-mercaptoethanol the complex dissociates and the corresponding peaks (12.64 ml and 13.56 ml) vanish after 30 min incubation. Fractions of the peak at 12.62 ml were loaded on the gel at lanes (3) and (4), of 13.56 ml at lanes (5) and (6) [Fig. 49]. This suggests a quite low stability of the complex as well as of the single components at pH 8 in a reducing environment. Upon this dissociation the same two peaks arise as is pH 6 (17.5 ml and 19.0 ml), which are probably degradation products. Lanes (7) and (8) show EF34 and the neck, respectively.

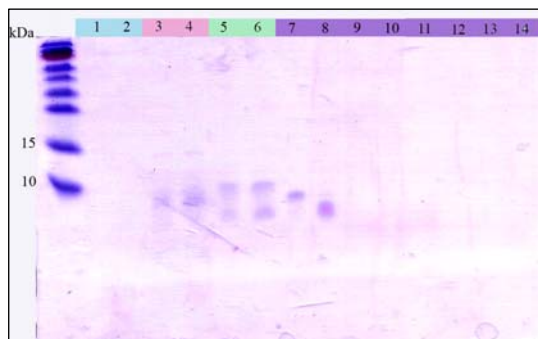


Fig. 49a Fractions of analytical gel filtration run at pH 6 applied to 18 % SDS PAGE gel. Gel was loaded without loading dye, using glycerol only.

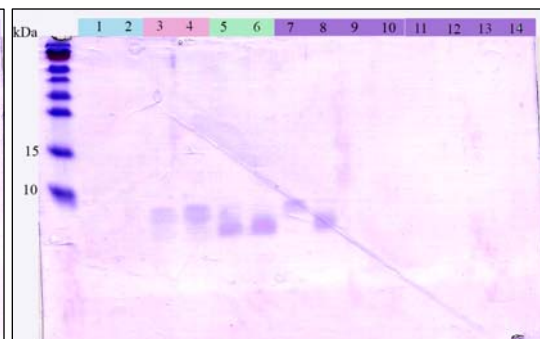


Fig. 49b Fractions of analytical gel filtration run at pH 6 applied to 18 % SDS PAGE gel. Gel was loaded with loading dye containing 1 M 2-mercaptoethanol.

4.2.2 Thermofluor measurements of free EF34 and bound to the neck

To determine the optimal buffer conditions for EF34, in which the protein is most stable and may form crystals with higher probability, several thermofluor experiments were done.

Many attempts were done to record melting curves from EF34, without any success. Only when the tests were run on the complex EF34-neck, some curves with expected shape could be obtained.

First of all varying dye-concentrations were titrated against increasing protein concentrations to determine the optimal [dye]:[protein] ratio.

Dye dilutions used were (pink) 1:1, (green) 1:100, (blue) 1:200, (grey) 1:400, (yellow) 1:800. Every dye dilution was tested with three different protein concentrations: 0.8 mg/ml, 1.5 mg/ml and 2 mg/ml. The best shift was obtained by a dye dilution of 1:100

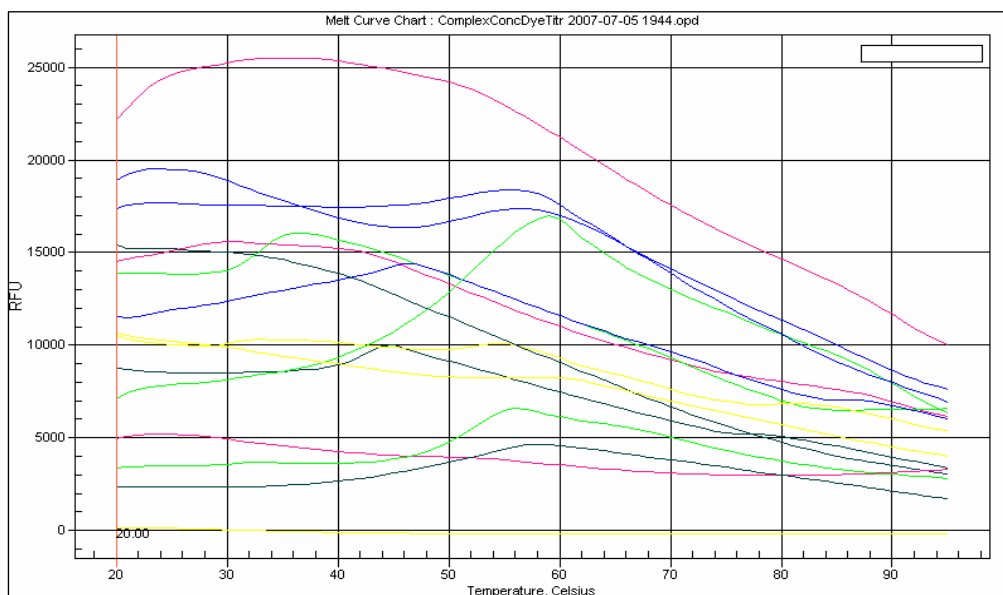


Fig. 50 Thermofluor measurements of the EF34-neck complex. The temperature is given in Celsius on the x-axis, the fluorescence signal in RFU on the y-axis.

with a final protein concentration of 1.5 mg/ml (green curve starting at 7000 RFU) [Fig. 50]. This ratio was used for all following thermofluor screens [Fig. 51].

Possible explanations for this phenomenon is that already in the folded state large hydrophobic patches are exposed to the surface. Therefore the dye can bind in the folded

state to the protein and cause high fluorescence signal already at the very beginning of the experiment. But the lack of another raise of fluorescence during the unfolding of the protein disproves this theory. On the other hand the shape of the profile of the pH-salt-screen with the EF34-neck complex shows two weak maxima at around 55 °C and 90 °C [Fig. 51]. This fact could be interpreted by some dye binding during unfolding of the protein causing a kind of melting curve. The first maxima would then indicate the dissociation of the complex, the second the unfolding of EF34. Nevertheless, these curves range in between a very weak signal to noise ratio and are therefore not highly reliable.

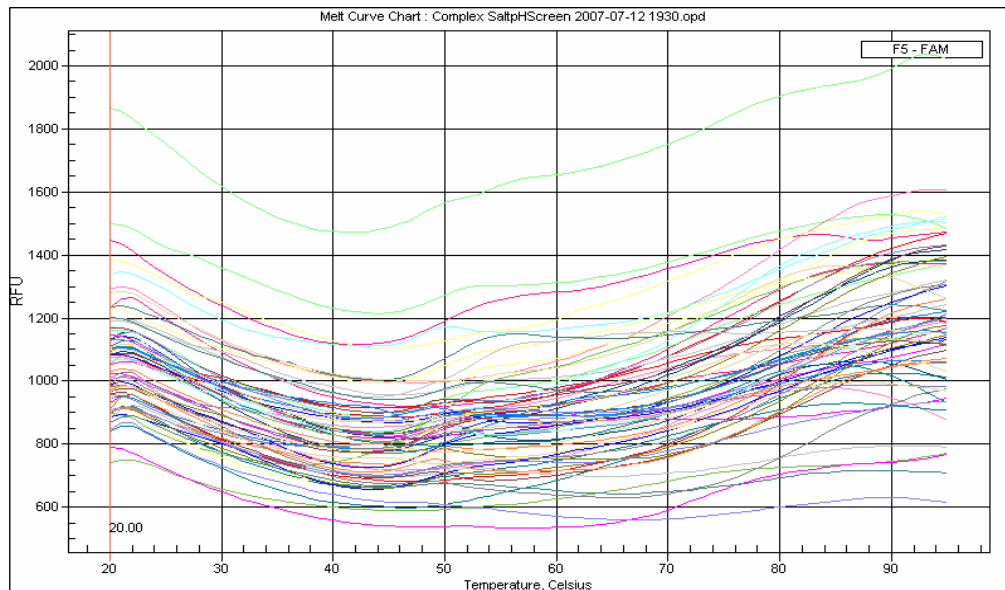


Fig. 51 Thermofluor salt-pH screen of EF34-neck complex. The temperature is given in Celsius on the x-axis, the fluorescence signal in RFU on the y-axis.

4.2.3 ITC measurement of EF34 and the neck

The present ITC result suggests a very high binding constant between EF34 and the neck [Fig. 52]. The fact, that only a single peak representing the binding of the neck to EF34 could be obtained, suggests, that the EF34 solution was saturated already after the first

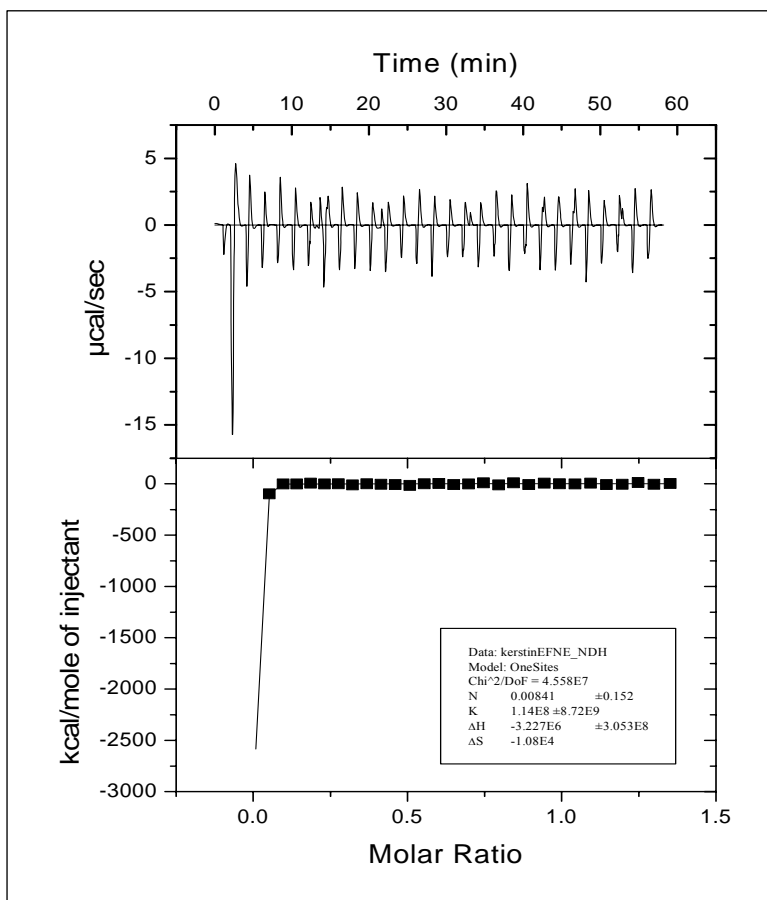


Fig. 52 EF34 and neck interaction demonstrated by isothermal calorimetry.

titration step. Therefore this has to be regarded as a preliminary result and another experiment with a ligand solution 5 – 10 times diluted would be necessary in order to gain more exact data.

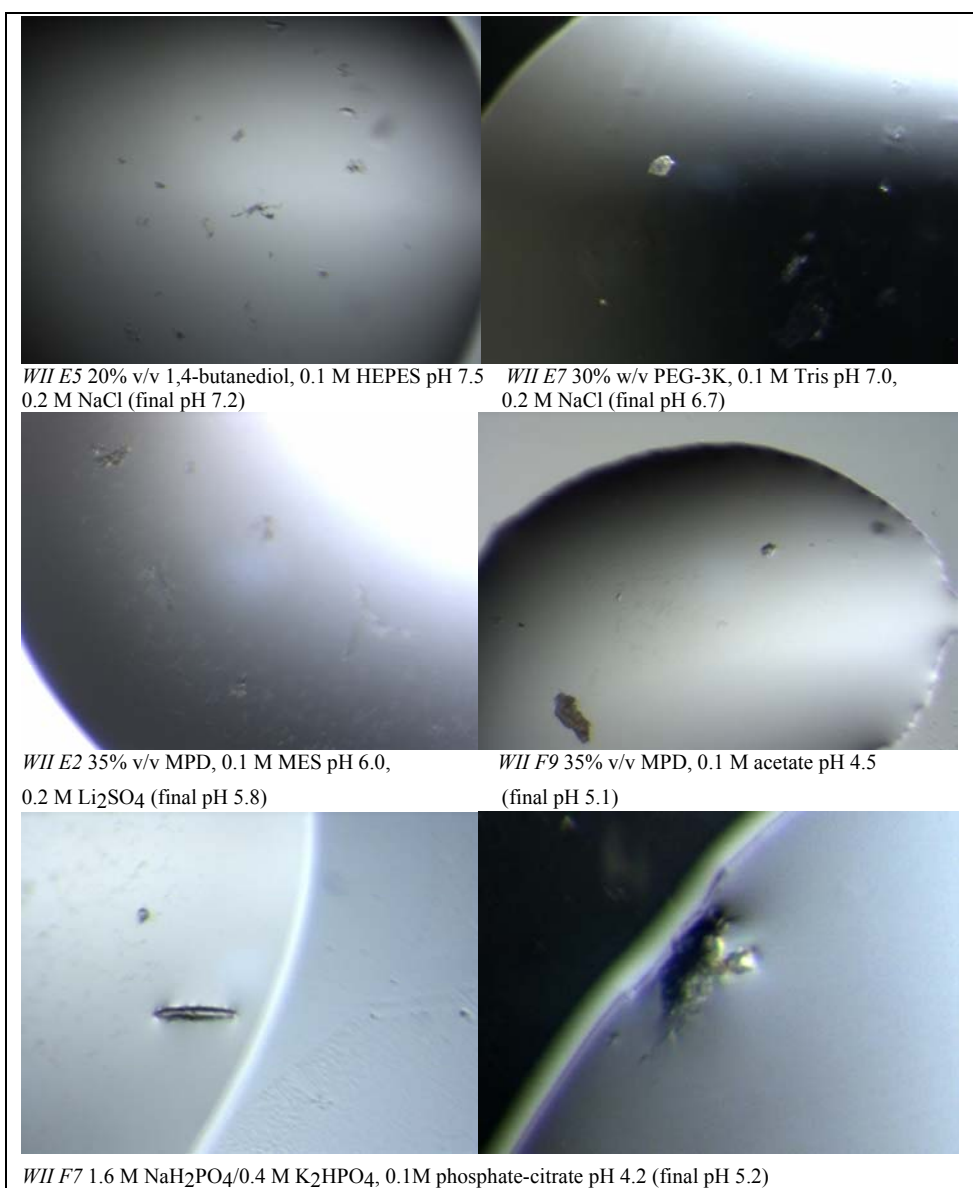
Nevertheless, the binding constant for ABD-R1 and CaM of 568 nM which was found in a former study (Young and Gautel, 2000) let us expect also a high binding constant for EF34 and the neck. The

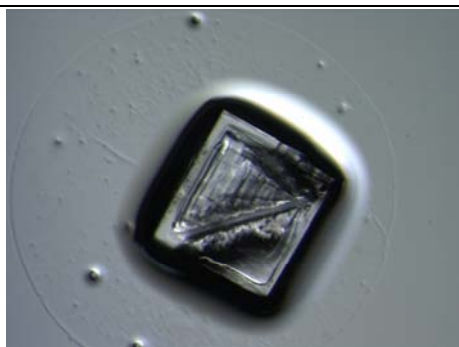
calculated K_d from the present data is around 100

nM, although with a single data point this value cannot be regarded as precise. Moreover a quite high heat of dilution was observed, causing the smaller peaks in the ITC spectrum. The negative numbers of heat capacity indicate hydrophobic contact formation (energy release), confirming the hypothesis that the hydrophobic patch in EF34 is involved in complex formation.

4.3 Crystallization of EF34-neck complex

The very first crystals appeared over night in conditions containing zinc ions. Later on crystals also grew in conditions containing other divalent cations, like calcium or magnesium. Subsequently, crystals in conditions with monovalent cations like lithium grew.

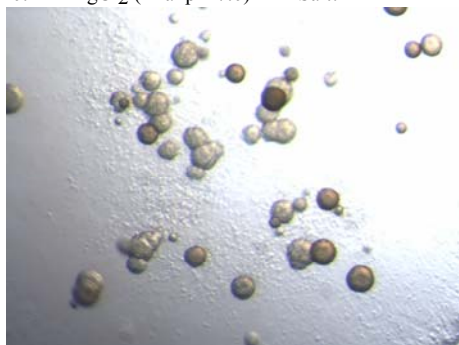




WII F5 2.5 M NaCl, 0.1 M Tris pH 7.0
0.2 M MgCl₂ (final pH 7.0) Salt!



WII F8 15% v/v ethanol, 0.1 M MES pH 6.0,
0.2 M Zn(OAc)₂ (final pH 6.0)



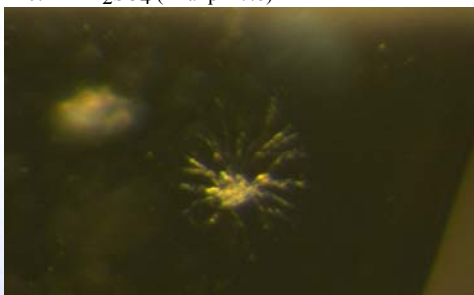
WII E8 10% w/v PEG-8K, 0.1 M Na/K phosphate
pH 6.2, 0.2 M NaCl (final pH 6.3)



WII H1 1 M K/Na tartrate, 0.1 M Tris pH 7.0,
0.2 M Li₂SO₄ (final pH 7.6)



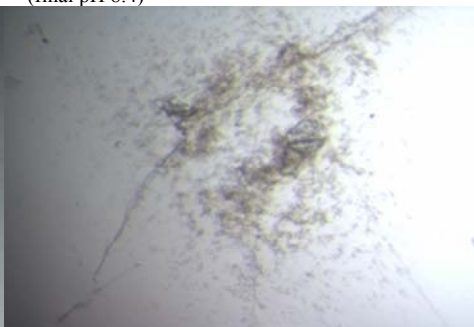
WII H6 30% v/v PEG-400, 0.1 M HEPES pH 7.5
0.2 M NaCl (final pH 7.4)



WII E10 1 M (NH₄)₂HPO₄, 0.1 M Tris pH 8.5
(final pH 8.4)



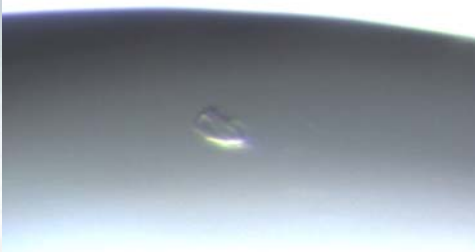
WII G12 10% w/v PEG-3K, 0.2 M NaCl
0.1 M phosphate-citrate pH 4.2 (final pH 4.3)



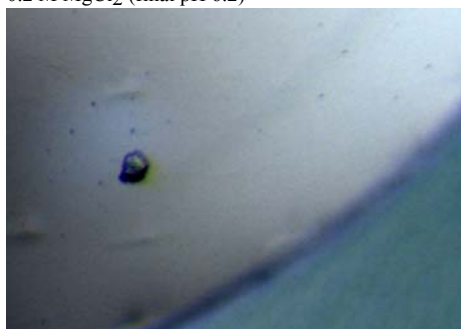
WII H7 10% w/v PEG-8K, 0.1 M Tris pH 7.0,
0.2 M MgCl₂ (final pH 6.6)



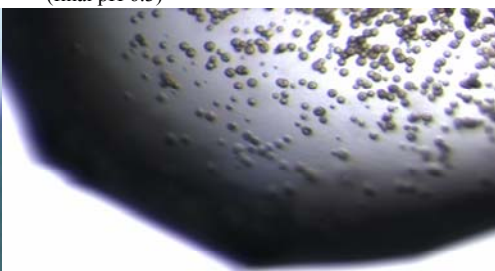
WII H8 20% w/v PEG-1K, 0.1 M cacodylate pH 6.5,
0.2 M MgCl_2 (final pH 6.2)



WII H9 1.26 M $(\text{NH}_4)_2\text{SO}_4$, 0.1 M MES pH 6.0
(final pH 6.3)



WII H11 2.5 M NaCl, 0.1 M imidazole pH 8.0,
0.2 M $\text{Zn}(\text{OAc})_2$ (final pH 6.0)



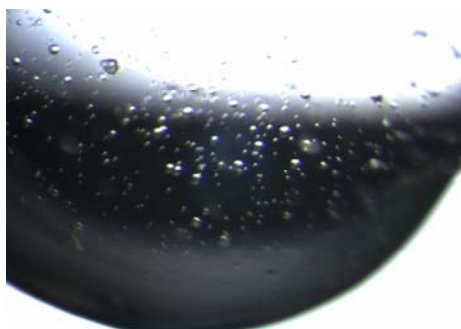
JCSGII E6 0.2 M zinc acetate,
0.1 M imidazole pH 8, 20% PEG 3000



JCSGII F5 0.2 M magnesium chloride,
0.1 M Tris pH 8.5, 50% ethylene glycol



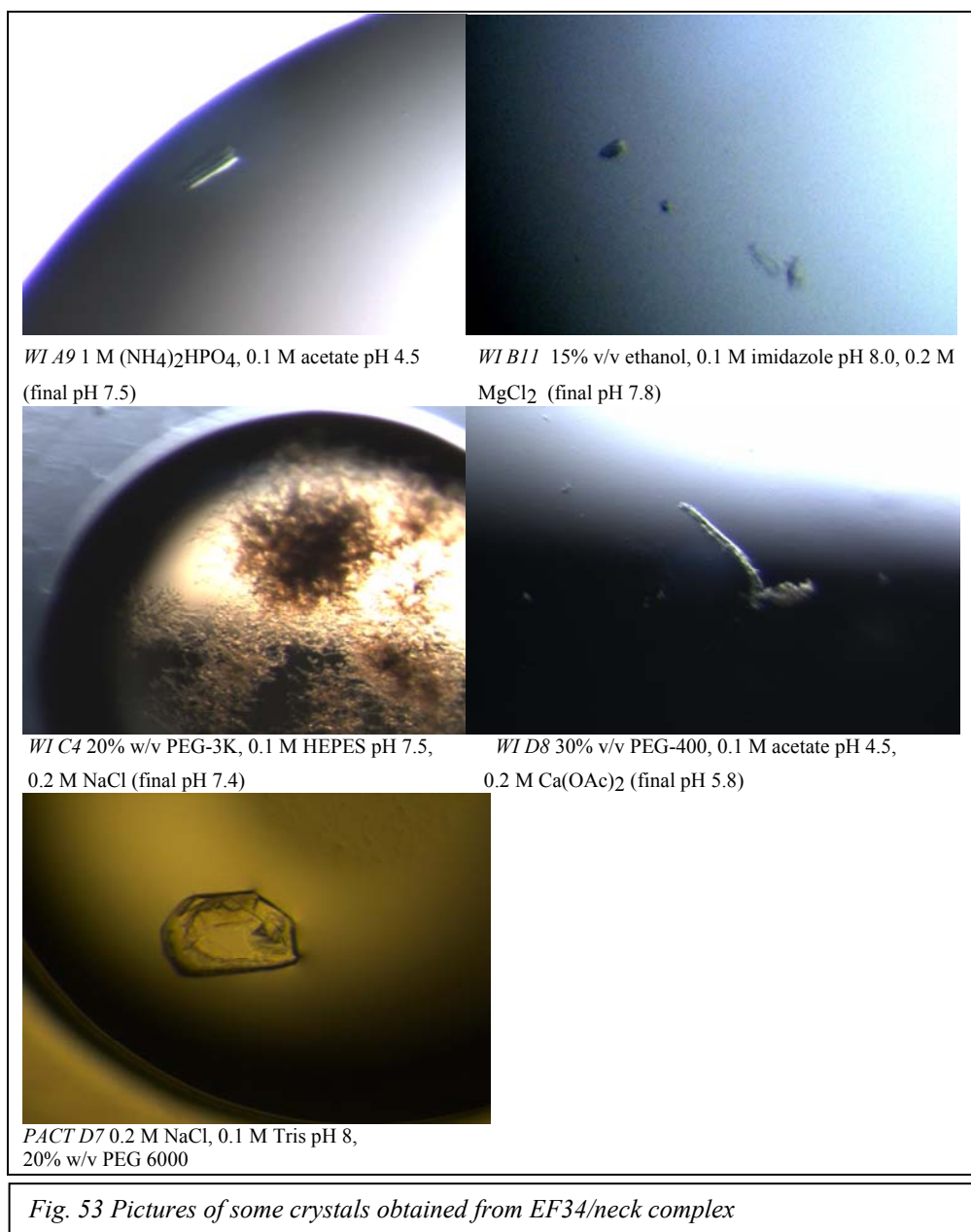
WI B1 1.26 M $(\text{NH}_4)_2\text{SO}_4$, 0.1 M cacodylate pH 6.5
(final pH 6.3)



WI A12 20% w/v PEG-1K, 0.1 M imidazole pH 8.0,
0.2 M $\text{Ca}(\text{OAc})_2$ (final pH 8.0)



WI A5 30% v/v PEG-400, 0.1 M CAPS pH 10.5
(final pH 10.5)



After a month crystals in conditions without metal ions appeared. Refinement screens were performed by analyzing all conditions in which crystals grew and combining the different components these conditions had in common. Metal ion screens were done with constant PEG smear concentration of 20 % v/v with varying MgCl_2 , Li_2SO_4 or $\text{Zn}(\text{OAc})_2$ concentrations, from 0- 250 mM against 20 mM Tris-HCl pH 7-pH 8.5. Refinement screens were repeated as described above with imidazole pH 7- pH 9 instead of Tris-HCl. Moreover it was screened for ammonium sulfate 1.6 mM- 2.2 mM versus varying pH,

from pH 5.5- pH 8 in 20 mM MES, 20 mM Bis-Tris and 20 mM Tris.

Crystals from conditions *PACT D7*, *WII H6*, *WII G12* and *JCSGII F5* were tested for diffraction at European Synchrotron Facility in Grenoble and at our home X-ray source (small focus rotating anode XProteum8 equipped with CCD detector and cryo-cooling device). Nevertheless none of the tested crystals diffracted X-rays.

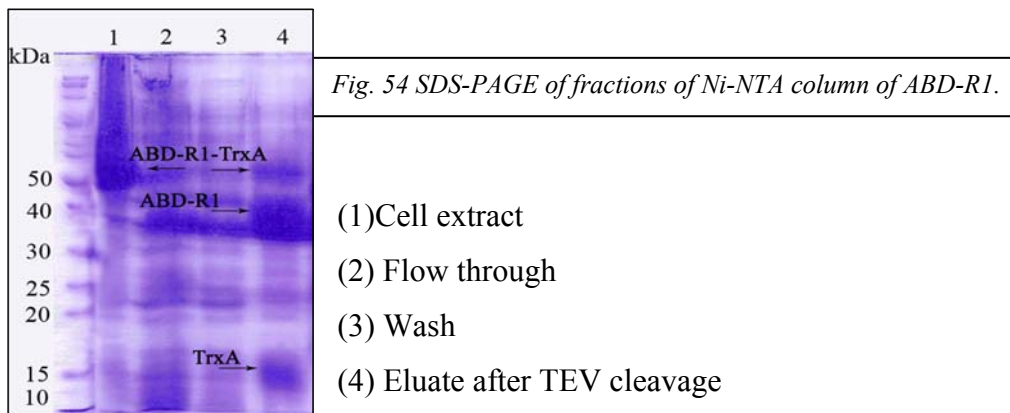
4.4 Complex formation and analysis of CaM/ABD-R1 and EF34/ABD-R1

4.4.1 Expression and Purification of ABD-R1

ABD-R1 was expressed and purified as described for the C-terminal alpha-actinin constructs.

The first purification step was again gravity Ni-NTA column [Fig. 54]. Nevertheless, due to rapid degradation if purified alone, ABD-R1 was mainly co-purified together either with EF34 or with CaM fusion proteins. After cells have been harvested, the pellets were re-suspended in Lysis Buffer and mixed in 1:1 ratio ABD-R1:EF34 and ABD-R1: CaM.

All other purification steps did not diverge from the standard procedure.



The samples were applied to gel filtration column directly after TEV protease cleavage and eluted with the profile shown in [Fig. 55] for ABD-R1/CaM and [Fig. 57] for ABD-R1/EF34.

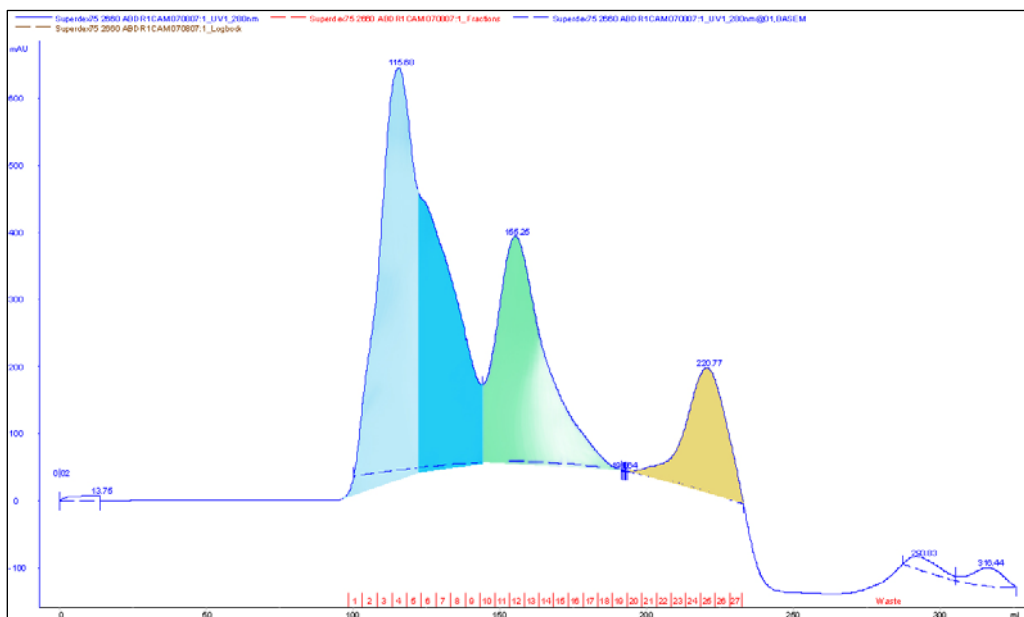


Fig. 55 Preparative size exclusion chromatogram of co-purified ABD-R1 and Cam. The abscissa shows the elution volume in ml and the ordinate the absorption at 280 nm in mAu.

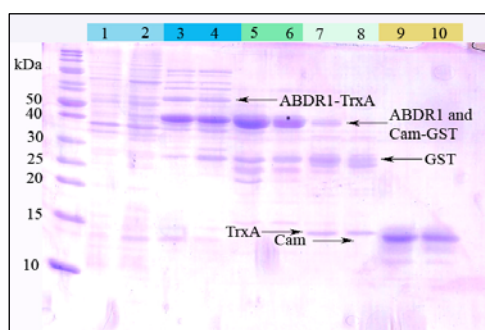


Fig. 56 Fractions of preparative size exclusion of co-purified ABD-R1 and Cam analyzed on 15 % SDS PAGE. In fractions 9 and 10 the pure Cam elutes, but nowhere in complex with ABD-R1.

TrxA.

First of all, it is obvious, that there are some interacting components, which elute together in one fraction in the preparative gel filtration. This refers to the shoulder of the peak eluted at 115 ml [Fig. 55] and the corresponding lanes (3) and (4)

on the gel in [Fig. 56], which contain ABD-R1-TrxA, ABD-R1, CaM-GST and GST, as well as to the peak eluted at 155 ml [Fig. 55] and the corresponding lanes (5)-(8) on the gel in [Fig. 56], containing ABD-R1, CaM-GST, GST and

The clearly visible GST tag in the peak eluting at 155 ml [Fig. 55 and Fig. 57] and in the corresponding fractions in lanes (3) – (8) in [Fig. 56] and lanes (10)-(16) in [Fig. 58] indicates a successful cleavage. The fact, that both, CaM [Fig. 55] and [Fig. 56] in lanes

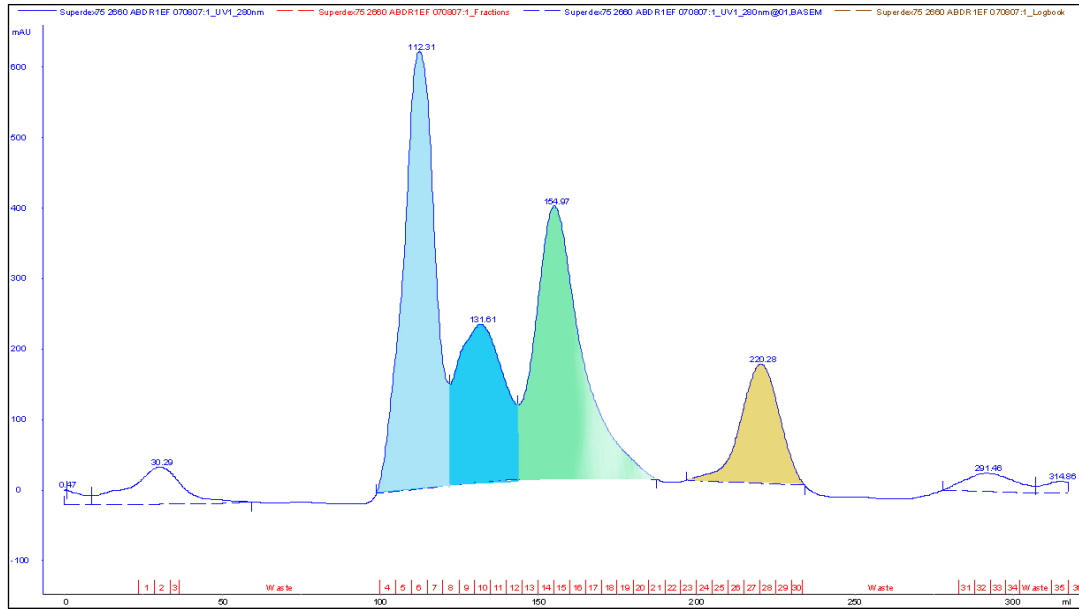


Fig. 57 Preparative size exclusion chromatography of co-purified ABD-R1-EF34. The abscissa shows the elution volume in ml and the ordinate the absorption at 280 nm in mAu.

(9) and (10) and EF34 [Fig. 57] and [Fig. 58] in lanes (27) and (28), elute at 220 ml, although their elution volumes are usually 178 ml for CaM and 208 ml for EF34, is quite peculiar and cannot be explained by now.

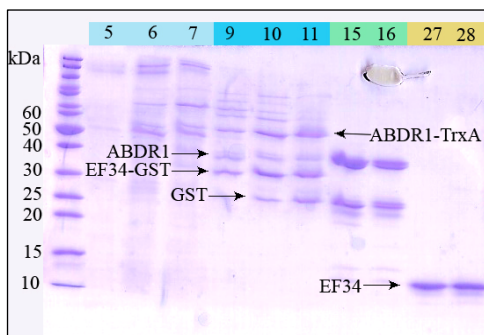


Fig. 58 Fractions of preparative size exclusion of co-purified ABD-R1 and EF34 analyzed on 15 % SDS PAGE.

Also the destination of the cleaved TrxA tag remains unclear. In the experiment with CaM one could assume that CaM elutes together with TrxA at 220 ml because of the same molecular weight: [Fig. 55] and [Fig. 56], lanes (9) and (10). Nevertheless in the experiment with EF34 TrxA is clearly absent: [Fig. 58], lanes (27) and (28). A successful TEV protease cleavage can be assumed, since cleaved ABD-R1 is clearly visible in lanes (3)-(6) in [Fig. 56] and lanes (9)-(16) in [Fig. 58].

Generally speaking, complex formation is only observed when the tags of the fusion proteins are still present, which implicates that the interaction rather involves the tags than the fusion protein. Another possible explanation is that the tag is necessary to bring the fusion protein in the conformation needed for interaction.

In contrast, it was possible in former studies (Young, Gautel, 2000) to form this complex. To reproduce the results of this former study, an on Ni-column binding assay was performed according to that work [Fig. 59].

4.4.2 On Column binding study of ABD-R1 and EF34

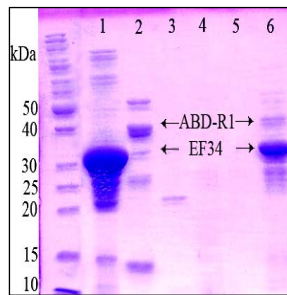


Fig. 59 SDS-PAGE gel of fractions of on column binding study of EF34 and ABD-R1

(1) EF34-GST

(2) ABD-R1

(3) Flow through EF34-GST

(4) Wash with 10 mM imidazole

(5) Flow through ABD-R1 (6) Elution of the complex

Apparently ABD-R1 and EF34 show interaction in this assay visible in [Fig. 59] in lane (6). Nevertheless it needs to be stated, that this analysis was done with the GST-tagged EF34. According to the previous gel filtration data it is possible, that ABD-R1 is not interacting with EF34 but with GST.

In a following experiment we tried to cleave the complex on column which would allow collecting the complex in the flow through. This experiment was performed at room temperature. It seems that the EF34-GST-His is bound to the Ni-resin in a way, that TEV protease is not able to cleave efficiently.

The collected flow through of the Ni-NTA was applied to analytical gel filtration for further analysis. This run was done on 4 °C.

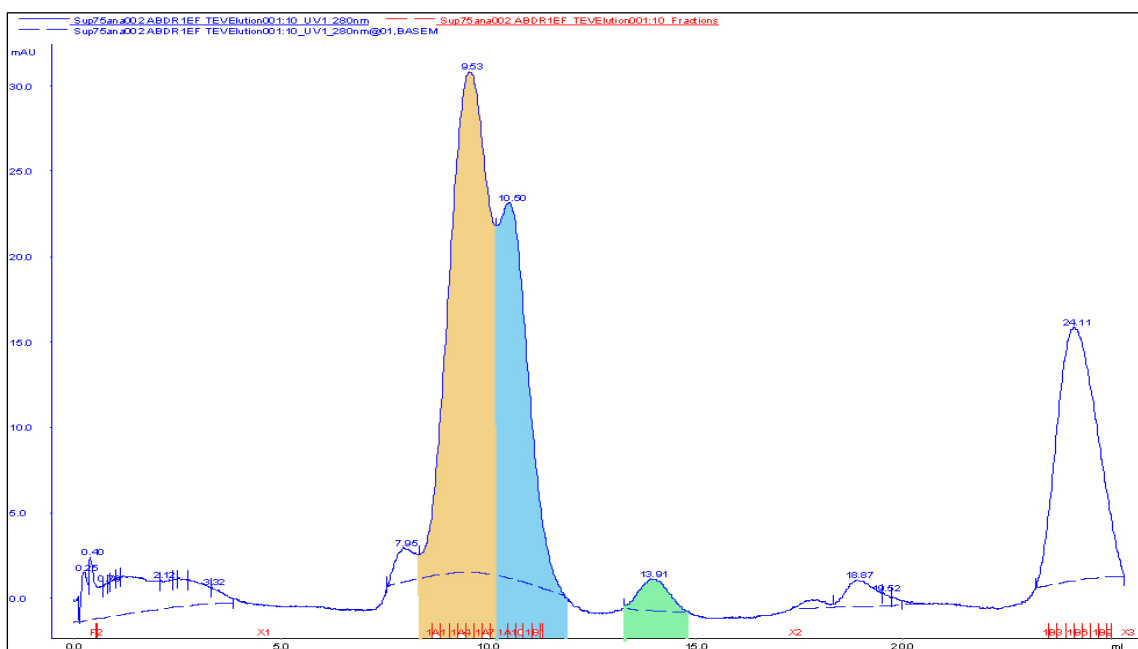
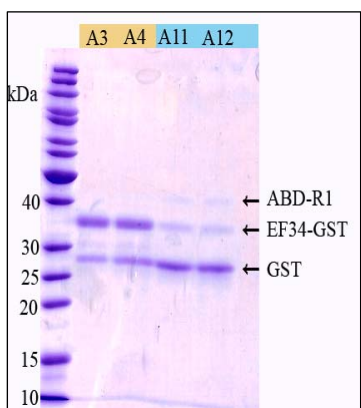


Fig. 60 Analytical gel filtration of flow through after on column TEV cleavage of ABD-R1/EF34. The abscissa shows the elution volume in ml and the ordinate the absorption at 280 nm in mAu.

A small amount of untagged EF34 was found in the eluate after the inefficient on column TEV protease cleavage, marked as the green peak in [Fig. 60] at 13.01 ml. This indicates that EF34 is binding to a binding partner, which is still binding the column. ABD-R1 and EF34-GST are the candidates for possible interaction. So, either EF34 is able to form dimers on column or there is indeed binding of ABD-R1 to EF34. The fractions of the peak eluted at 10.50 ml contain again ABD-R1, EF34-GST and GST as in the preparative gel filtration [Fig. 61]. Another attempt to bind ABD-R1 to CaM or EF34, respectively, was to purify ABD-R1 alone and mix the pure protein with CaM or EF34. No binding could be detected (data not shown).



The present results suggest that either the complex is only formed on room temperature, or that ABD-R1 binds to

Fig. 61 Fractions of analytical gel filtration of on-column TEV protease digested ABD-R1/EF34

GST, only.

Considering the results of the 2-mercaptoethanol study, it would be necessary to repeat the binding studies with low concentrations of reducing agents. If indeed disulfide

bridges play a role in this interaction, this procedure could change the results tremendously.

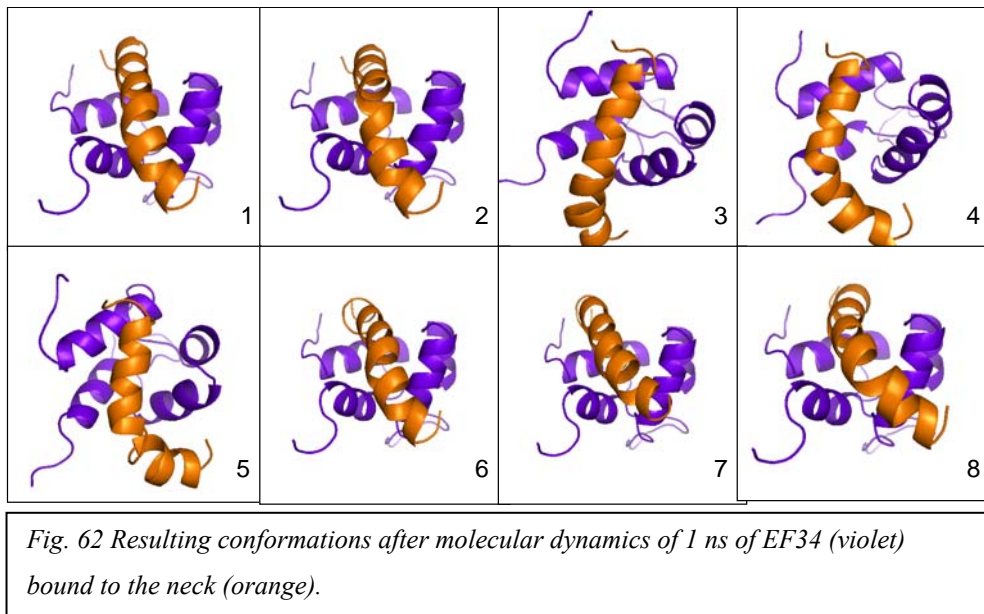
4.5 Mutants 834 Δ pBpa and 889 Δ pBpa

4.5.1 Selection of mutation sites

The structure of EF34 bound to Zr7 of titin (PDB entry: 1H8B) was used as a model to determine the putative interaction sites between EF34 and the neck. The sequence alignment of the C-terminal end of alpha-actinin and Zr-7 of titin shows very little similarity, implying a high plasticity of EF34 which enables it to bind to each of them (Young, Gautel, 2000).

Moreover, it might be important to note, that Zr-7 of titin is intrinsically unfolded when unbound and assumes a helical structure upon binding to EF34.

Since the secondary structure prediction of the neck is a helix, a perfect helix was built and was superimposed with the Zr7 of titin. The outcome of the eight 1ns molecular dynamics simulation of EF34 bound to the neck is illustrated in [Fig.62].



It is clearly visible that, as expected, that most flexible region of the neck is the unbound portion. Of course, these flexibilities might be impaired in the full length protein, where the neck is localized between two bulky domains of ABD and the rod domain.

The five most probable residues of EF34 to interact with the neck were chosen to be mutated to an artificial amino acid p-benzoyl-L-phenylalanine (pBpa), which has the property to crosslink residues within the range of 3 Å upon UV exposure (Ryu and Schultz 2006). This procedure was done to ensure that the whole complex (EF34-neck) is stable and therefore suitable for structural studies.

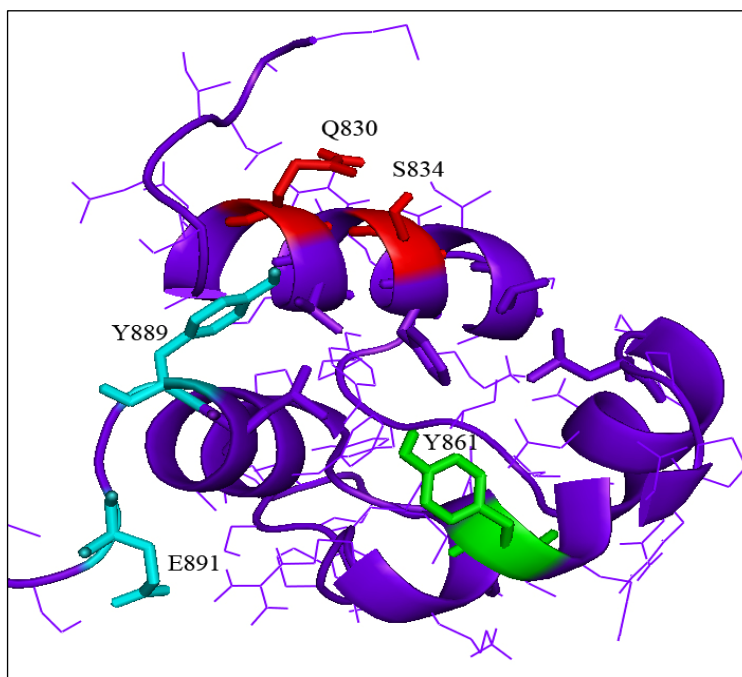


Fig. 63 Structure of EF34 (PDB:1H8B). The chosen residues to mutate have been highlighted. The different colors indicate the different positions on the three alpha helices.

We tried to choose at least one residue of each of the three helices EF34 consists of. By taking into consideration the distance matrices from our data, as well as available information from former studies (Atkinson, Joseph et al. 2001) we chose the most probable residues involved in interaction. These were the residues Q830, S834, Y861, Y889 and E891 [Fig. 63]. All these residues except E891 were found in

the interaction study and structure determination by Atkinson et. al to be involved in the interaction with Zr-7 of titin. According to the distance matrices S834 is the most likely to interact, even when the alpha helix of the neck breaks during molecular dynamics.

4.5.2 Cloning of mutants

Successful cloning of the mutant constructs was finally achieved by PCR mutagenesis of the whole vector, using primer with the amber stop codon mutation and Herculanase polymerase. The by PCR amplified mutated linear vector was incubated with DpnI for 1 h at 37 °C to remove the native template. 20 µl PCR mixes were then reduced in the speed vac to approximately 3 µl, which were used to transform E. coli strain XL1-blue. Successful mutagenesis was achieved for the constructs 834ΔpBpa [Fig. 64], 889ΔpBpa and 891ΔpBpa.

834	-----TCATCGCC	TAG	TTCCGGATCCTGGCTTCTGATAAGCCA
org	GACACCGACACTGCCGAGCAGGTCATCGCCTCCTTCCGGATCCTGGCTTCTGATAAGCCA		
	*****	*****	*****
834	TACATCCTGSCGGAGGAGCTGCGTCGGGAGCTGCCCCGGATCAGGCCAGTACTGCATC		
org	TACATCCTGGCGGAGGAGCTGCGTCGGGAGCTGCCCCGGATCAGGCCAGTACTGCATC		
	*****	*****	*****
834	AAGAGGATGCCCGCCTACTCAGGCCAGGCAGTGTGCCTGGTGCCTGGATTACGCTGCG		
org	AAGAGGATGCCCGCCTACTCAGGCCAGGCAGTGTGCCTGGTGCCTGGATTACGCTGCG		
	*****	*****	*****

Fig. 64 Sequencing result of 834ΔpBpa. The exchange of serine codon (TCC) to an amber stop codon (TAG) is marked in green

4.5.3 Expression and purification of mutants

Large scale expression in LB-media supplemented with 1 mM pBpa was done at 30 °C over night. The purification procedure was the same as for wild type EF34.

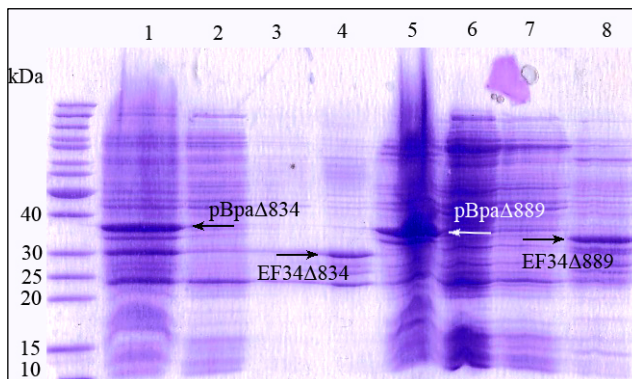


Fig. 65 SDS PAGE gel of Ni-NTA fractions of 834ΔpBpa and 889ΔpBpa

- (1) 834ΔpBpa insoluble fraction
- (2) Flow through
- (3) Wash

(4) EF34Δ834 elution

(7) Wash

(8) EF34Δ889 elution

(5) 889ΔpBpa insoluble fraction

(6) Flow through

The SDS-PAGE gel [Fig.65] shows that most of the mutant fusion protein (at this point still tagged with GST-His) is found in the insoluble fraction. Moreover, a truncated version of the mutated protein was observed, which terminates at the actual pBpa incorporation site. EF34Δ834 (deletion in residues 834-894) precipitates when the GST – tag is cleaved, while EF34Δ889 (deletion in residues 889-894) is soluble but very unstable; it degrades rapidly at 4 °C after the tag was cleaved.

The gel filtration profile of the truncated version obtained after TEV protease cleavage is diagrammed in [Fig. 66].

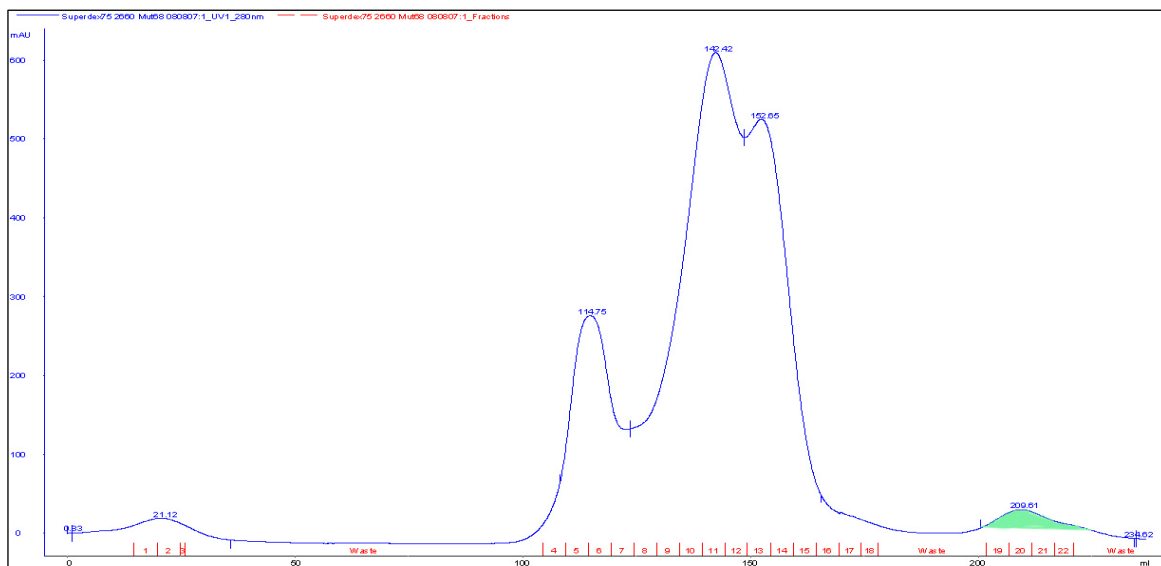


Fig. 66 Gel filtration profile of EF34Δ889 after TEV protease cleavage. The abscissa shows the elution volume in ml and the ordinate the absorption at 280 nm in mAu.

On the SDS-PAGE gel [Fig. 67] a comparison between the wild type EF34 and EF34 Δ 889 collected from fractions 19-21 of the gel filtration is shown. EF34 Δ 889 is

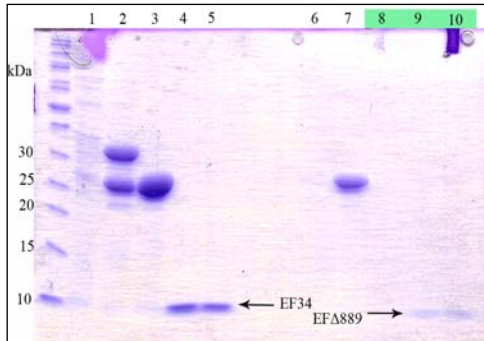


Fig.67 Comparison of EF34 and EF34 Δ 889 on 15 % SDS PAGE

clearly smaller and from the same expression volume only a fraction of the amount of protein compared to the wild type is obtained (2-3 mg/l).

Due to the failure of expressing soluble mutant protein in reasonable amounts, another expression attempt was done in GMML media supplemented with antibiotics and pBpa as described above for

LB media. The cells grew ~ 8-10 h to an OD₆₀₀ of 0.5, where they were induced with 0.5 M IPTG. Cells were harvested after 25 h of growth. Unfortunately also this procedure did not increase the amount of the soluble fraction of the mutant proteins.

In the control experiment where the mutated constructs were co-transformed with pSup-MjTyrRS-6TRN the amounts of full length mutants were comparably higher, but the

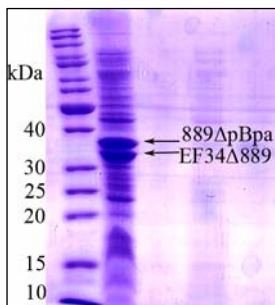


Fig. 68 Cell extract of 889 Δ Tyr expressed in GMML media

truncated version was still present with approximately 50 % [Fig.68]. Moreover also this mutant was found to be poorly soluble. These results could indicate that not sufficient amber codon-recognizing-tRNA is loaded with an amino acid (either tyrosine or pBpa) to proceed with the translation, which subsequently terminates the latter. The insolubility of the successfully mutated control protein remains unexplained, since 889 Δ Tyr should be absolutely the same as EF34. Nevertheless, the highly elongated expression times necessary for translation of the mutant proteins could possible reason for this fact.

All further experiments and analysis of the EF34 mutant protein were performed with the small soluble fraction obtained by expression in both, LB- and GMML media with 889 Δ pBpa.

4.5.4 Purification of inclusion bodies and refolding assay

In order to increase the amount of protein to work with, the insoluble fraction of 889 Δ pBpa was tried to refold.

Inclusion bodies were purified as described in section 3.2.3 according to the instructions of AthenaTM Refolding Kit via a Ni-NTA [Fig. 69 B]. Refolding attempts were performed with the 889 Δ pBpa mutant at a concentration of ~ 0.7 mg/ml. As described, the unfolded protein was diluted in several refolding buffers, incubated and analyzed. A rough analysis was done on a SDS PAGE, to determine the amount of soluble and insoluble fraction after refolding. [Fig. 69 A]. Only in three buffers a pellet was visible.

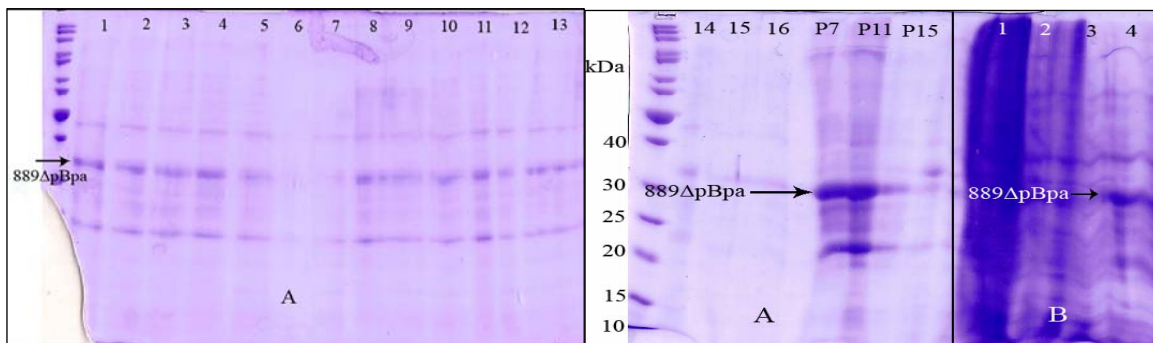


Fig. 69 A: SDS PAGE gel analysis of the refolding assay of 889 Δ pBpa
B: SDS PAGE gel fractions of Ni-NTA purification of 889 Δ pBpa in inclusion bodies

A:

- (1)- (15): dilutions of the unfolded 889 Δ pBpa in refolding buffers provided in AthenaTM Refolding Kit (see section 2.13)
- (16): dilution of unfolded 889 Δ pBpa into Gel Filtration Buffer.
- (P7)-(P9): visible insoluble fractions were found after 1 h incubation in refolding buffers #7, #11 and #15 after centrifugation.

B:

- (1) Cell extract of 889 Δ pBpa
- (2) Flow through
- (3) Wash
- (4) Elution of 889 Δ pBpa inclusion bodies

The next step was to measure the protein concentration at 280 nm and correlate it to the absorption at 320 nm, which enables one to estimate if the protein is mainly aggregate or folded (Tresaugues, Collinet et al. 2004). Since the absorptions at 320 nm were considerably low (~ 0.05) in buffers #1, #3 and #14, these dilutions were loaded on analytical size exclusion for further analysis. Unfortunately the majority of the protein eluted as aggregate. The refolded monodisperse portion was unreasonably small; therefore the refolding was not followed up any further.

4.5.5 Complex Formation and Photo cross-linking

Complex was formed between 889 Δ pBpa and the neck described before for the wild type construct: components of the complex were mixed in molar ratios 1:2 (889 Δ pBpa:neck) in Gel Filtration Buffer. The complex was incubated 30 min at 4 °C.

The best results were obtained by the BioDoc IT-Sytem UV Transilluminator UVP, exposing the complex 30 min to the UV light in a 2 ml eppendorf tube.

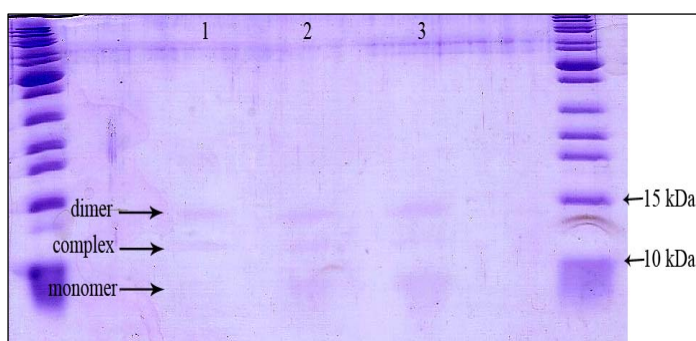


Fig. 70 Tricine gel of photo cross-linked 889 Δ pBpa/neck. Three expected bands are visible: the monomer (8 kDa), the complex (11 kDa) and the dimer (16 kDa)

Petri dishes and glass wear turned out to be unusable, since the heating of the sample is highly enhanced due to the extended surface, what resulted in precipitation of the protein. An irradiation time course of 889 Δ pBpa in complex with the neck has been carried out; lanes

1-3 show 10, 20 and 30 min of exposure [Fig. 70] (Farrell, Toroney et al. 2005). The samples were sent to mass spectroscopy to verify the incorporation of pBpa and the cross-linking. The samples were sent to mass spectroscopy to verify the incorporation of pBpa and the cross-linking, but unfortunately the amounts of complex in solution were not sufficient to perform mass-spectroscopy experiment that would unequivocally identify the insertion of the artificial amino acid residue in the complex.

Crystal screens like for EF34 were set up, which did not give any crystals by now.

4.5.6 Experiments on the truncated mutant EF34 Δ 889

It was also tried to form the complex between the truncated version EF34 Δ 889 and the neck. If the interaction was disrupted with the mutated protein, it would have proved that Y889 is crucial for binding of the neck. It was found, that this truncated version EF34 Δ 889 is degrading so fast, that binding studies are not possible.

The collected fractions of pure EF34 Δ 889 were mixed with lyophilized peptide of the neck and loaded on analytical gel filtration after 10 min incubation at 4 °C [Fig. 71]. The peak eluted around 14 ml contained the peptide of the neck, the other two peaks at 18.20 ml and 24.12 ml corresponding to approximately 1.5 kDa and 100 Da) were found to be degradation products of EF34 Δ 889.

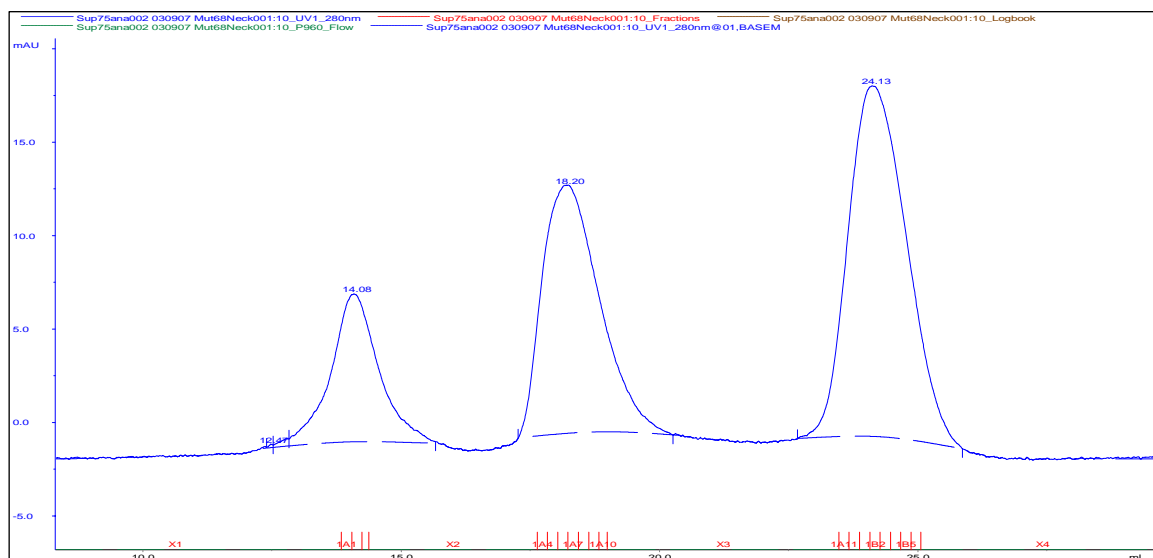


Fig. 71 Analytical gel filtration of EF34Δ889 and the neck. EF34Δ889 degrades rapidly giving two peaks eluting at 18.20 ml and 24.12 ml. No binding could be detected. The abscissa shows the elution volume in ml and the ordinate the absorption at 280 nm in mAu.

Adding the peptide of the neck to the tagged fusion protein before TEV protease cleavage, did not improve the results.

5.0 Conclusions and Perspectives

Alpha-actinin plays a dominant role in cross-linking of filamentous actin in muscle as well as in non muscle cells. It forms an important scaffold for numerous interaction partners involved in signaling and is crucial in any kind of cytoskeletal reassembly. To fulfill these manifold requirements and enable it to interact with many different binding partners, it is known, that alpha-actinin exists in two different conformations, a closed, uninduced state and an open, activated conformation. It is proposed, that the conformational change in muscle isoforms is triggered by binding of PiP_2 to the ABD domains of the alpha-actinin homodimer. Until now it is still unclear upon which physiological processes PiP_2 binds to alpha-actinin or if additional mechanisms are involved in the conformational change. Structural investigation of the closed conformation of the alpha-actinin, in which the CaM domain is bound to the neck connecting the ABD and the rod domain of the opposing subunit in the antiparallel dimer, shall provide further insights into the molecular architecture of the functional dimers and mechanisms of its regulation.

Concerning the mutant studies and photo cross-linking of 889 Δ pBpa and the neck, several changes may improve successful expression of the mutant protein. According to former studies (Farrell, Toroney et al. 2005) it might be helpful to re-clone the mutant constructs, since it was found, that the flanking nucleotides of the amber codon may highly influence the successful incorporation of pBpa and the solubility of the mutant protein. Nucleotides A or T following the amber codon were found to increase the probability of successful expression of the mutant protein. Alternatively, substitution of pBpa by p-azido-L-phenylalanine may also improve the mutant protein expression (Farrell, Toroney et al. 2005).

In this study it has been shown, that the binding between EF34 and the neck is salt independent, but slightly pH sensitive. Considering also the ITC results, indicating that the complex formation of EF34 and the neck is an exothermal reaction, we assume that the interaction is of hydrophobic nature. These findings are supported by presence of the hydrophobic patches within the neck and EF34 complex as observed in the three-dimensional structure generated by modeling. Additionally it was found that also disulfide bridge formation seems to play a role in this interaction, although this still needs to be confirmed for ABD-R1 and the C-terminal domain. It is reasonable to assume that the cysteine residues forming these disulfide bonds are only accessible in the short constructs used for the 2-mercaptoethanol study, but not in the full length protein. On the other hand the present results suggest that a reducing environment supports the change into the active state of alpha-actinin by loosening the interaction between EF34 and the neck.

6.0 References

- Atkinson, R. A., C. Joseph, et al. (2001). "Ca²⁺-independent binding of an EF-hand domain to a novel motif in the alpha-actinin-titin complex." Nat Struct Biol 8(10): 853-7.
- Au, Y., R. A. Atkinson, et al. (2004). "Solution structure of ZASP PDZ domain; implications for sarcomere ultrastructure and enigma family redundancy." Structure 12(4): 611-22.
- Bang, M. L., R. E. Mudry, et al. (2001). "Myopalladin, a novel 145-kilodalton sarcomeric protein with multiple roles in Z-disc and I-band protein assemblies." J Cell Biol 153(2): 413-27.
- Branden C, T. J. (1999). Introduction to Protein Structure 2nd ed. New York, Garland Publishing: New York.
- Beggs, A. H., T. J. Byers, et al. (1992). "Cloning and characterization of two human skeletal muscle alpha-actinin genes located on chromosomes 1 and 11." J Biol Chem 267(13): 9281-8.
- Berova, N. (2000). Circular Dichroism: Principles and Applications.
- Borrego-Diaz, E., F. Kerff, et al. (2006). "Crystal structure of the actin-binding domain of alpha-actinin 1: evaluating two competing actin-binding models." J Struct Biol 155(2): 230-8.
- Brooks, B., R. Bruccoleri, et al. (1983). "Charmm - a program for macromolecular energy, minimization, and dynamics calculations." J. Comp. Chem., 4, 187.
- Burridge, K., G. Nuckolls, et al. (1990). "Actin-membrane interaction in focal adhesions." Cell Differ Dev 32(3): 337-42.
- Chin, J. W., A. B. Martin, et al. (2002). "Addition of a photocrosslinking amino acid to the genetic code of Escherichiacoli." Proc Natl Acad Sci U S A 99(17): 11020-4.
- Crawford, A. W., J. W. Michelsen, et al. (1992). "An interaction between zyxin and alpha-actinin." J Cell Biol 116(6): 1381-93.
- Djinovic-Carugo, K. (2001). "The spectrin repeat: a structural platform for cytoskeletal protein assemblies." FEBS Letters 513 (2002): 119-123.
- Dubendorff, J. W. and F. W. Studier (1991). "Controlling basal expression in an inducible T7 expression system by blocking the target T7 promoter with lac repressor." J Mol Biol 219(1): 45-59.

- Ericsson, U. B., B. M. Hallberg, et al. (2006). "Thermofluor-based high-throughput stability optimization of proteins for structural studies." Anal Biochem 357(2): 289-98.
- Farrell, I. S., R. Toroney, et al. (2005). "Photo-cross-linking interacting proteins with a genetically encoded benzophenone." Nat Methods 2(5): 377-84.
- Faulkner, G., A. Pallavicini, et al. (2000). "FATZ, a filamin-, actinin-, and telethonin-binding protein of the Z-disc of skeletal muscle." J Biol Chem 275(52): 41234-42.
- Faulkner, G., A. Pallavicini, et al. (1999). "ZASP: a new Z-band alternatively spliced PDZ-motif protein." J Cell Biol 146(2): 465-75.
- Franzot, G., B. Sjoblom, et al. (2005). "The crystal structure of the actin binding domain from alpha-actinin in its closed conformation: structural insight into phospholipid regulation of alpha-actinin." J Mol Biol 348(1): 151-65.
- Galardy, R. E., L. C. Craig, et al. (1973). "Benzophenone triplet: a new photochemical probe of biological ligand-receptor interactions." Nat New Biol 242(117): 127-8.
- Galkin, V. E., A. Orlova, et al. (2002). "The utrophin actin-binding domain binds F-actin in two different modes: implications for the spectrin superfamily of proteins." J Cell Biol 157(2): 243-51.
- Geiger, B., A. H. Dutton, et al. (1981). "Immunoelectron microscope studies of membrane-microfilament interactions: distributions of alpha-actinin, tropomyosin, and vinculin in intestinal epithelial brush border and chicken gizzard smooth muscle cells." J Cell Biol 91(3 Pt 1): 614-28.
- Gillespie, D. T. (1996). "The mathematics of brownian motion." Americam Journal of Physics 38.
- Gimona, M. and R. Mital (1998). "The single CH domain of calponin is neither sufficient nor necessary for F-actin binding." J Cell Sci 111 (Pt 13): 1813-21.
- Heiska, L., C. Kantor, et al. (1996). "Binding of the cytoplasmic domain of intercellular adhesion molecule-2 (ICAM-2) to alpha-actinin." J Biol Chem 271(42): 26214-9.
- Honda, K., T. Yamada, et al. (1998). "Actinin-4, a novel actin-bundling protein associated with cell motility and cancer invasion." J Cell Biol 140(6): 1383-93.
- Ikura, M. (1996). "Calcium binding and conformational response in EF-hand proteins." Trends Biochem Sci 21(1): 14-7.

- Langanger, G., M. Moeremans, et al. (1986). "The molecular organization of myosin in stress fibers of cultured cells." J Cell Biol 102(1): 200-9.
- Lazarides, E. and B. L. Granger (1978). "Fluorescent localization of membrane sites in glycerinated chicken skeletal muscle fibers and the relationship of these sites to the protein composition of the Z disc." Proc Natl Acad Sci U S A 75(8): 3683-7.
- Lazaridis, T. and M. Karplus (1999). "Effective energy function for proteins in solution." Proteins, 35:133-152.
- Litjens, S. H., K. Wilhelmsen, et al. (2005). "Modeling and experimental validation of the binary complex of the plectin actin-binding domain and the first pair of fibronectin type III (FNIII) domains of the beta4 integrin." J Biol Chem 280(23): 22270-7.
- Lowry, O. H., N. J. Rosebrough, et al. (1951). "Protein measurement with the Folin phenol reagent." J Biol Chem 193(1): 265-75.
- Macarthur, D. G., J. T. Seto, et al. (2007). "Loss of ACTN3 gene function alters mouse muscle metabolism and shows evidence of positive selection in humans." Nat Genet.
- MacKerell, A., D. Bashford, et al. (1998). "All-atom empirical potential for molecular modeling and dynamics studies of proteins." J. Phys. Chem. B.
- Maiti, R., G. V. Domselaar, et al. (2004). "SuperPose: a simple server for sophisticated structural superposition." Nucleic Acids Res. 2004 July 1; 32 (Web Server issue): W590W594.
- Masaki, T., M. Endo, et al. (1967). "Localization of 6S component of a alpha-actinin at Z-band." J Biochem (Tokyo) 62(5): 630-2.
- McElhinny, A. S., S. T. Kazmierski, et al. (2003). "Nebulin: the nebulous, multifunctional giant of striated muscle." Trends Cardiovasc Med 13(5): 195-201.
- McGough, A., M. Way, et al. (1994). "Determination of the alpha-actinin-binding site on actin filaments by cryoelectron microscopy and image analysis." J Cell Biol 126(2): 433-43.
- Nave, R., D. O. Furst, et al. (1990). "Interaction of alpha-actinin and nebulin in vitro. Support for the existence of a fourth filament system in skeletal muscle." FEBS Lett 269(1): 163-6.
- Nikolopoulos, S. N., B. A. Spengler, et al. (2000). "The human non-muscle alpha-actinin protein encoded by the ACTN4 gene suppresses tumorigenicity of human neuroblastoma cells." Oncogene 19(3): 380-6.

- Ohtsuka, H., H. Yajima, et al. (1997). "The N-terminal Z repeat 5 of connectin/titin binds to the C-terminal region of alpha-actinin." Biochem Biophys Res Commun 235(1): 1-3.
- Otey, C. A., F. M. Pavalko, et al. (1990). "An interaction between alpha-actinin and the beta 1 integrin subunit in vitro." J Cell Biol 111(2): 721-9.
- Pomies, P., H. A. Louis, et al. (1997). "CRP1, a LIM domain protein implicated in muscle differentiation, interacts with alpha-actinin." J Cell Biol 139(1): 157-68.
- Ryu, Y. and P. G. Schultz (2006). "Efficient incorporation of unnatural amino acids into proteins in Escherichia coli." Nat Methods 3(4): 263-5.
- Salmikangas, P., O. M. Mykkanen, et al. (1999). "Myotilin, a novel sarcomeric protein with two Ig-like domains, is encoded by a candidate gene for limb-girdle muscular dystrophy." Hum Mol Genet 8(7): 1329-36.
- Schagger, H. (2006). "Tricine-SDS-PAGE." Nat Protoc 1(1): 16-22.
- Small, J. V. (1985). "Geometry of actin-membrane attachments in the smooth muscle cell: the localisations of vinculin and alpha-actinin." Embo J 4(1): 45-9.
- Sorimachi, H., A. Freiburg, et al. (1997). "Tissue-specific expression and alpha-actinin binding properties of the Z-disc titin: implications for the nature of vertebrate Z-discs." J Mol Biol 270(5): 688-95.
- Tresaugues, L., B. Collinet, et al. (2004). "Refolding strategies from inclusion bodies in a structural genomics project." J Struct Funct Genomics 5(3): 195-204.
- Vallénus, T., K. Luukko, et al. (2000). "CLP-36 PDZ-LIM protein associates with nonmuscle alpha-actinin-1 and alpha-actinin-4." J Biol Chem 275(15): 11100-5.
- Virel, A., B. Addario, et al. (2007). "Characterization of Entamoeba histolytica alpha-actinin2." Mol Biochem Parasitol 154(1): 82-9.
- Virel, A. and L. Backman (2006). "Characterization of Entamoeba histolytica alpha-actinin." Mol Biochem Parasitol 145(1): 11-7.
- Wachsstock, D. H., J. A. Wilkins, et al. (1987). "Specific interaction of vinculin with alpha-actinin." Biochem Biophys Res Commun 146(2): 554-60.
- Wang, L., J. Xie, et al. (2006). "Expanding the genetic code." Annu Rev Biophys Biomol Struct 35: 225-49.

Xia, H., S. T. Winokur, et al. (1997). "Actinin-associated LIM protein: identification of a domain interaction between PDZ and spectrin-like repeat motifs." J Cell Biol 139(2): 507-15.

Ylanne, J., K. Scheffzek, et al. (2001). "Crystal Structure of the alpha-Actinin Rod: Four Spectrin Repeats Forming a Thight Dimer." Cell Mol Biol Lett 6(2): 234.

Yao, X., G. C. Perez-Alvarado, et al. (1999). "Solution structure of the chicken cysteine-rich protein, CRP1, a double-LIM protein implicated in muscle differentiation." Biochemistry 38(18): 5701-13.

Young, L. and Q. Dong (2004). "Two-step total gene synthesis method." Nucleic Acids Res 32(7): e59.

Young, P., C. Ferguson, et al. (1998). "Molecular structure of the sarcomeric Z-disk: two types of titin interactions lead to an asymmetrical sorting of alpha-actinin." Embo J 17(6): 1614-24.

Young, P. and M. Gautel (2000). "The interaction of titin and alpha-actinin is controlled by a phospholipid-regulated intramolecular pseudoligand mechanism." Embo J 19(23): 6331-40.

Curriculum Vitae

Name: Kerstin Schorn

Adresse: Felberstraße 28/12, 1150 Wien

Geburtsdatum: 21.01.1983

Geburtsort: Steyr

1989-1993: Volksschule Tragwein

1993-2001: Wirtschaftskundliches Realgymnasium
der Kreuzschwestern Linz

2001-2007: Studium der Molekularen Biologie an der
Universität Wien mit den Schwerpunktsfächern
Zellbiologie, Strukturbioogie und Bioinformatik